# University of California, Merced

# Isothermal Titration Calorimetry Investigation of the Crowding Effects of Immobilized Aptamers on Gold Nanoparticle Surfaces

A dissertation submitted in partial satisfaction of the requirements for the degree Doctor of Philosophy

in

Chemistry and Biochemistry

by

Zachary James Petrek

2024

Committee Members:

Professor Anne Kelley, Chair

Professor Tao Ye, Advisor

Professor Hrant Hratchian

Jing Li, Ph.D.

The dissertation of Zachary Petrek is approved, and it is acceptable in quality and form for publication on microfilm and in digital formats.

---

Professor Tao Ye, Advisor

---

Professor Hrant Hratchian

---

Jing Li. Ph.D.

---

Professor Anne Kelley, Chair

University of California, Merced

2024

*To my mother, father, brother, and sister.*

# Contents

# Acknowledgements

I would like to express my sincere gratitude to my doctoral advisor, Dr. Tao Ye, for his guidance and support over my tenure at the University of California, Merced. Tao was encouraging, guiding, and never gave up on my efforts to complete this degree. My journey through graduate school included many roadblocks but having a persistent advisor such as Tao helped me navigate and stay the course. I would also like to thank my committee, Dr. Anne Kelley, Dr. Hrant Hratchian, and Dr. Jing Li for their continuous support and patience with my progress. My gratitude is also extended to Dr. Maria Zoghbi and Dr. Victor Muñoz for allowing me to use their equipment for sample preparation.

I would also like to thank Dr. David Kelley. Through the daily grind of graduate school, it can become easy to lose the love for the fields of study we step into. Dave's science discussions and mentoring through my time at the University of California, Merced helped me keep sight of the reason I fell in love with chemistry.

Thanks goes to my undergraduate advisor, Dr. Ashley Ringer McDonald, for encouraging me to pursue Ph.D. education. Her faith in me has been unwavering and provided me guidance for navigating the many hurdles I encountered throughout graduate school.

A very special thanks goes to Gallo for the collaboration effort that produced the results contained in this dissertation. Dr. Hui Chong, Dr. Thomas Giagou, and Dr. Nick Dokoozlian's guidance and willingness to collaborate with me and the University of California, Merced are a chief reason I was able to complete the Ph.D. degree requirements. I am forever grateful.

I am very grateful for the fellow graduate students and friends I have met throughout graduate school: Dr. Huan Cao, Dr. Qufei Gu, Dr. Yehan Zhang, Dr. Gary Abel Jr., Dr. Melissa Goodlad, Dr. Paniz Rahmani, Dr. David Morgan, Dr. William Spalder, Dr. Morgan Quail, Dr. Austin Perry, Dr. John Wilson, Dr. Arjan Bains, Veronica Luna, Warren Nanney, Cheetar Lee, Yichen Li, Ivan Vasquez, Andrew DeMello, Robert Durdkin, Bala Lwin, Ding Li, Lisa Paggeot, Alexandra Moniz, Karen Mous, Dirk Mous, Hassan Khan, and Richard Senegor. Our numerous invaluable discussions greatly contributed to my experience as a graduate student and citizen of Merced. My slow-pitch softball team mates on the Bad News Bobcats and Wasted Talent deserve thanks for helping me stay balanced and providing me with an enjoyable outlet. I would also like to extend thanks to Kennedy Nguyen for assistance in the Imaging and Microscopy Facility.

All my previous teachers and mentors dating back to my kindergarten days deserve a fair accolade in this dissertation. Ever obvious in science, education is about standing on others' shoulders. All my previous teachers' desires to share knowledge and open minds influenced and shaped me into who I am today.

Special thanks and recognition go to my family. I would not be in this position without the support of my mother, Heather, and my father, Jay. Constantly and throughout my time as a graduate student, they believed in me when I did not, and they loved me when I did not. My

brother, Aaron, and my sister, Brooke, deserve recognition for their availability to help me with technical skills or programs at a moment's notice, as well as answering an occasional phone call to help me stay balanced. My late maternal and paternal grandfathers, Lou and John, respectively, inspired my young scientific mind and my maternal and paternal grandmothers, Lynne and Janice, deserve thanks for their love and support. My extended family members deserve thanks for their support and encouragement. I would also like to thank my cat, Kelvin, for his company and willingness to cheer me up after the most defeating days.

# Curriculum Vitae

Zachary James Petrek

## Education

- Ph.D. Chemistry and Biochemistry

  University of California, Merced (2016 – 2024)

- M.S. Chemistry and Biochemistry

  University of California, Merced (2016 – 2022)

- B.S. Biochemistry

  California Polytechnic State University, San Luis Obispo (2012 – 2015)

## Publications

**Petrek, Z**.; DeMello, A.; Chong, H.; Ye, T. Isothermal Titration Calorimetry Investigation of Molecular Crowding Effects on Target Binding on Colloidal Gold Nanoparticles. In preparation, **2024**.

Zhang, Y; Allen, A; **Petrek, Z**; Cao, H; Kumar, D; Goodlad, M; Martinez, V; Singh, J; Zhang, J; Ye, T. Formation of Linear Plasmonic Heterotrimers Using Nanoparticle Docking to DNA Origami Cage. The Journal of Physical Chemistry, C. **2024**.

Gu, Q.; **Petrek, Z**.; Rezayan, R.; Ye, T. Single molecule insights into interfacial molecular recognition for model electrochemical DNA biosensors. Current Opinion in Electrochemistry. **2023.**

Gu, Q.; Cao, H. H.; Josephs, E.; Zhang, Y; Wang, H.; **Petrek, Z**.; Ye, T. Predicting Hybridization Kinetics of E-DNA Sensors with Nanoscale Probe Spatial Organization. ACS Sensors **2021**.

## Presentations

Stability Study of Bi-functionalized Gold Nanoparticles in High Ionic Strength Solutions: An Emphasis on Biosensor Development – ACS National Conference, San Francisco CA, 2023.

Varying DNA Aptamer Loading Densities on Gold Nanoparticles for Biosensor Development – ACS National Conference, San Diego CA, 2022.

Investigating the Ability of a Gold Nanoparticle / Aptamer System for Convenient and Rapid Detection of SARS-CoV-2 – UC Merced, 2021.

UC Merced Grad Slam Finalist 2019 – 2020.

Doctorless Disease Detection – California Council of Science and Technology's Science Translators Showcase, Sacramento CA, 2019.

Hydrophobic Mesoporous Silica Thin Film Chemical Sensors for Space Applications – NASA Ames Research Center, Mountain View CA, 2019.

DNA Origami Substrate for Reproducible Surface Enhanced Raman Spectroscopy – ACS National Conference, New Orleans LA, 2018.

Mesoporous Silica Thin Films for Single Walled Carbon Nanotube Sensors – NASA Ames Research Center, Mountain View CA, 2018.

DNA Origami Substrate for Reproducible Surface Enhanced Raman Spectroscopy – MACES Thrust Meeting, Merced CA, 2017.

Carbon Nanotube Based Chemical Sensor for Detection of Biomolecules in Water Samples – NASA Ames Research Center, Mountain View CA, 2017.

**Teaching Experience**

Inorganic Chemistry Teaching Assistant, UC Merced, January – May 2024

Physical Chemistry Teaching Assistant, UC Merced, January – May 2023

Instrumental Analysis Teaching Assistant, UC Merced, January – May 2017 – 2018, August – December 2022 – 2023

General Chemistry Teaching Assistant, UC Merced, August – December 2016

**Professional Service and Trainings**

E&J Gallo Winery Lab Technician, July – December 2023, March – May 2024

Non-Denominational Wedding Officiant, 2017 - current

UC Merced Authorship Dispute Board Member, 2022

Intern for Congressman Jim Costa, January – June 2022

Intern at NASA Ames Research Center, June – August 2017 - 2019

Toastmasters International, 2017 – 2022

Linguistic Lynx, Sunrise Clubs

President, 2018 – 2022

Vice President of Education, 2021 - 2022

California Council of Science and Technology Science Translators Showcase, 2019

UC Merced Center for Cellular and Biomolecular Machines (CCBM) Cleanroom and Lithography Module, June – July 2018

Team Lead for Merced Nanomaterials Center for Energy and Sensing (MACES) High School Science Outreach, 2017 – 2018

# Abstract of the Dissertation

## Isothermal Titration Calorimetry Investigation of the Crowding Effects of Immobilized Aptamers on Gold Nanoparticle Surfaces

by

Zachary Petrek

Doctor of Philosophy in Chemistry and Biochemistry

University of California, Merced, 2024

Isothermal titration calorimetry (ITC) is a powerful tool for investigating interactions between biomolecules – which are especially pertinent to many biosensing platforms. Interactions between nucleic acid aptamers and protein targets are of particular interest as aptamers offer a versatile alternative to traditionally used molecular recognition elements. ITC has been used to characterize interactions between protein targets and aptamer molecular receptors for a better understanding of the target binding process.

ITC experiments often consist of interacting biomolecules in dilute solutions. However, many aptamer-based applications require immobilization to a solid support. Interactions between neighboring immobilized aptamers change the local environment around each aptamer. Furthermore, as the solid support surface becomes increasingly crowded, aptamer / target binding is likely to deviate from what is known about binding in a dilute solution. Several barriers exist that complicate incorporating aptamer functionalized gold nanoparticles into the ITC platform. Barriers stemming from low signals produced from interacting biomolecules require unique resolutions. Overcoming these barriers is necessary for accurate characterization of binding events.

This dissertation details how ITC was enabled for investigating target binding between immobilized aptamers on gold nanoparticle surfaces and target proteins – a novel approach for characterizing target binding of immobilized aptamer-based systems. By precisely accounting for reaction stoichiometry, matching titrant and titrate buffers, and countering non-specific adsorption, we demonstrate that ITC can be used to characterize systems that feature immobilized aptamers on colloidal gold nanoparticles and protein targets – unveiling ITC as

an additional means for guiding biosensor design. Additionally, an investigation into how aptamer loading density affects target binding reveals an improvement to binding affinity as loading density increases. ITC analysis reveals that entropic compensation stemming from prepaid entropic penalties from aptamer immobilization explains the counterintuitive trend of binding affinity improvements as loading density increases. Of important note, at sufficiently high loading densities, a precipitous decline of target binding is observed, likely from increased steric hindrance from neighboring aptamers. Limitations of ITC on aptamer functionalized gold nanoparticle systems are discussed as well as future directions for using ITC to better understand target binding in crowded environments.

# List of Figures

# List of Tables

***Prologue***

Set on the surface of a gold nanoparticle, this dissertation aims to understand how crowded receptors influence the capture of a molecule of interest, *i.e.*, target. By better understanding the thermodynamics of the target binding process, an explanation to a counterintuitive trend can be used to help transform biosensing platforms and point of care diagnostics to have far-reaching implications for how we monitor the environments around and within us.

# Chapter 1: Introduction

## 1.1 Overview

When Richard Feynman gave his famous lecture "There's Plenty of Room at the Bottom" to a room full of scientists at Caltech in 1959, only he and a few others could have imagined the field that would manifest from the ideas presented. Feynman discussed manipulating matter on an atomic scale and the impacts this new perspective would have on society, science, and technology.[1] Ideas stemming from this talk would branch into a new field called "nanotechnology" and would reach and impact human lives in fields of medicine, communications, computing, and chemical analysis.

'Nano' finds its origin from the Greek prefix 'νᾶνος' meaning "dwarf." In 1960, nano was adopted by the General Conference on Weights and Measurements as a standard prefix measuring $10^{-9}$.

It is difficult to conceptualize how small a nanometer (nm), one billionth of a meter, is – though several relatable examples can be used from objects that we commonly encounter. The nominal value of the width of a human hair is approximately 75,000 nm. The finest sand on a white sand beach measures up to roughly 60,000 nm. The smallest snowflakes falling gracefully towards the Earth measure about 200,000 nm – all seemingly gigantic when fitted to the nanoscale.

Small sizes contrasted with massive room for research and development, nanotechnology has grown to a multi-disciplinary field with research competing for Nobel Prize bids and funding from the most prestigious agencies.[2, 3]

Objects in the nanoscale find themselves bordering classical (bulk) and quantum (molecular) domains as dimensional confinement shapes their properties. Their versatility and ability to bridge the gap between the macroscopic and molecular realms make them a focal point of scientific research and technological innovation. Large surface area to volume ratios lead to increased surface effects, as surface atoms have different bonding environments and energy levels compared to bulk materials. Surface effects impact reactivity of nanomaterials, making them excellent catalysts and constituents for drug delivery and sensing applications. Quantum confinement is responsible for changes in electronic structure, band gap, and optical properties of nanomaterials. Quantum confinement occurs when the motion of electrons within a material becomes restricted in one or more dimensions by the material's physical size, leading to discrete energy levels within a nanomaterial. Therefore, altering the physical size of the nanomaterial allows for precise control over its optical and electrical properties. Nanomaterials are on the size scale of biological molecules and cellular structures. Surface modifications allow nanomaterials to be engineered for cellular uptake for specific intracellular processes such as drug delivery or to target specific cells. Already miniaturized, nanomaterials fit nicely into technology's drive for compactness. These phenomena have integrated nanotechnology into seemingly every aspect of modern life – from computer chips to advanced sensing

techniques and coatings.[4] A field appreciably enjoying the boom of nanotechnological research and development is chemical and biological sensing.

Sensors are devices that quantitatively describe an environment by producing an output signal for the purpose of detecting a physical phenomenon. Examples of sensors can be found ubiquitously in our daily lives such as the heart rate monitors on smart watches, the tire pressure gauges in an automobile, or an at-home pregnancy test strip. These sensors detect or quantify signals of analytes of interest – blood volume changes through skin per unit time, pound-force per square inch of atmospheric molecules / elements (namely $N_2$, $O_2$, and argon) inside a tire, or the presence of chorionic gonadotrophin in urine – and relay the quantity or presence of the analyte to the user. Nanomaterials are exceptionally well-suited for incorporation into sensors due to the unique properties of the nanoscale. The high surface-to-volume ratio of nanomaterials enhances sensitivity, allowing for detection of minute quantities of analytes. Nanomaterials exhibit rapid response times, crucial for real-time monitoring, and their tunable properties, such as size and surface chemistry, allow for precise customization. The biocompatibility of some nanomaterials makes them suitable for sensing in biological and medical contexts. Multiplexing capabilities enable the detection of multiple analytes, while miniaturization facilitates the development of compact, portable sensors. Advances in nanomaterial synthesis techniques have improved cost-effectiveness, paving the way to widespread adoption. The enhanced signal-to-noise ratio and versatility across optical, electrochemical, and piezoelectric sensors further underscores the significance of nanomaterials in sensing technologies.

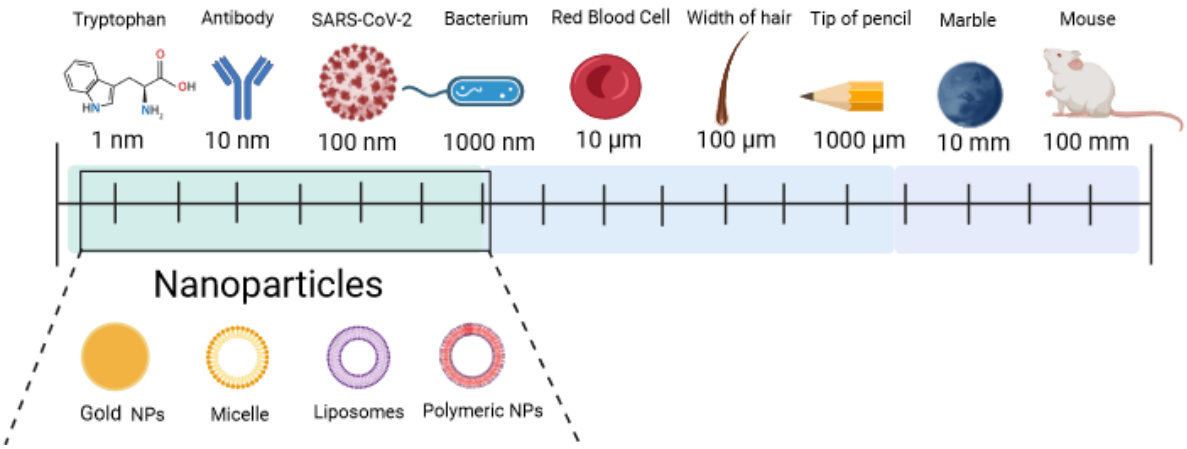


Figure 1.1: Visualization of the nanoscale. Created with BioRender.com

## 1.2 Fundamentals of Biosensing

Almost all biosensors consist of three essential components working in conjunction, including a receptor designed to bind or react specifically to a target, a signal transducer that can effectively translate the presence or changes in the target into a detectable signal, and a readout system that measures the raw signal and converts it into usable data. All sensors must possess three essential evaluation criteria to guarantee the accurate and reliable interpretation of a sample.

**Selectivity**: A sensor must only interact with a particular analyte so that the user can be confident that the signal generated is originating from the analyte. For this to be the case, sensors employ a "recognition element," which is a molecule that is designed to only specifically interact with a particular analyte even in the presence of other similar molecules.

**Sensitivity**: In the most basic sense, sensors display a signal for a given concentration. Ideally, a small change in concentration results in a large signal change, which can be quantified by the slope of a sensor's calibration curve. A sensor's detection limit is the smallest quantity of analyte that can be reliably detected – commonly corresponding to a signal that is three standard deviations above the noise.

A sensor's dynamic range is usually considered to be the range of concentrations that produce a linear or logarithmically linear change with respect to the generated signal. At high enough concentrations, sensors eventually reach a non-linear range where the signal transduction mechanism saturates the sensor's detection apparatus.

**Reproducibility / Reliability:** Sensors must be designed in a way that minimizes batch-to-batch variation. Partly a challenge in engineering, ensuring that two sensors made from the same materials produce the same result gives the user confidence that the signal produced is reliable and reproducible.

Fouling is a term used to describe a sensor's inability to produce a reliable signal after non-specific interactions with macromolecules in a solution containing the target analyte.[5] Fouling either produces a false-positive signal or does not allow the molecular recognition element to interact with the target molecule. In either case, the sensor fails to produce a signal that can be trusted by the user. Sensor design aims to eliminate non-specific adsorption to the sensor surface in order to combat fouling and produce a reliable signal.

## 1.3 Colloidal Gold Nanoparticles and Surface Functionalization

Gold nanoparticles are commonly incorporated into numerous sensing platforms. Their unique properties translate to remarkable signal transduction capabilities that have elevated the performance of these sensing platforms. The surface of gold nanoparticles can also be easily modified to incorporate a molecular receptor that can facilitate the binding process.

Understanding how gold nanoparticles can integrate molecular recognition and signal transduction is crucial to understanding why these nanomaterials are so prolific.

Gold nanoparticles possess a handful of attractive qualities and advantages that make them well-suited for signal transduction in biological and chemical detection. Gold nanoparticles are biocompatible, which allows for versatility for *in vivo* sensing applications and interactions with biomolecules without sacrificing biomolecular integrity.[6] Most often through well-established thiol – gold chemistry, gold nanoparticles are relatively easy to chemically modify, enhancing their versatility in various solvents, including aqueous solutions with various ionic strengths. Gold nanoparticles have a characteristic red color when dispersed in solution. However, when aggregated together, they change color to blue or purple due to inter-particle plasmon coupling.[7] This drastic color change has been leveraged in making colorimetric sensors where the presence of a target molecule can induce a color change that serves as a user-friendly approach to detection. Electronic properties of gold nanoparticles can be utilized to design gold nanoparticle-based biosensors. Gold is conducting in nature, so changes in current stemming from surface functionalized ligands can be used for detection of quantification.[8] Gold nanoparticles also serve as quenchers in fluorescence-based detection mechanisms.[9] When fluorophores move away from the gold nanoparticle surface, the quenching by gold is diminished, increasing the fluorescence signal. Lastly, the high surface area to volume ratio of gold nanoparticles allows a single gold nanoparticle to accommodate large numbers of capturing ligands and target molecules.[10]

Bare, unfunctionalized gold nanoparticles have very little practical use due to their stability issues in ionic strength solutions. When introduced to an ionic solution, charge screening by ions in the solution cause gold nanoparticles to irreversibly aggregate. This aggregation causes a redshift in the localized surface plasmon wavelength.[11, 12] Though this has been leveraged as a detection technique, the uncontrolled nature of this process makes it difficult to leverage as a reproducible strategy for detection.[13] In addition, bare gold nanoparticles are incapable of specific interactions, which are necessary for most chemical and biosensing applications. The absence of surface groups on gold nanoparticles exposes the surface to non-specific adsorption.[14] Without surface groups, non-specific adsorption often leads to fouling, leading to poor reproducibility or even outright failure in sensing.

Functionalizing gold nanoparticles with ligands solves the aforementioned issues. Firstly, functionalization provides stability for gold nanoparticles so they can exist in ionic strength solutions without aggregating. Certain ligands used for gold nanoparticle functionalization alter the surface charge, increasing electrostatic repulsion between neighboring particles – a process known as electrostatic stabilization. Alternatively, the presence of ligands on the gold nanoparticle surface serves as a 'buffer zone' around the corona of each gold nanoparticle which serves to prevent gold nanoparticles from aggregating together from attractive van der Waals interactions between neighboring nanoparticles. Secondly, surface functionalization passivates the gold nanoparticle surface, *i.e.*, suppressing non-specific adsorption. These two

attributes improve the reproducibility, selectivity, and reliability of gold nanoparticle-based sensing platforms.

Many surface functionalization techniques take place through thiol (-SH) gold chemistry. The Au-S bond (~232 kJ/mol) is sufficient to anchor molecules with thiol functional groups to the gold nanoparticle surface.[15] The resultant dense monolayer that forms vastly improves the practicality and utility of gold nanoparticles. DNA is a common ligand used to functionalize the surface of gold nanoparticles. Through both electrostatic stabilization (negatively charged DNA backbone) and steric stabilization, DNA oligonucleotides vastly improve gold nanoparticle stability, versatility, and programmability. Several approaches to functionalizing gold nanoparticles with DNA oligonucleotides have been developed over the past 30 years. Mirkin *et al.* pioneered the field of functionalizing gold nanoparticles with DNA ligands with a "salt aging" technique.[16] In their approach, sodium chloride is slowly added over several hours to reduce the electrostatic repulsion between citrate-capped gold nanoparticles and the negatively charged DNA phosphate backbone. At higher salt concentrations, more DNA strands will cover the gold surface, as sodium chloride screens the electrostatic repulsions between neighboring DNA ligands tethered to the surface.[10] While this method requires lengthy preparation, it has been proven to work with many different gold nanoparticle sizes and can be readily scaled up for larger functionalization batches. Liu *et al*. established a rapid method for DNA functionalized gold nanoparticles by freezing solutions of gold nanoparticles and DNA.[17] As the solution freezes, volume in the solution is excluded by ice crystals. Gold nanoparticles and DNA oligomers are forced together in close proximity, allowing thiol – gold bonding to commence. The main advantage of this approach is eliminating lengthy intervals that are necessary for the salt aging method. While being a rapid approach, this technique is sometimes ineffective with larger gold nanoparticles, as these particles are more likely to aggregate together when forced together during the freezing process. Additionally, dynamic light scattering (DLS) revealed that AuNPs functionalized by the freezing method often contain small amounts of aggregation, which may lead to disadvantageous downstream effects. Liu also developed a low pH method of functionalizing DNA oligonucleotides to gold nanoparticles.[18] The nucleobase adenine can be protonated at low pH (pH < 3), which positively charges the DNA oligonucleotide and allows the DNA strand to overcome the electrostatic repulsion from the gold surface. Although this approach uses less DNA than other methods, it works best with adenine-rich sequences, which limits its applicability. Lastly, and most recently, Deng *et al*. developed an alternative method to functionalize gold nanoparticles with a dense DNA layer through the assistance of butanol.[19] In the presence of excess butanol, hydrophilic DNA and gold nanoparticles are forced together in small water droplets. The approach is rapid, and the overall methodology is similar to the freezing method. This rapid method works well with larger gold nanoparticles and can achieve DNA loading densities about 2-3 times higher than the salt aging and freezing methods. Although technically able to scale up, this method does generate large quantities of butanol waste when functionalizing large quantities of gold nanoparticles, as butanol is added to the gold nanoparticle / DNA

reaction mixture in a 9:1 ratio. Therefore, each of the methods to functionalize gold nanoparticles has advantages and disadvantages. The choice of the surface functionalization methods depends on the specific requirements of the applications, such as loading.

The highly programmable base pairing of nucleic acids allows DNA functionalized gold nanoparticles to be assembled into higher order structures that possess unique geometries and properties. Higher order structures have been studied and assembled to increase plasmonic resonance, which increases the sensitivity of such structures.[20, 21] Moreover, the DNA ligands can be used for specific recognition of target molecules. While the recognition of nucleic acids by these DNA ligands is well known, certain DNA sequences, known as DNA aptamers, are known to specifically interact with proteins, small molecules, and even cells. Hence, gold nanoparticles functionalized with DNA aptamers attracted significant attention due to their potential in biosensing applications.[22, 23]

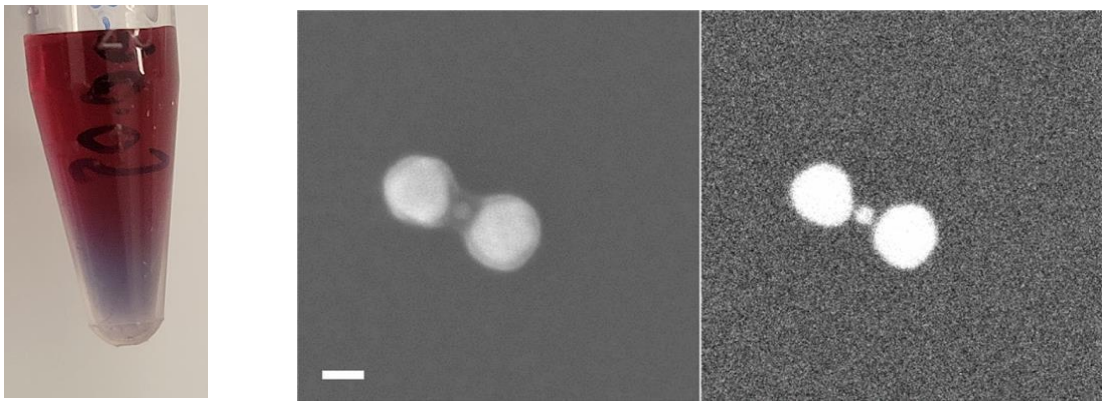

Figure 1.2: (Left) Photo of instability within a solution containing gold nanoparticles. Stable 10nm AuNP at the top of the microcentrifuge tube appear red while larger AuNP aggregates (caused by the addition of NaCl) appear purple. (Right) Scanning electron microscope image of DNA functionalized gold nanoparticle assembly. Complementary DNA binding between AuNP allows for the fabrication of higher order structures for advanced sensing techniques such as surface enhanced Raman spectroscopy (SERS). Scale bar is 20nm. Images taken by Zachary Petrek.

## 1.4 Aptamers as Molecular Recognition Elements

Aptamers are short, synthetic nucleic acid strands that exhibit affinity for various target molecules.[24] Aptamers undergo a conformational change to assume a unique tertiary structure that allows for specific yet non-covalent interactions with their targets.[25]

Before aptamers, antibodies were the chief molecular recognition element for detection strategies for decades, dating back to the 1950s.[26] Antibodies are the immune system's method of recognizing antigens inside a host. They show a high affinity and specificity for a particular

antigen. Despite the success in harvesting antibodies from host organisms, such as rats, antibodies do suffer from a few drawbacks in sensing applications.

Because antibodies are produced and harvested from a host organism, they tend to show variation between batches. This variation can lead to challenges in reproducibility.[24, 27] Additionally, because antibodies are made of proteins, they are subject to irreversible denaturation in harsh conditions. After denaturation, the antibody will no longer be able to bind to the target molecule. Furthermore, antibody production and identification is a time and labor-intensive process that is limited to targets that elicit an immune response, rendering certain conditions, such as poisoning from specific toxins, incapable of generating antibody molecular recognition.[28]

Aptamers have the potential to overcome some of these limitations of antibodies, making them attractive for sensing applications.[29] Because they are identified and produced *in vitro* and under denaturing conditions, they are not subject to batch-to-batch variations. Additionally, because they are not made of proteins, but rather flexible nucleic acids, their denaturation process is reversible, which increases their shelf life and versatility in harsh environments and makes aptamers thermally stable. There is also a wider range of target molecules that aptamers can be generated for because an immune response is not necessary for aptamer production. Aptamers are also typically much cheaper to synthesize compared to antibody harvesting.

The process of selecting DNA aptamers is known as SELEX. Though not the focus of this dissertation, understanding the SELEX process highlights how DNA oligonucleotides can be engineered to specifically interact with a range of target analytes.

Table 1.1: Comparison between nucleic acid aptamers and monoclonal antibodies when considering biosensor design.

| | Nucleic Acid Aptamers | Monoclonal Antibodies |
|---|---|---|
| Preparation | In vitro SELEX. Cheap to synthesize. No batch-to-batch variation. Time required is about 8 weeks. | Requires in vivo production. Batch-to-batch variations are often present. Expensive process compared to SELEX. Time required is about 4 months. |
| Stability | Long shelf life. Stable at room temperature and temperature resistant. Can undergo repeated rounds of denaturation / renaturation. Able to be lyophilized. | Limited shelf life. Temperature sensitive and often require refrigeration. Refrigeration is required for transport and storage. Easily denatured. |

| | | |
|---|---|---|
| Target Potential | Not limited by immune response. Targets range from small molecules and ions to whole cells. | Limited to targets that create a strong immune response. |
| Size | Small molecules that lead to decreased steric hinderance. | Relatively large when compared to the target. |
| Affinity | Can select for a range of affinities depending on application. | Dependent on the number of epitopes on the antigen. |
| Specificity | Single point mutations are easily identifiable with sequencing techniques. | Specific, but different antibodies are known to bind to the same antigen. |
| Modifiability | Easily modifiable.<br>Affinity is typically not sacrificed. | Difficult to modify.<br>Modification often leads to reduced activity. |

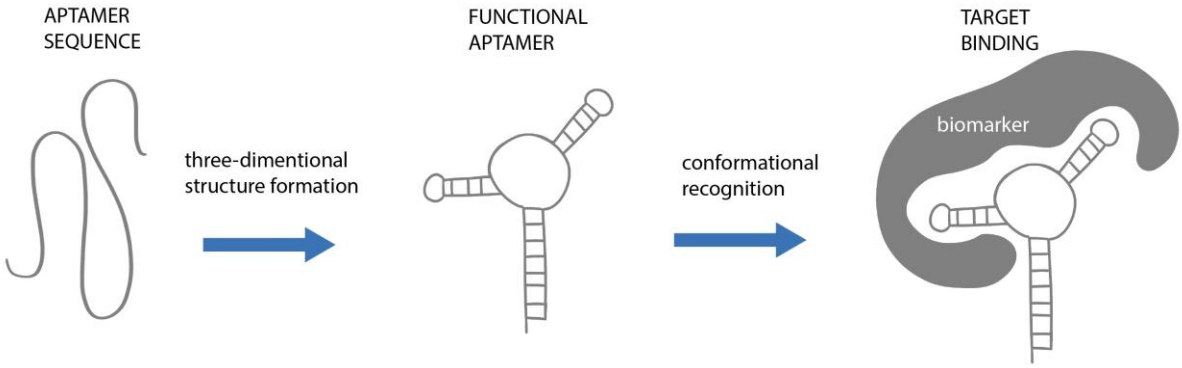


Figure 1.3: Illustration of aptamer conformation required for target binding. Secondary structure maximizes non-covalent interactions with the target.

### 1.4.1 SELEX

SELEX (systematic evolution of ligands by exponential enrichment) is used to identify and select for nucleic acid sequences that non-covalently interact with a target molecule. The target molecule can take many forms ranging in sizes and complexities, including ions, peptides, proteins, viruses, and even whole cells.[30] The technique was first proposed in 1990 by independent groups and has grown to be the standard for identifying nucleic acid aptamers that bind to a target molecule with high specificity and affinity.[31, 32] Starting from a random pool of oligonucleotides, multiple cycles select for aptamers with high affinity for a target. The SELEX process can be broken down into 5 steps.

1) *Preparation of the initial oligonucleotide pool*: At the start of the SELEX selection process, a random library of oligonucleotides is introduced to the target. These libraries are obtained from commercial vendors (such as Sigma Aldrich) and typically contain between $10^{14} – 10^{15}$ random oligonucleotide sequences. Each oligonucleotide sequence contains a recognition sequence (30 – 50 nucleotides) sandwiched between primer binding sites, which are used to amplify the sequence in subsequent steps.
2) *Incubation between target and oligonucleotides*: Upon solvation, oligonucleotides will fold into secondary and tertiary structures that will interact with target molecules. Because the target molecules are often bound to a surface, oligonucleotides that show affinity for the target molecules will be immobilized. The immobilization of oligonucleotides serves as a partitioning strategy for purification.
3) *Partitioning the bound versus unbound oligonucleotides*: Bound oligonucleotides are separated from unbound oligonucleotides. Bound oligonucleotides will move on to subsequent SELEX rounds, while unbound oligonucleotides will be removed through a method of purification that is specific to the SELEX experimental setup. A few common methods for partitioning bound versus unbound oligonucleotides are affinity columns, magnetic beads, capillary electrophoresis, or membrane filtration.[33]
4) *Amplification*: Oligonucleotides that show affinity for the target molecule are amplified for subsequent SELEX rounds. DNA aptamers are amplified by PCR (polymerase chain reaction) while RNA aptamers are amplified by RT-PCR (reverse transcription polymerase chain reaction). With the primer binding sites on each side of the oligonucleotide sequence, amplification can proceed in the presence of primers, a polymerase and nucleotides.
5) *Sequencing*: Binding oligonucleotide sequences are sequenced by Sanger sequencing or high-throughput sequencing methods. This helps ensure the binding is reproducible.

The entire SELEX process takes weeks to months, depending on the number of SELEX cycles. Between 8 and 20 cycles are typically required to obtain high affinity aptamers. Additionally, negative-target selections are introduced throughout the SELEX process to screen against non-specific binding. Other strategies include modulating the target concentration to ensure that higher affinity aptamers out-compete lower affinity sequences.[34]

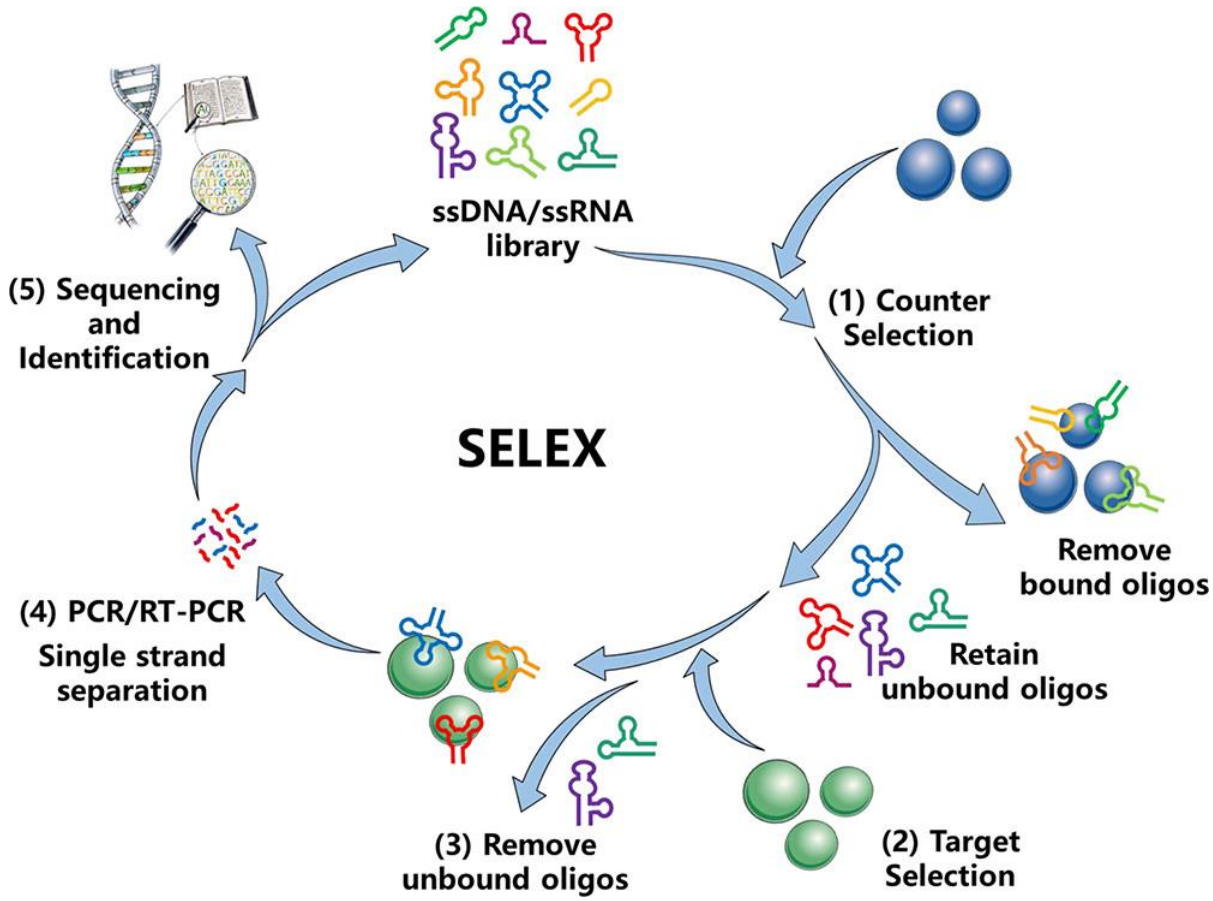


Figure 1.4: Schematic of the SELEX process. Nucleic acid aptamers are selected from primary libraries. Multiple rounds of SELEX identify high affinity aptamers. Reprinted with permission from Recent Advances in Aptamer-Based Liquid Biopsy. J. L. Zhang, Y. H. Huang, M. Sun, S. Wan, C. Y. Yang and Y. L. Song. *ACS Appl. Bio Mater.* 2022. Copyright © 2022 American Chemical Society.

### 1.4.2 Interactions with Targets

While the specific interactions between aptamers and targets vary from case to case, there are a handful of intermolecular forces that are responsible for affinity between aptamers and target molecules. These interactions work in concert with each other and are highly dependent on the chemistry between the aptamer and the target molecule.[35] External factors, such as pH, metal ion strength, and temperature, can affect the interaction energy of binding forces.

**Hydrogen bonding**

Hydrogen bonding is the most ubiquitous interaction between aptamers and targets.[28] Nucleic acid base pairs are capable of being hydrogen bond donors or acceptors while the negatively

charged phosphate backbone functions as a hydrogen bond acceptor.[36] Hydrophilic residues of the side chains of proteins often serve as hydrogen bond donors. Hydrogen bonding is also known to stabilize G-quadruplex structures, a common aptamer motif when interacting with proteins such as thrombin.[37]

**Electrostatic interactions**

Electrostatic interactions are another class of interactions that aptamers use to recognize target molecules. Electrostatic interactions mostly arise from the negatively charged phosphate backbone of a nucleic acid aptamer and positively charged amino acid residues, such as lysine and arginine.[38] As water is most often the solvent for any protein or biological macromolecule, charged amino acid residues often reside on the surface of the protein where interaction with the aptamer phosphate backbone can readily take place. Electrostatic interactions can be non-specific in nature and tend to be influenced by the surrounding media and salt concentrations.

**Hydrophobic effects and pi-stacking**

Hydrophobic effects refer to the tendency of nonpolar constituents to associate together while excluding water molecules in an aqueous solution. Though the phosphate backbone of the aptamer is charged and readily associates with water molecules, aptamer bases, especially purines adenine and guanine, have hydrophobic aromatic rings consisting of pi electrons. Pi-stacking of purine-rich sequences is known to stabilize the nucleic acid secondary structure.[39] Hydrophobic residues of amino acids, such as tyrosine and tryptophan, are likely to associate with hydrophobic regions of aptamers.[35]

**Van der Waals interactions**

Van der Waals interactions are omnipresent in molecular interactions as random changes in electron density result in attractive or repulsive forces between atoms, molecules, and surfaces. While characteristically weak, van der Waals interactions typically couple with other non-covalent interactions, such as electrostatic interactions, and contribute to interaction energies between aptamers and target molecules.[40, 41] These interactions become more prevalent with increased molecular size.

## 1.5 Thrombin and its Aptamers

Thrombin is classified as an allosteric serine protease and acts as a central protein in the coagulation cascade in mammals.[42, 43] Activated thrombin cleaves fibrinogen into fibrin, resulting in blood clots that stop bleeding. Because of its relevance in physiological homeostasis, studies involving thrombin and its detection serve as practical examples for biosensing development.

The discovery of Thrombin Binding Aptamer (TBA) was among the first nucleic acid aptamers discovered though the SELEX process.[44] Thrombin is often used as a model system in many

aptamer-based sensor studies because it has two known aptamers that bind to different locations on the thrombin protein independently.[45] The short sequences of thrombin's aptamers make them relatively inexpensive to synthesize. The affinities of these two well-characterized aptamers differ by two orders of magnitude, which can be leveraged for biosensing platforms.

Bock *et al*. discovered the first aptamer that binds to human α-thrombin in 1992.[44] The 15 base-pair aptamer sequence (5' - GGT TGG TGT GGT TGG – 3') is guanine-rich and in the presence of potassium cations, forms a stable G – quadruplex: a structure that adopts an antiparallel chair-like conformation from parallel guanine residues.[46, 47] When in this folded conformation, 15mer-TBA binds to the fibrinogen – recognition exosite, also known as Exosite I, of thrombin and has an affinity for this exosite of ~ 100 nM.[27] When this aptamer binds to an active exosite of thrombin, the fibrinogen cleaving activity is reduced.

More recently, an aptamer that binds to a different exosite of thrombin was discovered. Twenty-nine nucleotides in length, the 29mer aptamer (5' – AGT CCG TGG TAG GGC AGG TTG GGG TGA – 3') recognizes the heparin-binding exosite, also known as Exosite II, and has an affinity of 0.5 nM.[27, 48] The difference in binding affinities and recognition sites from these two aptamers has prompted the development of sandwich assays for thrombin detection.[45]

Many iterations and alterations of these two aptamers have been produced and studied for their effects on binding to thrombin. Adding a long, poly-T tail to Bock's TBA was shown to increase affinity by nearly a factor of ten.[49] Additionally, Tian *et al.* showed how combining the 15mer TBA sequence with the 29mer TBA sequence using a polyethylene glycol phosphoramidite linker to enable multivalent binding increased binding affinity by 97-fold.[50] These modifications to the TBA highlight the versatility of aptamers and how they can be leveraged to maximize binding efficiency to enhance biosensor performance.

The understanding of thrombin and its aptamers make it a relatively user-friendly system for studying biosensing platforms. Thus, thrombin is the target captured by TBA, which serves as the molecular recognition element. Many biosensing platforms require immobilizing a molecular recognition element onto a solid support. Several factors, including the local environment of the molecular recognition element, are known to influence target binding. Molecular crowding is a factor that has been investigated in hopes of improving sensor performance and leveraging conditions that are favorable to target binding.

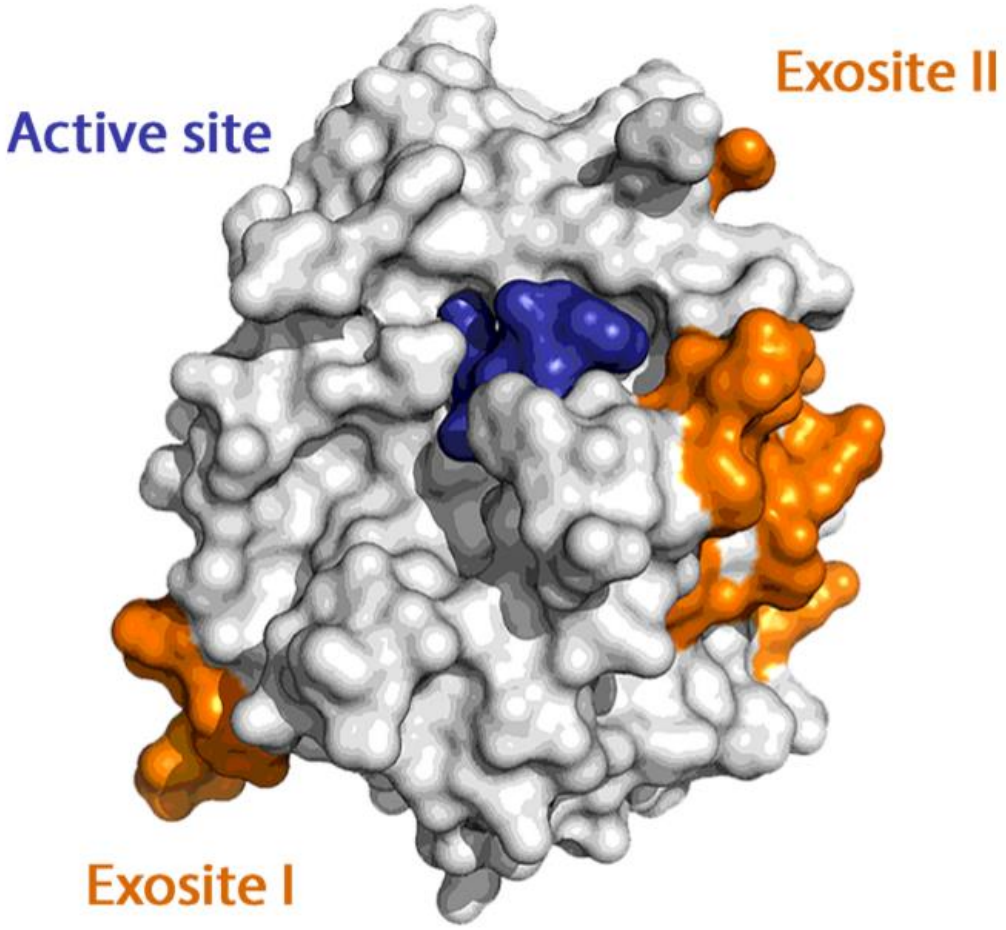


Figure 1.5: Thrombin protein with its exosites highlighted in orange. Exosite I, the fibrinogen – recognition site, is the binding site for 15mer TBA. Exosite II, the heparin – recognition site, is the binding site for 29mer TBA. Reproduced from reference 44. 

## 1.6 Crowding on Flat and Curved Surfaces

Molecular crowding is a term used to describe the effects of neighboring molecules on chemical reactions, target recognition, and binding inhibition.[51] Such instances occur naturally in cells and other heterogeneous solutions. The idea of molecular crowding was first introduced in the 1960 but did not break into mainstream research until the late 1990s. Minton *et al.* first described the idea of excluded volume in 1980, explaining how the thermodynamics of protein folding and stability was influenced by other macromolecules in a cell cytoplasm.[52] Because cytoplasm density inside a cell is often large, he cautioned researchers against assuming results of experiments performed in dilute solution to match the conditions found in *vivo*. Minton's

thermodynamic interpretation of excluded volume effects on protein stability catapulted in-solution crowding effects into an active field of study.[53]

Interest around crowding on flat surfaces ensued with the development techniques immobilizing DNAs on solid support. Immobilized DNAs would take root in many notable biotechnological platforms such as eDNA sensors, DNA microarrays, and DNA sequencers. [54-57] All these technologies used immobilized DNA as a molecular recognition element for target capture.

Complementary DNA (cDNA) was a common target as these new technologies could be used to detect genes of interest. Researchers focused on how the density of immobilized DNA influenced cDNA capture efficiency, as the ability to understand crowding on solid support systems could be applied to eDNA sensors, DNA microarrays, and DNA sequencers. From a polymer physics perspective, DNA can be viewed as a negatively charged polymer. Counterions are required to stabilize DNA when tethered to a surface. Crowding the surface with large numbers of tethered DNA oligonucleotides represents an electrostatic barrier for cDNA hybridization.[58] Conditions required to overcome electrostatic barriers and steric effects from tethered DNA brushes became a focus for the first crowding experiments pertaining to flat surfaces.

Tarlov *et al.* developed a method of controlling the surface coverage of DNA immobilized on a gold surface by introducing a mercaptohexanol (MCH) spacer.[59] MCH was demonstrated to displace non-specifically adsorbed DNA strands from the gold surface and helped extend the immobilized DNA into the solution phase. The MCH backfilling approach became mainstream in many DNA sensors as it greatly improved signal to noise ratios and hybridization efficiencies. Tarlov *et al.* further developed the field by introducing an electrochemical method of quantifying DNA immobilized on gold using chronocoulometry.[60] This study allowed researchers to prepare different density DNA brushes to further optimize hybridization conditions. Southern *et al.* demonstrated how steric factors stemming from tethered DNA brushes affected cDNA hybridization on DNA microarrays.[61] This study determined that spacer regions aided in cDNA hybridization and helped relate DNA brush density to cDNA hybridization. Geordiadis *et al*. was among the first to study how tethered DNA density influenced kinetics of cDNA hybridization.[62] The conclusion that hybridization efficiency decreases with increasing probe density was not unexpected but opened the door for researchers to better understand the conditions necessary for cDNA hybridization to tethered surfaces. Levicky *et al.* studied the impact of immobilized DNA surface density and ionic strength on cDNA target capture.[63] While it has been established that cDNA target capture efficiency decreases with increasing surface density, increasing the solution's ionic strength can help overcome the dense electrostatic DNA brush barrier. Given solution ionic strength and surface density conditions, Levicky *et al*. characterized non-hybridizing, suppressed hybridizing, and pseudo-Langmuir hybridizing regimes that can be used to predict cDNA hybridization efficiency. Levicky suggests that the Langmuir hybridization regime is where

immobilized probes do not interact with each other – a region where target binding would readily occur due to the lack of crowding interactions between immobilized DNA strands.

While these studies have afforded insights into how the crowding interactions impact the hybridization of immobilized DNA probes, crowding effects on immobilized aptamer-based biosensors are not as well understood. Steric hinderance from neighboring bound aptamers, bound and unbound target macromolecules, and excluded volume from unbound aptamers is likely to hinder target capture. Xiao *et al*. illustrated how immobilizing DNA aptamers in a folded conformation increases signal gain in hairpin DNA sensors.[25] Aptamers immobilized in their folded state have room to undergo conformational change when re-introduced to a target. The increased separation between probes results in a greater percentage of probes capturing target molecules, increasing the signal gain on a flat gold surface.

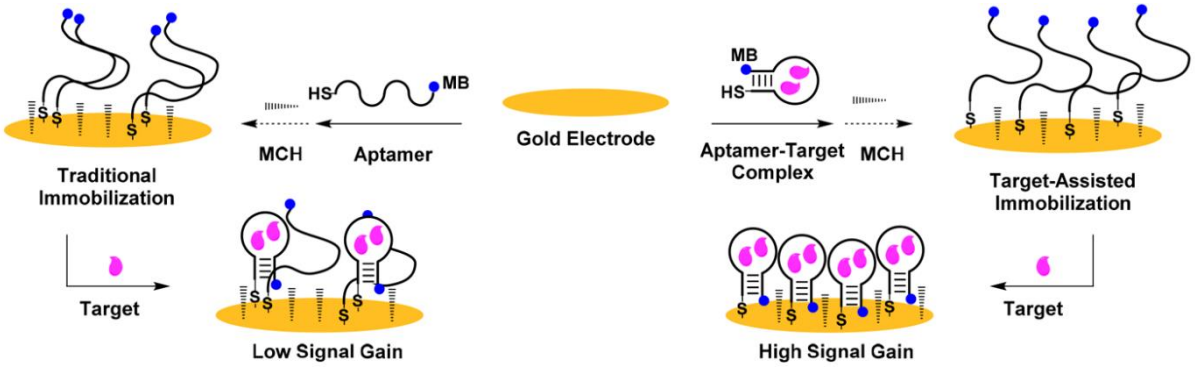


Figure 1.6: Illustration of how aptamer crowding on planar gold surfaces hinders target capture. Aptamers immobilized when complexed with targets showed increased signal gain compared to aptamers immobilized without complex. Reprinted with permission from Immobilization Strategies for Enhancing Sensitivity of Electrochemical Aptamer-Based Sensors. Yingzhu Liu, Juan Canoura, Obtin Alkhamis, and Yi Xiao. *ACS Applied Materials & Interfaces* **2021** *13* (8), 9491-9499. DOI: 10.1021/acsami.0c20707. Copyright © 2021 American Chemical Society.

Due to nanoparticle curvature, colloidal surfaces smaller than 60 nm in diameter likely display unique crowding effects when compared to flat surfaces. Gooding *et al.* studied how target capture may be affected by different DNA loading densities on colloidal gold nanoparticles by using the binding induced conformational change that turns on fluorescence of a reporter.[22] They discovered that increasing DNA aptamer loading densities on 49 nm diameter gold nanoparticles increases aptamer / target affinity when using a protein macromolecule target. While this study apparently contradicts the conventional wisdom regarding target capture in crowded environments, the mechanism of enhanced target binding on aptamer functionalized nanoparticles remains unclear. A first step toward such mechanistic understanding is to quantify the thermodynamics of aptamer / target binding in crowded, colloidal systems. Enthalpic and entropic contributions to aptamer target capture may illuminate how the driving forces of target binding are altered by the crowded environment, which in turn may help

researchers to improve biosensor design and preparation of nanoparticles to increase biosensor performance.

## 1.7 Isothermal titration calorimetry (ITC) as a method of studying molecular interactions

Isothermal titration calorimetry (ITC) is the standard for determining quantitative thermodynamic data for biomolecular studies. ITC measures the heat evolved or absorbed during the formation of a ligand / macromolecule complex.[64] ITC is highly versatile, allowing the study of various biomolecular interactions without the need for fluorescent, radioactive, or redox labels. By measuring heat associated with a reaction, ITC is a direct method of thermodynamic characterization of the target binding process. The ability to provide a detailed thermodynamic profile makes ITC an invaluable tool in understanding the intricacies of molecular recognition.[65, 66] Adapting ITC to study molecular crowding effects could help explain the deviation from the target capture trends observed in cDNA systems.

In the context of molecular crowding, biomolecular interactions are commonly studied by fluorescence spectroscopy or potentiometry. In each of these techniques, the signal is generated by a tag located on the molecular recognition element: a fluorophore for fluorescence spectroscopy and a redox tag for potentiometry. Upon binding, the position of the tag changes in relation to the gold surface, which generates a change in signal (fluorescence or electrical current). These techniques reveal the association constant ($K_a$) for two interacting molecules, but rely on conformational changes of the molecular recognition element.[67] This indirect method of analysis is subject to crowding effects, raising questions of the origin of the generated signal.

Furthermore, it is difficult to use fluorescence and redox based detection strategies to quantify entropic or enthalpic contributions of target binding – leaving knowledge gaps surrounding the nature of the interaction between target and recognition molecules. Several studies have concluded that molecular crowding effects can have an impact on the position of the tag, which is necessary for such studies.[68, 69]

Few ITC studies have incorporated gold nanoparticles or studies involving crowding effects. Mirkin *et al.* used ITC to study how the DNA density on a gold nanoparticle affects the target capture of a complementary DNA oligonucleotide.[70] They also demonstrated that DNA strands tethered to a gold nanoparticle surface enhanced cDNA target capture by preventing DNA strands on the gold surface from adopting unfavorable binding conformations.

However, they did not study how varying crowding densities may affect target capture. Additionally, because this study focused on cDNA as a target, interactions between aptamers and targets remain unexplored. As such non-covalent interactions are distinct from base-pairing interactions, the trends concerning how the nanoparticles alter DNA hybridization cannot be readily extrapolated to target binding by immobilized aptamers.

De *et al.* incorporated gold nanoparticles into ITC to study complex formation of amino acid functionalized gold nanoparticles functionalized with various proteins.[71] The effects of crowding on complex formation were not the focus of this study. Due to the lack of quantitative information concerning thermodynamics, we still do not understand how molecular recognition is influenced by the local environment of the gold nanoparticles.

### 1.7.1 ITC Working Principles

An ITC consists of a sample well, reference well, and a syringe. The syringe delivers small, regular volumes of ligand to the sample well, which contains the macromolecule under study. The reference well is filled with buffer identical to the sample well, but lacking reactants. The concentration of the ligand in the syringe is typically 10x the concentration of the macromolecule in the sample well to ensure the reaction reaches saturation. Both the sample and reference wells sit inside an adiabatic jacket, ensuring that there is negligible heat exchange with the environment.

Upon injection, ligands bind to unbound macromolecules in the sample well. The heat evolved from ligand / macromolecule interactions is measured by thermocouples that surround the sample well. The amount of power required to return the sample cell to the same temperature as the reference cell is recorded and directly related to the heat evolved during the reaction between ligand and macromolecule. Initially, because all the macromolecules in the sample well are unbound, ligands readily interact with macromolecules. However, after successive injections from the syringe, the macromolecules become saturated with ligands and binding begins to slow. As binding slows, less heat is evolved.

By analyzing the resulting thermograms, crucial information including the binding affinity, free energy changes, enthalpy changes, entropy changes, and reaction stoichiometry can be extracted.

**Determining the binding affinity ($K_A$)**

Consider the following equilibrium reaction between thrombin and aptamer interacting to form a complex…

$$[A] + [T] \overset{K_A}{\leftrightarrow} [AT]$$

Where:

$[A]$ is the concentration of free aptamer.

$[T]$ is the concentration of free thrombin.

$[AT]$ is the concentration of the aptamer / thrombin complex.

The association constant is used to quantify the binding affinity of the aptamer for the thrombin.

$$K_A = \frac{[AT]}{[A][T]}$$

*(~~Equation~~ 1)*

The association constant, $K_A$, has units of $M^{-1}$ and can be used to determine the amount of bound aptamer at a specified concentration of aptamer and thrombin. The above equation can be arranged to more clearly show the ratio of the aptamer – thrombin complex to free thrombin, $[AT]/[T]$.

$$K_A[A] = \frac{[AT]}{[T]}$$

*(~~Equation~~ 2)*

Notice:

$$[T]_{bound} + [AT] = [T]_{total}$$

*(~~Equation~~ 3)*

When half of the thrombin binding sites are occupied by the aptamer, the other half are bound to the aptamer. At these conditions, [AT] equals [T], the value of $K_A$ can be expressed as simply 1/[A].

Another view of equilibrium can be observed by comparing the fraction of binding sites occupied to the total number of binding sites, θ. The total number of binding sites is the sum of thrombin with and without aptamers bound. This ratio can be described in relation to the concentrations of thrombin without aptamers bound, [T], and the concentration of the total protein. $[T]_{total.}$

$$\theta = \frac{Binding\ sites\ occupied}{Total\ number\ of\ binding\ sites} = \frac{[AT]}{[T]_{total}} = \frac{[AT]}{[AT] + [T]}$$

*(~~Equation~~ 4)*

By substituting $[AT] = K_A [A][T]$, the fraction of binding sites can be expressed as:

$$\theta = \frac{[AT]}{[AT] + [T]} = \frac{K_A[A][T]}{K_A[A][T] + [T]} = \frac{K_A[A]}{1 + K_A[A]}$$

*(~~Equation~~ 5)*

In the context of ITC measurements, the heat, $q$, released or absorbed during an injection is directly proportional to the moles of the AT complex formed. This quantity can be expressed in terms of the total volume, V, and concentration [AT]. Utilizing the expression for the fraction, θ, enables the representation of heat in relation to the association constant.

$$q \propto V[AT] = V[T]_{total}\,\theta = V[T]_{total}\left(\frac{K_A[A]}{1 + K_A[A]}\right)$$

*(~~Equation~~ 6)*

Therefore, the heat profiles obtained from ITC experiments can be employed to determine the binding affinity of the drug to the protein. The proportionality constant is determined by the quantity of heat released or absorbed during the binding of each molecule.

Conventionally, the dissociation constant – the inverse of the association constant – is used because it has units of molar rather than inverse molar. The same relationship applies – when [AT] equals [T], the dissociation constant is [A].

$$K_D = \frac{[A][T]}{[AT]}$$

*(~~Equation~~ 7)*

**Determining the free energy change (ΔG)**

As discussed above, ITC uses heat to determine the association constant of an interaction by calculating the heat evolved after each injection and relating it to the formation of the complex between aptamer and thrombin. The equilibrium constant is then used to determine the free energy change, ΔG, of the reaction by the following relationship:

$$\Delta G = -RTln(K_A)$$

*(~~Equation~~ 8)*

**Determining the enthalpy change (ΔH)**

New non-covalent interactions form when two molecules interact. The rearrangement of non-covalent interactions releases heat into the system or absorbs heat from the system. The formation of new non-covalent interactions between biomolecules is generally exothermic, meaning it releases energy and contributes to the stabilization of the system. This occurs because non-covalent interactions, such as hydrogen bonds, ionic interactions, van der Waals forces, and hydrophobic interactions, typically lower the overall free energy of the system. When two biomolecules come together, the attractive forces between complementary regions of the molecules result in a net release of energy. As the heat dissipates into the solution, the ITC cools to the sample cell so it can return to the temperature of the reference cell. This is represented as a negative value on the difference in power (DP) and corresponds to downward spikes when the titrant is introduced to the titrate.

However, under certain conditions, the formation of new non-covalent interactions between two biomolecules can be endothermic. For instance, reactions that proceed by disrupting pre-existing interactions within the biomolecules or with solvent molecules may require more energy than is released by the formation of the new interactions. In aqueous solutions, displacing strongly hydrogen-bonded water molecules from the biomolecules can be energetically costly. Conformational changes needed to accommodate new interactions may also require an energy input, as can overcoming electrostatic repulsion between charged groups on the biomolecules. As energy is taken from the surroundings for the reaction to proceed, the temperature of the sample cell drops. The ITC compensates for this cooling by adding heat to make the sample cell the same temperature as the reference cell. The difference in power is positive and is noted by upward spikes when the titrant is introduced to the titrate.

The heat absorbed or released after each injection can be expressed as…

$$q_{injection} = V\Delta H\, \Delta[L_B]$$

*(~~Equation~~ 9)*

Where…

$q_{injection}$ is the heat associated after the injection (measured by the ITC).

$V$ is the reaction volume.

$\Delta H$ is the enthalpy of binding.

$\Delta[L_B]$ is the change in the bound ligand concentration.

$\Delta H$ for a given injection can be calculated from the equation above.

The difference in power needed to keep the sample cell at the same temperature as the reference cell is integrated with respect to time, which produces a binding isotherm. The binding isotherm represents the total heat evolved or absorbed during the titration. The enthalpy change can be quickly determined graphically by measuring the difference between the initial injections and the injections after the titrant has saturated the titrate.

After each injection, the bound ligand concentration increases. Since q is directly proportional to the increase in bound ligand, the magnitude of heat evolved or absorbed after each injection decreases in a stepwise fashion as the titrant saturates the titrate.

The total amount of heat absorbed or released by the system is directly proportional to the total amount of bound ligand, which can be expressed as…

$$Q = V\ \Delta H \sum \Delta\ [L_B] = V\ \Delta H\ [L_B]$$

*(~~Equation~~ 10)*

Where…

Q is the cumulative heat

*V* is the reaction volume

$L_B$ is the concentration of bound ligand

By integrating the total heat evolved from the reaction, the total enthalpy change, ΔH, of the reaction can be solved using Equation 10.

**Determining the entropy change (ΔS)**

There is a change in entropy in a system where two molecules bind together. In the case of DNA aptamers and target proteins, entropy changes relate to…

- the restriction of DNA conformations because of target binding
- the restriction of target protein conformations because of target binding
- release of ordered water molecules after binding
- the loss of some translational degrees of freedom for the aptamers and proteins
- the rearrangement of neighboring DNA aptamers in crowded environments because of target binding

Change in entropy is often difficult to measure directly. ITC deduces entropy changes from thermodynamic quantities that were previously discussed.

ITC determines the entropy change in a system of interacting biomolecules by the following relationship…

$$\Delta G = \Delta H - T\Delta S$$

*(~~Equation~~ 1~~0~~)*

Where…

$\Delta G$ is the system's change in free energy

$\Delta H$ is the system's change in enthalpy

$T$ is the system's temperature (K)

$\Delta S$ is the system's change in entropy

Previous sections outlined the determination of $\Delta G$ and $\Delta H$. Because ITC takes place at constant temperature, $T$ is constant. $\Delta S$ can be found by mathematical rearrangement.

**Determining the binding stoichiometry (N)**

ITC determines the stoichiometry of a reaction by analyzing heat changes during the titration of one reactant into another. Heat changes, $q$, are measured for each injection, and the area under the resulting peaks represents the total heat change. By calculating the heat change per mole of titrant and identifying the steepest part of the heat signal, which corresponds to the region of approaching equilibrium, ITC allows for the determination of stoichiometry. The stoichiometry is then calculated by comparing the total heat change to the heat change per mole. It's essential to note that ITC assumes a one-to-one binding, which is the case for thrombin interacting with an apatamer that binds to one exosite. For reactions with more complex stoichiometry or multiple steps, complementary analyses or techniques may be required for a comprehensive understanding of the reaction mechanism.

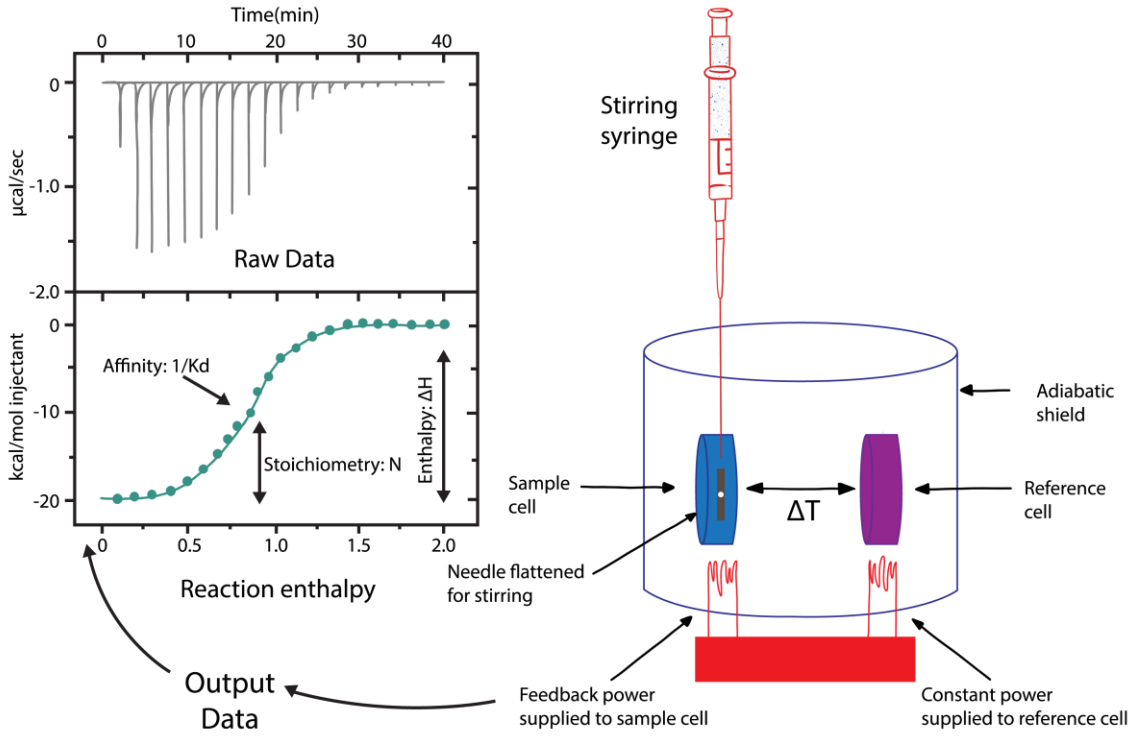


Figure 1.7: The diagram illustrates the basic principle of isothermal titration calorimetry (ITC), featuring a schematic of the calorimeter (right) and a typical titration experiment (upper left) along with its evaluation (lower left). In the upper left image, the titration thermogram shows the heat per unit of time released after each injection of the ligand into the protein. The lower left image depicts the relationship between the heat released per injection and the ratio of total ligand concentration to total protein concentration. Experimental data points are represented by circles, and the line indicates the best fit to a model with n identical and independent binding sites. The process involves inserting a syringe into the sample cell and performing a series of injections.

## 1.8 Roadmap of the Dissertation

After a discussion of relevant background knowledge and information in chapter 1, chapter 2 more thoroughly details how practical limitations were overcome to incorporate gold nanoparticles into ITC studies. Chapter 2 also examines how different aptamer crowding densities were fabricated on 10nm gold nanoparticles and quantified using a label free approach. Chapter 3 presents how molecular crowding on 10nm gold nanoparticle surfaces affects target binding and discusses how the nearest neighbor distance can be used to leverage high affinity binding. A discussion of the impacts of overcrowding along with misconceptions found in the literature is also presented.

Chapter 1 References


(1) Feynman, R. P. There's Plenty of Room at the Bottom. *Resonance* **2011**, *16* (9), 890-904. DOI: DOI 10.1007/s12045-011-0109-x.

(2) Cademartiri, L.; Ozin, G. A. *Concepts of nanochemistry*; Wiley-VCH;, ;John Wiley Distributor, **2009**.

John Wiley distributor, 2009.

(3) Tourney, C. From nano machines to Nobel prizes. *Nat Nanotechnol* **2017**, *12* (1), 1-1. DOI: 10.1038/nnano.2016.289.

(4) Nasrollahzadeh, M.; Sajadi, S. M.; Sajjadi, M.; Issaabadi, Z.; Atarod, M. *An introduction to green nanotechnology*; Academic Press, **2019**.

(5) Desai, T.; Hansford, D.; Leoni, L.; Essenpreis, M.; Ferrari, M. Nanoporous anti-fouling silicon membranes for biosensor applications. *Biosensors & Bioelectronics* **2000**, *15* (9-10), 453-462.,, Article. DOI: 10.1016/S0956-5663(00)00088-9.

(6) Kus-Liskiewicz, M.; Fickers, P.; Ben Tahar, I. Biocompatibility and Cytotoxicity of Gold Nanoparticles: Recent Advances in Methodologies and Regulations. International Journal of Molecular Sciences *Int J Mol Sci* **2021**, *22* (20). DOI: ARTN 10952

10.3390/ijms222010952.

(7) Elghanian, R.; Storhoff, J. J.; Mucic, R. C.; Letsinger, R. L.; Mirkin, C. A. Selective colorimetric detection of polynucleotides based on the distance-dependent optical properties of gold nanoparticles. *Science* **1997**, *277* (5329), 1078-1081. DOI: DOI 10.1126/science.277.5329.1078.

(8) Morita, T.; Lindsay, S. Determination of single molecule conductances of alkanedithiols by conducting-atomic force microscopy with large gold nanoparticles. *Journal of the American Chemical Society* **2007**, *129* (23), 7262-+. DOI: 10.1021/ja072040+.

(9) Chen, Y.; O'Donoghue, M. B.; Huang, Y. F.; Kang, H. Z.; Phillips, J. A.; Chen, X. L.; Estevez, M. C.; Yang, C. Y. J.; Tan, W. H. A Surface Energy Transfer Nanoruler for Measuring Binding Site Distances on Live Cell Surfaces. *Journal of the American Chemical Society* **2010**, *132* (46), 16559-16570. DOI: 10.1021/ja106360v.

(10) Hurst, S.; Lytton-Jean, A.; Mirkin, C. Maximizing DNA loading on a range of gold nanoparticle sizes. *Analytical Chemistry* **2006**, *78* (24), 8313-8318., Article. DOI: 10.1021/ac0613582.

(11) Moitra, P.; Alafeef, M.; Dighe, K.; Frieman, M. B.; Pan, D. Selective Naked-Eye Detection of SARS-CoV-2 Mediated by N Gene Targeted Antisense Oligonucleotide Capped Plasmonic Nanoparticles. *Acs Nano* **2020**, *14* (6), 7617-7627. DOI: 10.1021/acsnano.0c03822.

(12) Zhao, W. A.; Chiuman, W.; Lam, J. C. F.; McManus, S. A.; Chen, W.; Cui, Y. G.; Pelton, R.; Brook, M. A.; Li, Y. F. DNA aptamer folding on gold nanoparticles: From colloid chemistry to biosensors. *Journal of the American Chemical Society* **2008**, *130* (11), 3610-3618. DOI: 10.1021/ja710241b.

(13) Zhou, W.; Hu, K. Q.; Kwee, S.; Tang, L.; Wang, Z. H.; Xia, J. F.; Li, X. J. Gold Nanoparticle Aggregation-Induced Quantitative Photothermal Biosensing Using a Thermometer: A Simple and Universal Biosensing Platform. *Analytical Chemistry* **2020**, *92* (3), 2739-2747. DOI: 10.1021/acs.analchem.9b04996.

(14) Ma, W. W.; Saccardo, A.; Roccatano, D.; Aboagye-Mensah, D.; Alkaseem, M.; Jewkes, M.; Di Nezza, F.; Baron, M.; Soloviev, M.; Ferrari, E. Modular assembly of proteins on nanoparticles. *Nature Communications* **2018**, *9*. DOI: ARTN 1489

10.1038/s41467-018-03931-4.

(15) Pensa, E.; Cortés, E.; Corthey, G.; Carro, P.; Vericat, C.; Fonticelli, M. H.; Benítez, G.; Rubert, A. A.; Salvarezza, R. C. The Chemistry of the Sulfur-Gold Interface: In Search of a Unified Model. *Accounts of Chemical Research* **2012**, *45* (8), 1183-1192. DOI: 10.1021/ar200260p.

(16) Mirkin, C. A.; Letsinger, R. L.; Mucic, R. C.; Storhoff, J. J. A DNA-based method for rationally assembling nanoparticles into macroscopic materials. *Nature* **1996**, *382* (6592), 607-609. DOI: DOI 10.1038/382607a0.

(17) Liu, B.; Liu, J. Freezing Directed Construction of Bio/Nano Interfaces: Reagentless Conjugation, Denser Spherical Nucleic Acids, and Better Nanoflares. *Journal of the American Chemical Society* **2017**, *139* (28), 9471-9474., Article. DOI: 10.1021/jacs.7b04885.

(18) Zhang, X.; Servos, M. R.; Liu, J. W. Instantaneous and Quantitative Functionalization of Gold Nanoparticles with Thiolated DNA Using a pH-Assisted and Surfactant-Free Route. *Journal of the American Chemical Society* **2012**, *134* (17), 7266-7269. DOI: 10.1021/ja3014055.

(19) Hao, Y.; Li, Y. J.; Song, L.; Deng, Z. X. Flash Synthesis of Spherical Nucleic Acids with Record DNA Density. *Journal of the American Chemical Society* **2021**, *143* (8), 3065-3069. DOI: 10.1021/jacs.1c00568.

(20) Ding, S.; Yi, J.; Li, J.; Ren, B.; Wu, D.; Panneerselvam, R.; Tian, Z. Nanostructure-based plasmon-enhanced Raman spectroscopy for surface analysis of materials. *Nature Reviews Materials* **2016**, *1* (6), Review. DOI: 10.1038/natrevmats.2016.21.

(21) Heck, C.; Prinz, J.; Dathe, A.; Merk, V.; Stranik, O.; Fritzsche, W.; Kneipp, J.; Bald, I. Gold Nanolenses Self-Assembled by DNA Origami. *Acs Photonics* **2017**, *4* (5), 1123-1130, Article. DOI: 10.1021/acsphotonics.6b00946.

(22) Chen, X. Q.; Lisi, F.; Bakthavathsalam, P.; Longatte, G.; Hoque, S.; Tilley, R. D.; Gooding, J. J. Impact of the Coverage of Aptamers on a Nanoparticle on the Binding Equilibrium and Kinetics between Aptamer and Protein. *ACSes Sensors* **2021**, *6* (2), 538-545. DOI: 10.1021/acssensors.0c02212.

(23) Wang, R.; Zhang, Y.; Cai, J.; Cai, W.; Gao, T. Aptamer-Based Fluorescent Biosensors. *Current Medicinal Chemistry* **2011**, *18* (27), 4175-4184, Review.

(24) Jayasena, S. Aptamers: An emerging class of molecules that rival antibodies in diagnostics. *Clinical Chemistry* **1999**, *45* (9), 1628-1650., Article|Proceedings Paper.

(25) Liu, Y. Z.; Canoura, J.; Alkhamis, O.; Xiao, Y. Immobilization Strategies for Enhancing Sensitivity of Electrochemical Aptamer-Based Sensors. *Acs Applied Materials & Interfaces* **2021**, *13* (8), 9491-9499. DOI: 10.1021/acsami.0c20707.

(26) Sun, H. G.; Zu, Y. L. A Highlight of Recent Advances in Aptamer Technology and Its Application. *Molecules* **2015**, *20* (7), 11959-11980. DOI: 10.3390/molecules200711959.

(27) Deng, B.; Lin, Y. W.; Wang, C.; Li, F.; Wang, Z. X.; Zhang, H. Q.; Li, X. F.; Le, X. C. Aptamer binding assays for proteins: The thrombin example-A review. *Analytica Chimica Acta* **2014**, *837*, 1-15. DOI: 10.1016/j.aca.2014.04.055.

(28) Mairal, T.; Özalp, V. C.; Sánchez, P. L.; Mir, M.; Katakis, I.; O'Sullivan, C. K. Aptamers:: molecular tools for analytical applications. *Analytical and Bioanalytical Chemistry* **2008**, *390* (4), 989-1007. DOI: 10.1007/s00216-007-1346-4.

(29) Ni, S. J.; Zhuo, Z. J.; Pan, Y. F.; Yu, Y. Y.; Li, F. F.; Liu, J.; Wang, L. Y.; Wu, X. Q.; Li, D. J.; Wan, Y. Y.; et al. Recent Progress in Aptamer Discoveries and Modifications for Therapeutic Applications. *ACSes Applied Materials & Interfaces* **2021**, *13* (8), 9500-9519. DOI: 10.1021/acsami.0c05750.

(30) Zhang, J. L.; Huang, Y. H.; Sun, M.; Wan, S.; Yang, C. Y.; Song, Y. L. Recent Advances in Aptamer-Based Liquid Biopsy. *ACSes Applied Bio Materials* **2022**, *5* (5), 1954-1979. DOI: 10.1021/acsabm.1c01202.

(31) Tuerk, C.; Gold, L. Systematic Evolution of Ligands by Exponential Enrichment - Rna Ligands to Bacteriophage-T4 DNA-Polymerase. *Science* **1990**, *249* (4968), 505-510. DOI: DOI 10.1126/science.2200121.

(32) Ellington, A. D.; Szostak, J. W. Invitro Selection of Rna Molecules That Bind Specific Ligands. *Nature* **1990**, *346* (6287), 818-822. DOI: DOI 10.1038/346818a0.

(33) Darmostuk, M.; Rimpelova, S.; Gbelcova, H.; Ruml, T. Current approaches in SELEX: An update to aptamer selection technology. *Biotechnology Advances* **2015**, *33* (6), 1141-1161. DOI: 10.1016/j.biotechadv.2015.02.008.

(34) Komarova, N.; Kuznetsov, A. Inside the Black Box: What Makes SELEX Better? *Molecules* **2019**, *24* (19). DOI: ARTN 3598

10.3390/molecules24193598.

(35) Cai, S. D.; Yan, J. H.; Xiong, H. J.; Liu, Y. F.; Peng, D. M.; Liu, Z. B. Investigations on the interface of nucleic acid aptamers and binding targets. *Analyst* **2018**, *143* (22), 5317-5338. DOI: 10.1039/c8an01467a.

(36) Hermann, T. Strategies for the design of drugs targeting RNA and RNA - Protein complexes. *Angewandte Chemie-International Edition* **2000**, *39* (11), 1891-1905.

(37) Nagatoishi, S.; Isono, N.; Tsumoto, K.; Sugimoto, N. Loop residues of thrombin-binding DNA aptamer impact G-quadruplex stability and thrombin binding. *Biochimie* **2011**, *93* (8), 1231-1238. DOI: 10.1016/j.biochi.2011.03.013.

(38) Lang, P. T.; Brozell, S. R.; Mukherjee, S.; Pettersen, E. F.; Meng, E. C.; Thomas, V.; Rizzo, R. C.; Case, D. A.; James, T. L.; Kuntz, I. D. DOCK 6: Combining techniques to model RNA-small molecule complexes. *RNAna* **2009**, *15* (6), 1219-1230. DOI: 10.1261/rna.1563609.

(39) Chou, S. H.; Chin, K. H.; Wang, A. H. J. DNA aptamers as potential anti-HIV agents. *Trends in Biochemical Science* **2005**, *30* (5), 231-234. DOI: 10.1016/j.tibs.2005.03.004.

(40) Unruh, J. R.; Gokulrangan, G.; Lushington, G. H.; Johnson, C. K.; Wilson, G. S. Orientational dynamics and dye-DNA interactions in a dye-labeled DNA aptamer. *Biophysical Journal* **2005**, *88* (5), 3455-3465. DOI: 10.1529/biophysj.104.054148.

(41) Zhang, C. Z.; Wang, L.; Tu, Z.; Sun, X.; He, Q. H.; Lei, Z. J.; Xu, C. X.; Liu, Y.; Zhang, X.; Yang, J. Y.; et al. Organophosphorus pesticides detection using broad-specific single-stranded DNA based fluorescence polarization aptamer assay. *Biosensors & Bioelectronics* **2014**, *55*, 216-219. DOI: 10.1016/j.bios.2013.12.020.

(42) Huntington, J. A. Molecular recognition mechanisms of thrombin. *Journal of Thrombosis and Haemostasis* **2005**, *3* (8), 1861-1872. DOI: DOI 10.1111/j.1538-7836.2005.01363.x.

(43) Davie, E. W.; Kulman, J. D. An overview of the structure and function of thrombin. *Seminars in Thrombosis and Hemostasis* **2006**, *32*, 3-15. DOI: 10.1055/s-2006-939550.

(44) Bock, L. C.; Griffin, L. C.; Latham, J. A.; Vermaas, E. H.; Toole, J. J. Selection of Single-Stranded-DNA Molecules That Bind and Inhibit Human Thrombin. *Nature* **1992**, *355* (6360), 564-566. DOI: DOI 10.1038/355564a0.

(45) Pica, A.; Krauss, I. R.; Parente, V.; Tateishi-Karimata, H.; Nagatoishi, S.; Tsumoto, K.; Sugimoto, N.; Sica, F. Through-bond effects in the ternary complexes of thrombin sandwiched by two DNA aptamers. *Nucleic Acids Research* **2017**, *45* (1), 461-469. DOI: 10.1093/nar/gkw1113.

(46) Macaya, R. F.; Schultze, P.; Smith, F. W.; Roe, J. A.; Feigon, J. Thrombin-Binding DNA Aptamer Forms a Unimolecular Quadruplex Structure in Solution. *Proceedings of the National Academy of Sciences of the United States of America* **1993**, *90* (8), 3745-3749. DOI: DOI 10.1073/pnas.90.8.3745.

(47) Russo Krauss, I.; Merlino, A.; Randazzo, A.; Novellino, E.; Mazzarella, L.; Sica, F. High-resolution structures of two complexes between thrombin and thrombin-binding aptamer shed light on the role of cations in the aptamer inhibitory activity. *Nucleic Acids Research* **2012**, *40* (16), 8119-8128. DOI: 10.1093/nar/gks512.

(48) Tasset, D. M.; Kubik, M. F.; Steiner, W. Oligonucleotide inhibitors of human thrombin that bind distinct epitopes. *Journal of Molecular Biology* **1997**, *272* (5), 688-698. DOI: DOI 10.1006/jmbi.1997.1275.

(49) Bai, Y. L.; Li, Y. P.; Zhang, D. P.; Wang, H. L.; Zhao, Q. Enhancing the Affinity of Anti-Human α-Thrombin 15-mer DNA Aptamer and Anti-Immunoglobulin E Aptamer by PolyT Extension. *Analytical Chemistry* **2017**, *89* (17), 9467-9473. DOI: 10.1021/acs.analchem.7b02313.

(50) Tian, L.; Heyduk, T. Bivalent Ligands with Long Nanometer-Scale Flexible Linkers. *Biochemistry-Us* **2009**, *48* (2), 264-275. DOI: 10.1021/bi801630b.

(51) Watkins, H. M.; Simon, A. J.; Ricci, F.; Plaxco, K. W. Effects of Crowding on the Stability of a Surface-Tethered Biopolymer: An Experimental Study of Folding in a Highly Crowded Regime. *Journal of the American Chemical Society* **2014**, *136* (25), 8923-8927. DOI: 10.1021/ja411486g.

(52) Minton, A. P. Excluded Volume as a Determinant of Protein-Structure and Stability. *Biophysical Journal* **1980**, *32* (1), 77-79. DOI: Doi 10.1016/S0006-3495(80)84917-4.

(53) Minton, A. P. Effect of a concentrated "inert" macromolecular cosolute on the stability of a globular protein with respect to denaturation by heat and by chaotropes: A statistical-thermodynamical model. *Biophysical Journal* **2000**, *78* (1), 101-109. DOI: Doi 10.1016/S0006-3495(00)76576-3.

(54) Southern, E. M.; Casegreen, S. C.; Elder, J. K.; Johnson, M.; Mir, K. U.; Wang, L.; Williams, J. C. Arrays of Complementary Oligonucleotides for Analyzing the Hybridization Behavior of Nucleic-Acids. *Nucleic Acids Research* **1994**, *22* (8), 1368-1373. DOI: DOI 10.1093/nar/22.8.1368.

(55) Schena, M.; Shalon, D.; Davis, R. W.; Brown, P. O. Quantitative Monitoring of Gene-Expression Patterns with a Complementary-DNA Microarray. *Science* **1995**, *270* (5235), 467-470. DOI: DOI 10.1126/science.270.5235.467.

(56) Fodor, S. P. A.; Read, J. L.; Pirrung, M. C.; Stryer, L.; Lu, A. T.; Solas, D. Light-Directed, Spatially Addressable Parallel Chemical Synthesis. *Science* **1991**, *251* (4995), 767-773. DOI: DOI 10.1126/science.1990438.

(57) Millan, K. M.; Mikkelsen, S. R. Sequence-Selective Biosensor for DNA-Based on Electroactive Hybridization Indicators. *Analytical Chemistry* **1993**, *65* (17), 2317-2323. DOI: DOI 10.1021/ac00065a025.

(58) Rao, A. N.; Grainger, D. W. Biophysical properties of nucleic acids at surfaces relevant to microarray performance. *Biomaterials Science-Uk* **2014**, *2* (4), 436-471. DOI: 10.1039/c3bm60181a.

(59) Levicky, R.; Herne, T. M.; Tarlov, M. J.; Satija, S. K. Using self-assembly to control the structure of DNA monolayers on gold: A neutron reflectivity study. *Journal of the American Chemical Society* **1998**, *120* (38), 9787-9792. DOI: DOI 10.1021/ja981897r.

(60) Steel, A. B.; Herne, T. M.; Tarlov, M. J. Electrochemical quantitation of DNA immobilized on gold. *Analytical Chemistry* **1998**, *70* (22), 4670-4677. DOI: DOI 10.1021/ac980037q.

(61) Shchepinov, M. S.; CaseGreen, S. C.; Southern, E. M. Steric factors influencing hybridisation of nucleic acids to oligonucleotide arrays. *Nucleic Acids Research* **1997**, *25* (6), 1155-1161. DOI: DOI 10.1093/nar/25.6.1155.

(62) Peterson, A. W.; Heaton, R. J.; Georgiadis, R. M. The effect of surface probe density on DNA hybridization. *Nucleic Acids Research* **2001**, *29* (24), 5163-5168. DOI: DOI 10.1093/nar/29.24.5163.

(63) Gong, P.; Levicky, R. DNA surface hybridization regimes. *Proceedings of the National Academy of Sciences of the United States of America* **2008**, *105* (14), 5301-5306. DOI: 10.1073/pnas.0709416105.

(64) Freire, E.; Mayorga, O. L.; Straume, M. Isothermal Titration Calorimetry. *Analytical Chemistry* **1990**, *62* (18), A950-A959. DOI: DOI 10.1021/ac00217a002.

(65) Ladbury, J. E.; Chowdhry, B. Z. Sensing the heat: The application of isothermal titration calorimetry to thermodynamic studies of biomolecular interactions. *Chemical Biology* **1996**, *3* (10), 791-801. DOI: Doi 10.1016/S1074-5521(96)90063-0.

(66) Song, C. C.; Zhang, S. C.; Huang, H. Choosing a suitable method for the identification of replication origins in microbial genomes. *Frontiers in Microbiology* **2015**, *6*. DOI: ARTN 1049

10.3389/fmicb.2015.01049.

(67) Sun, J. F.; Guo, A. T.; Zhang, Z. Y.; Guo, L.; Xie, J. W. A Conjugated Aptamer-Gold Nanoparticle Fluorescent Probe for Highly Sensitive Detection of rHuEPO-α. *Sensors-Basel* **2011**, *11* (11), 10490-10501. DOI: 10.3390/s111110490.

(68) Ricci, F.; Lai, R. Y.; Heeger, A. J.; Plaxco, K. W.; Sumner, J. J. Effect of molecular crowding on the response of an electrochemical DNA sensor. *Langmuir* **2007**, *23* (12), 6827-6834. DOI: 10.1021/la700328r.

(69) Kang, D.; Zuo, X.; Yang, R.; Xia, F.; Plaxco, K.; White, R. Comparing the Properties of Electrochemical-Based DNA Sensors Employing Different Redox Tags. *Analytical Chemistry* **2009**, *81* (21), 9109-9113, Article. DOI: 10.1021/ac901811n..

(70) Fong, L. K.; Wang, Z. W.; Schatz, G. C.; Luijten, E.; Mirkin, C. A. The Role of Structural Enthalpy in Spherical Nucleic Acid Hybridization. *Journal of the American Chemical Society* **2018**, *140* (20), 6226-6230. DOI: 10.1021/jacs.8b03459.

(71) De, M.; You, C. C.; Srivastava, S.; Rotello, V. M. Biomimetic interactions of proteins with functionalized nanoparticles: A thermodynamic study. *Journal of the American Chemical Society* **2007**, *129* (35), 10747-10753. DOI: 10.1021/ja071642q.

# Chapter 2: Enabling ITC for Binding Studies Featuring Immobilized Aptamers on Gold Nanoparticles and Protein Targets

## 2.1 Introduction

Isothermal titration calorimetry (ITC) is a label free approach for studying two interacting biomolecules.[1, 2] ITC incrementally introduces two binding partners and extrapolates the magnitude of heat evolved that is resultant from binding partner association. A complete thermodynamic profile can be extrapolated in a single ITC experiment - providing insight into the driving forces of biomolecular interactions. Biomolecules that interact specifically with a target molecule are of particular interest for applied research applications such as sensing or bioimaging.[3-6]

Studies that characterize biomolecular interactions commonly use ITC to generate a thermodynamic profile in a dilute solution. However, many applied research fields require immobilizing one binding partner on a solid support.[7, 8] Once immobilized, the local environment of the molecular recognition element greatly differs from the dilute solution.[9, 10] Crowding between immobilized neighbors results in localized electrostatic repulsions and steric hinderance, which is likely to affect binding. Therefore, the propensities of immobilized molecules to interact with targets cannot be readily extrapolated from behavior in the dilute solution.

To the best of our knowledge, ITC has not been used to study interactions between aptamer conjugated gold nanoparticles and protein targets. Several hurdles represent barriers to experimental success and leave an open question of whether it is possible to incorporate ITC into immobilized aptamer binding studies with protein targets. Potential difficulties include the requirement of large concentrations of aptamers to produce heat signatures detectable using calorimetry, the need to precisely control reaction stoichiometry, matching buffer components between the titrant and titrate, and countering non-specific adsorption between target proteins and exposed gold nanoparticle surfaces. Overcoming these challenges may enable ITC for immobilized aptamer studies, affording insight into how aptamer immobilization affects target binding.

Here we explored how barriers for immobilized aptamer interactions with target proteins can be mitigated, enabling ITC to study the target recognition by surface immobilized aptamers. We dissected the components of the ITC experimental set-up to maximize the signal produced by target binding. We also provide insight into the limitations of this approach and discuss the applicability to similar systems involving immobilized aptamers.

Future studies may utilize this tool for thermodynamic characterization of the target binding process of a variety of aptamers, which can aid in more rational design of materials and devices that incorporate immobilized aptamers.

## 2.2 Materials

Potassium chloride (KCl), magnesium chloride ($MgCl_2$), sodium citrate dihydrate, tris borate EDTA (TBE), polyethylene glycol (PEG) 8000, sodium chloride (NaCl), tris acetate, and tris

(2-carboxyethyl) phosphine hydrochloride (TCEP) were purchased from Fisher Scientific. Sodium dodecyl sulfate (SDS) and dithiothreitol (DTT) were purchased from Sigma-Aldrich. Butanol was purchased from Spectrum Chemical Manufacturing Group. Calcium chloride hexahydrate ($CaCl_2$) was purchased from Acros Organics. Thiol-OEG was purchased from Prochimia. All chemicals listed above were used without further purification or modifications. α-Thrombin (thrombin) was purchased from BSP Biosciences. Thiolated DNA aptamers were purchased from Integrated DNA Technologies (IDT). 10 nm gold nanoparticles were purchased from Ted Pella in Redding, CA. 3 kDa Amicon columns were purchased from Millipore Sigma. NAP-5 columns were purchased from Cytiva.

## 2.3 Results and Discussions

Several hurdles make using ITC to study interactions between immobilized aptamers and protein targets challenging. The root of these hurdles is often the magnitude of signal produced from interacting biomolecules. Interacting biomolecules tend to have small enthalpic changes upon binding, meaning that reactant concentrations need to be increased to produce detectable signals.[11-13] Of a similar concern is minimizing experimental noise as to have less ambiguity from the collected signal. Recognizing the root causes, we outlined an experimental plan that could counter the limitations of ITC in studying such interactions.

Fundamental to the success of these experiments is the preparation of materials and understanding the roles of loading density, buffer matching, and passivating agents to counter non-specific adsorption, which determine the magnitude of heat signals and the experimental noise. Below, we discuss in detail how these barriers were approached and overcome to enable ITC for study of immobilized aptamers on gold nanoparticles with protein targets.

### 2.3.1 Reaction stoichiometry

Over the past three decades, a handful of strategies have been developed to immobilize thiolated DNA oligonucleotides to gold nanoparticle surfaces. While all the strategies achieve the same goal, the loading density can vary considerably. Because it is the immobilized aptamer that interacts with the target protein, quantifying the loading density is a crucial step in experimental setup to arrive at the proper stoichiometric ratios between titrant and titrate. Furthermore, the stoichiometry of the reaction between immobilized aptamers and thrombin is directly tied to the amount of reactants required. ITC requires knowledge regarding the concentration of reactants so analysis software can be used to calculate binding affinity and thermodynamic profiles based on the reaction's heat signatures and ratio of titrant to titrate per a given injection. The immobilized aptamer strands bind to the thrombin target, thus quantifying the number of aptamer strands per particle is an essential step in experimental planning.

We employed three different functionalization strategies to immobilize DNA aptamers to the gold nanoparticle surface.[14-16] While many studies rely on fluorescent tags (ref), which may alter the loading density in ways that are difficult to predict, we used a label free approach to quantifying immobilized aptamers to obtain more reliable measurements of the loading density

for nanoparticles used for ITC experimentation. In the salt aging method, NaCl is slowly, incrementally added to a reaction containing gold nanoparticles and thiolated DNA aptamers. Because NaCl is used to screen electrostatic repulsions between neighboring immobilized aptamers, the aptamer loading density is expected to increase as the NaCl concentration inside the reaction vessel increases. Hence the loading density can be tuned to some extent by the final NaCl concentration. The freezing method uses the principle of excluded volume to drive aptamer immobilization. Ice crystals force aptamers and nanoparticles into close proximity where thiol-gold interactions can immobilize aptamers. The butanol dehydration method operates under a similar principle but uses butanol to remove excess water molecules from the gold nanoparticle / aptamer matrix. As the effective concentration of aptamers and nanoparticles rises, thiol-gold interactions anchor aptamers to the gold nanoparticles.

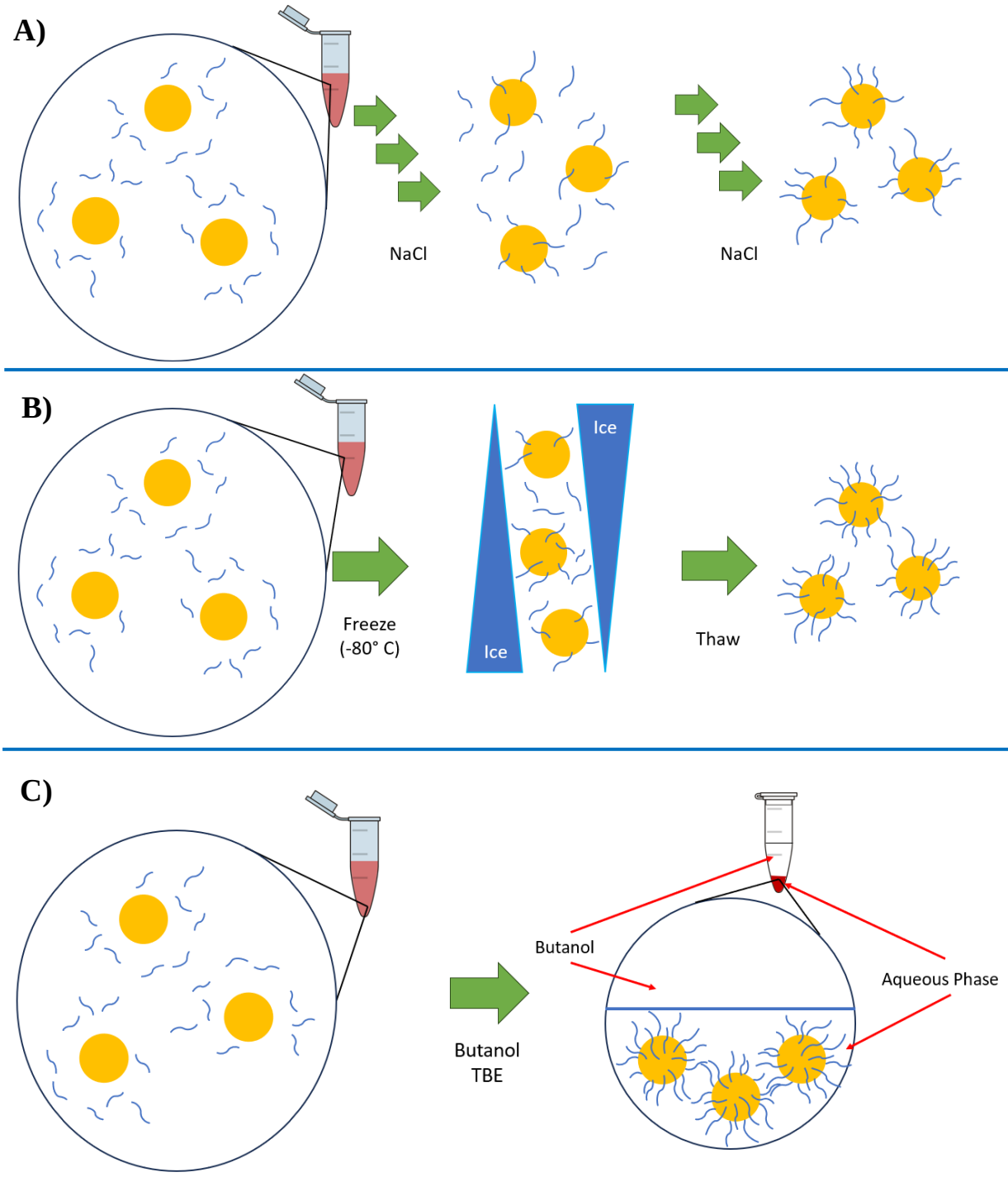


Figure 2.1: Schematics of various strategies to immobilize aptamers on gold nanoparticle surfaces. A) salt aging method B) freezing method C) butanol dehydration method, consisting of butanol phase (blank) on top and aqueous phase containing gold nanoparticles and excess DNA ligands on bottom. 300:1 ratio of aptamers to gold nanoparticles were used in all reactions. Following each functionalization protocol, thiol-OEG was added in a 300:1 ratio with respect to gold nanoparticles and allowed to react for 18 hours to passivate the exposed gold surface before purification.

As discussed in Chapter 1, immobilized DNA aptamers provide stability to colloidal gold nanoparticles. The negative charge of a DNA polymer grants electrostatic stabilization from the negatively charged phosphate backbone while also creating a ligand shell around each nanoparticle, which presents a steric barrier toward aggregation.[17] During the immobilization process, thiolated DNA aptamers are present in excess to favor immobilization over destabilizing van der Waals forces that irreversibly aggregate unfunctionalized gold nanoparticles. However, excess aptamers in solution must be removed to ensure accurate quantification of the loading density. Solutions with weak ionic strength (*i.e.*, resuspending in nanopure water) require ultra-centrifugation (99 k RCF) to pellet 10 nm gold nanoparticles at reasonable time scales (< 55 minutes) and remove unbound aptamers from the supernatant. While ionic strength does allow 10 nm gold nanoparticles to pellet at slower centrifugation speeds, we found that speeds slower than 25 k RCF failed to produce a compact pellet of functionalized 10 nm gold nanoparticles after 55 minutes in a 0.171 mol / L ionic strength solution.

After a homogeneous solution of aptamer functionalized gold nanoparticles is obtained, immobilized aptamers can be liberated from the gold nanoparticle surface and quantified by UV-Vis spectroscopy to determine the average loading density on each gold nanoparticle. As DTT strongly interacts with gold,[18, 19] the addition of DTT in excess is a common technique for removing immobilized thiolated DNA oligonucleotides from gold nanoparticles.[20] After the removal of the supernatant (containing DTT and thiolated DNA oligonucleotides), oligonucleotides can be purified from excess DTT through size exclusion chromatography. This important step ensures the absorbance signal at 260 nm is generated by thiolated DNA oligonucleotides instead of contributions from DTT. The extinction coefficient of 265,000 $M^{-1}$ $cm^{-1}$ was provided by the DNA oligonucleotide manufacturer and used to quantify DNA at 260 nm.

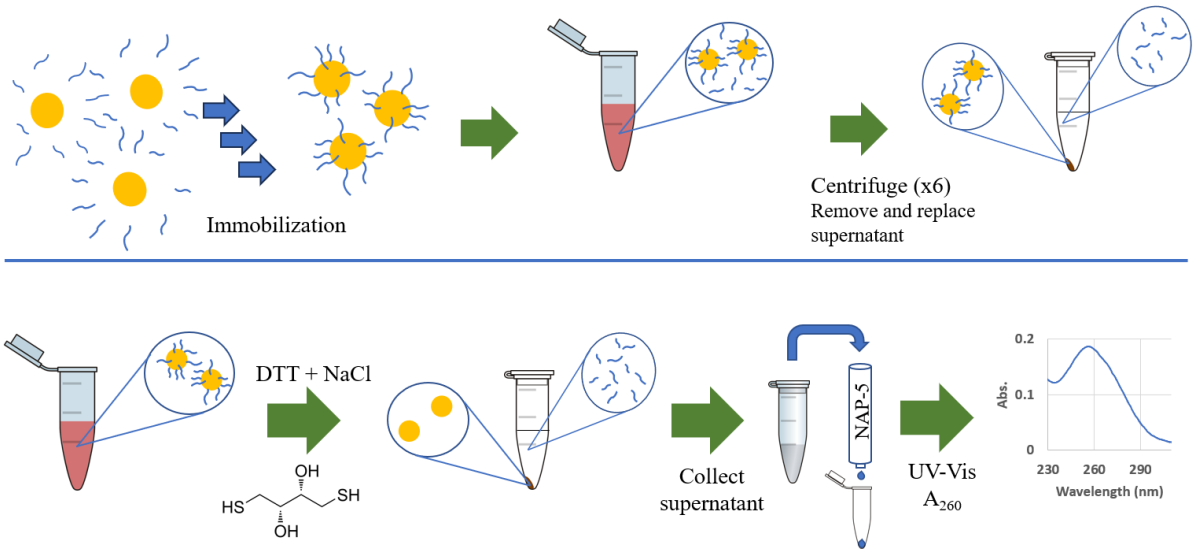


Figure 2.2: Schematics of the label free quantification process used to characterize immobilized aptamer loading density. Salt aging, freeze method, and butanol dehydration were used for aptamer immobilization.

A wide range of aptamer loading densities were achieved by the three different immobilization techniques. Notably, the freeze and butanol dehydration methods produced very high aptamer loading densities. A modular approach with the salt aging technique enabled tailoring the loading density based on the final salt concentration.

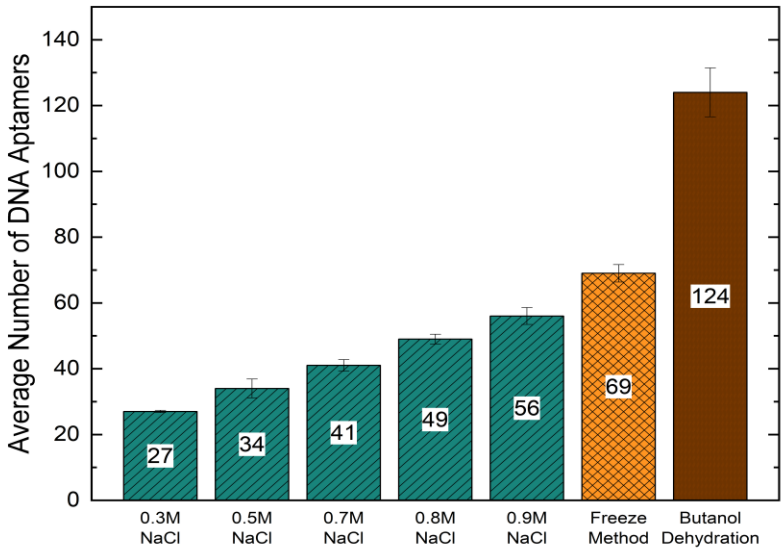


Figure 2.3: Average number of immobilized aptamers for nanoparticles prepared using three different methods, salt aging (0.3 M to 0.9 M NaCl), freeze, and butanol dehydration.

A better understanding of the reactant demand for ITC studies featuring immobilized aptamers on gold nanoparticles is seen after the loading densities are quantified. Assuming 225 µL of functionalized gold nanoparticles are required for triplicate ITC trials and a blank for background subtraction, Table 2.1 illustrates the volume of gold nanoparticles required to have a 10-fold aptamer concentration excess of titrant with respect to titrate.

Table 2.1: Volumes of stock (8.2 nM) gold nanoparticles required for triplicate ITC trials. Final volume of functionalized gold nanoparticles is 225 µL. Final aptamer concentration is 50 µM.

| ***Functionalization Method*** | **Number of immobilized aptamers** | **Final [AuNP] for ITC trial (µM)** | **Volume of 10 nm AuNP stock solution (mL)** |
|---|---|---|---|
| *0.3M NaCl* | 27 | 1.85 | 50.81 |
| *0.5M NaCl* | 34 | 1.47 | 40.35 |
| *0.7M NaCl* | 41 | 1.22 | 33.46 |
| *0.8M NaCl* | 49 | 1.02 | 28.00 |
| *0.9M NaCl* | 56 | 0.89 | 24.50 |
| *Freeze Method* | 69 | 0.72 | 19.88 |
| *Butanol Dehydration* | 124 | 0.40 | 11.06 |

Figure 2.4 reveals a potential barrier toward ITC characterization of target binding of aptamer functionalized nanoparticles. Although larger gold nanoparticles can accommodate larger aptamer loading densities, the low stock concentrations of these nanoparticles require more starting materials when planning an ITC experiment. *E.g.*, to study the binding to aptamers on 50 nm gold nanoparticles at a common loading density, $10^{13}/cm^2$, ~200 ml of the stock nanoparticle solution is needed for just a single data point. Synthesizing gold nanoparticles in house may be a cost-effective strategy for designing ITC experiments with larger gold nanoparticles, but this approach could have other barriers such as nanoparticle size homogeneity, costs of starting materials, and the requirement of larger batches of thiolated DNA aptamers.

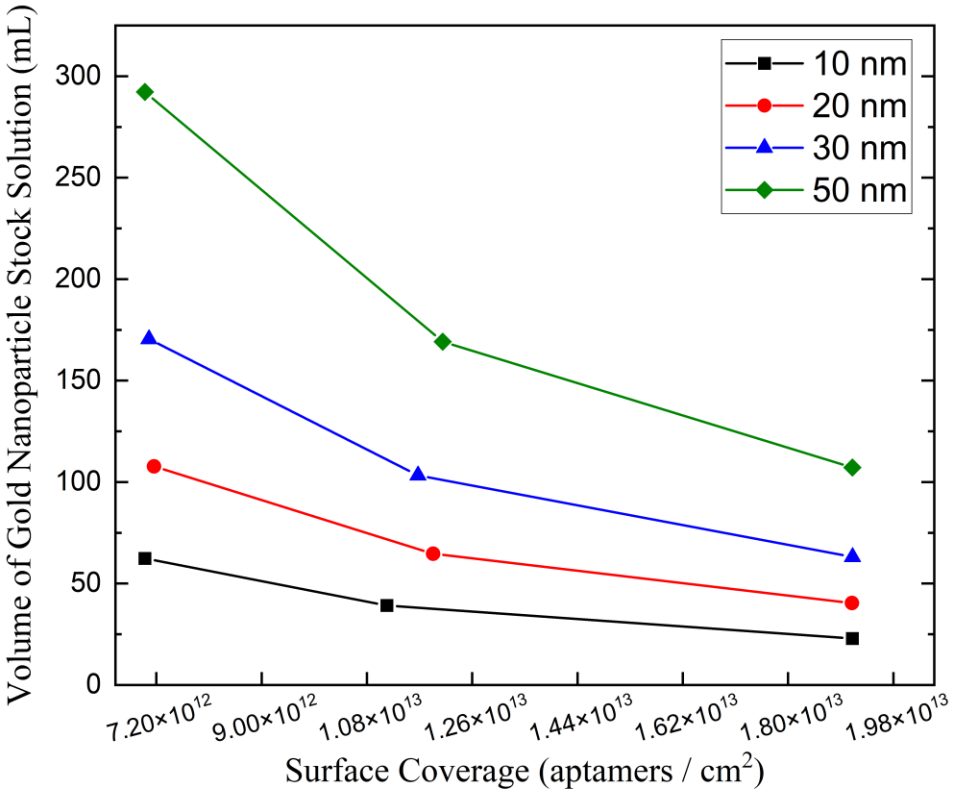


Figure 2.4: Estimated volumes of stock gold nanoparticles required for ITC experiments assuming a final aptamer concentration of 50 µM and final volume of 225 µL. Stock solution concentrations used were provided by Ted Pella: 1.16 nM, 0.33 nM, and 0.07 nM for 20 nm, 30 nm, and 50 nm gold nanoparticles, respectively.

Table 2.2: Aptamer strands per gold nanoparticle given surface coverage and nanoparticle size.

| Gold Nanoparticle Size (nm) | Surface Coverage (strands / $cm^2$) | Strands / gold nanoparticle |
|---|---|---|
| **10** | $7.00 \times 10^{12}$ | 22 |
| | $1.11 \times 10^{13}$ | 35 |
| | $1.91 \times 10^{13}$ | 60 |
| **20** | $7.16 \times 10^{12}$ | 90 |
| | $1.19 \times 10^{13}$ | 150 |
| | $1.91 \times 10^{13}$ | 240 |
| **30** | $7.07 \times 10^{12}$ | 200 |
| | $1.17 \times 10^{13}$ | 330 |
| | $1.91 \times 10^{13}$ | 540 |
| **50** | $7.00 \times 10^{12}$ | 550 |
| | $1.21 \times 10^{13}$ | 950 |
| | $1.91 \times 10^{13}$ | 1,500 |

### 2.3.2 Titrant and titrate buffer matching

Sizeable heat artifacts are often introduced when ITC titrant and titrate do not have matching buffers.[21] The mixing of buffers can have a wide range of heat signatures, all of which lead to ambiguity in the signal generation and potentially faulty binding analysis. It is the best practice to match buffers of both species in the ITC experimental design to have a clear origin of the signal.

Consider the two binding isotherms and integrated heat plots in figure 2.5. The top plots feature 15mer TBA titrated into thrombin residing in the sample cell. The heat plot paints a clear picture of target binding and reaches saturation after sufficient titrant injections. However, the bottom plots, featuring a buffer mismatch between 15mer TBA and thrombin, fail to paint a clear picture of target binding. The binding isotherm fails to reach saturation because heat artifacts resultant from buffer dilutions are present. This also muddies the integrated heat plot, where target binding is not obvious.

There are practical difficulties in ensuring that titrant and titrate buffers have identical buffer composition. Thrombin that was purchased from BPS Bioscience arrived in a buffer solution (referred to as BPS buffer) containing 50 mM sodium citrate pH 6.5, 200 mM NaCl, and 0.1% PEG 8000. However, numerous studies have demonstrated the requirement of potassium ion to stabilize the g-quadruplex secondary aptamer structure for target binding to take place.[22-24] As such, it was necessary to resuspend thrombin in a buffer appropriate for target binding with 15mer TBA.

We used a freeze-drying strategy to resuspend thrombin in a buffer solution that would enable target binding. 92 µL of 3.55 mg/mL α-thrombin was frozen in a -80º C freezer and subsequently freeze-dried using a Labconco freeze dryer at -80º C and 0.2 mbar for several hours. Once the freeze-drying process was completed, freeze dried thrombin and buffer components were resuspended in 1,606 µL of thrombin binding buffer (TBB), which consists of 20 mM tris acetate pH 7.4, 140 mM NaCl, 5 mM KCl, 1 mM $MgCl_2$, and 1 mM $CaCl_2$. The TBB was the buffer used when 15mer TBA was discovered and commonly used for TBA / thrombin binding studies.[12, 22, 25, 26] The final concentration of thrombin was 5.5 µM. Samples were aliquoted and frozen until use to best prevent denaturation. Of important note is the ratio of the thrombin stock buffer solution and the TBB. This ratio was used to match the buffer components between titrant and titrate. As such, we freeze dried 20 mL of BPS buffer and resuspended it into 349mL of TBB. As gold nanoparticles were functionalized and purified for ITC analysis, this new conjugation buffer (CB), consisting of BPS and TBB in a volumetric ratio of 0.0573, was used to replace the removed supernatant after each centrifuge spin.

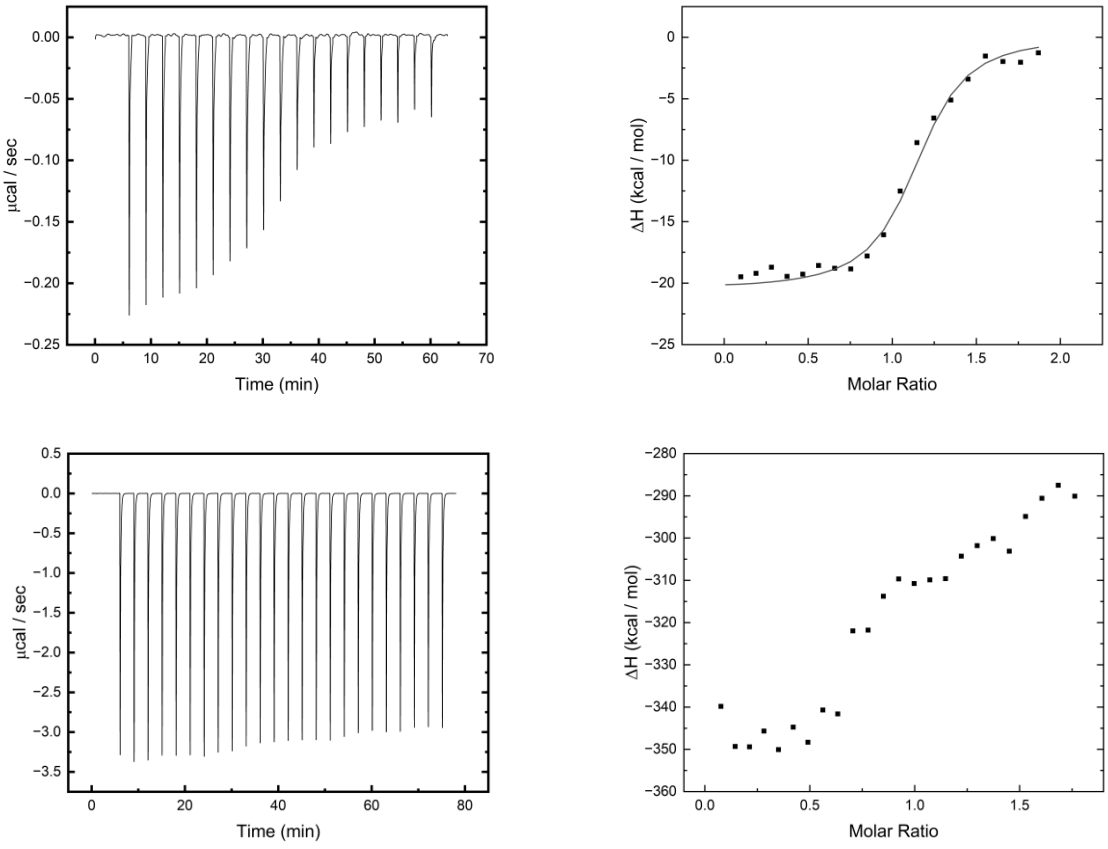


Figure 2.5: Binding isotherm and integrated heat plots of 15mer TBA and thrombin highlighting heat artifacts from mismatching buffers. Top plots consist of 15mer TBA and thrombin in matching CBs. Bottom plot has 15mer TBA in TBB and thrombin in CB. In both plots, concentration of 15mer TBA is 50 µM and concentration of thrombin is 5.5 µM.

### 2.3.3 Countering non-specific adsorption

Non-specific adsorption between thrombin and gold nanoparticle surfaces can cause heat signatures that do not originate from aptamer binding to the target. In biosensing, this can lead to false positives and pose a challenge to reproducibility.[27, 28] When gold nanoparticles are incorporated into the ITC experimental setup, an interface with which the thrombin target can interact must be accounted for to correctly identify the signal and characterize the thermodynamic profiles of binding partners.

We functionalized 15mer TBA to 10 nm gold nanoparticles using the salt aging method until the final salt concentration was 0.3 M NaCl. After gold nanoparticles were functionalized with DNA aptamers, thiolated oligoethylene glycol (thiol OEG) was added in a 300:1 ratio with respect to gold nanoparticles to backfill the bare gold nanoparticle surface regions. Thiol OEG has been used in several studies for passivating gold surfaces.[17, 28, 29] Immobilized aptamers on gold nanoparticles were loaded into the ITC syringe and titrated into the sample cell containing thrombin after purification and stoichiometric adjustment. Figure 2.6A shows the binding isotherms and integrated heat plots for 15mer TBA functionalized gold nanoparticles backfilled with thiol-OEG to prevent non-specific adsorption. The plots paint a clear picture of target binding while the negative control experiment (figure 2.6B) featuring 10 nm gold nanoparticles functionalized with CoV-1C-RBD aptamer, which recognizes SARS-CoV-2 spike protein and backfilled with thiol-OEG does not exhibit binding behavior or produce sizable heat signatures.[30] CoV-1C-RBD functionalized gold nanoparticles were titrated into a blank solution containing CB. The evolved heat is similar to that of the experimental trial containing thrombin. While there is a small difference between the binding isotherms, the blank experiment suggests that the evolved heat mainly originates from gold nanoparticle dilution, suggesting that contributions from non-specific adsorption between thrombin and gold nanoparticle surfaces are minimal. The blank experiments (figure 2.6 C&D) also confirm that the heat signature from 15mer TBA functionalized gold nanoparticles titrated into thrombin (figure 2.6A) is caused by specific recognition. Differences in heat signatures from blank experimental trials is low (~0.025 µcal / sec) but likely attributed to differences in gold nanoparticle concentrations in the syringe (concentration of gold nanoparticles for figure 2.6C is 1.85 µM, concentration of gold nanoparticles for figure 2.6D is 1.3 µM).

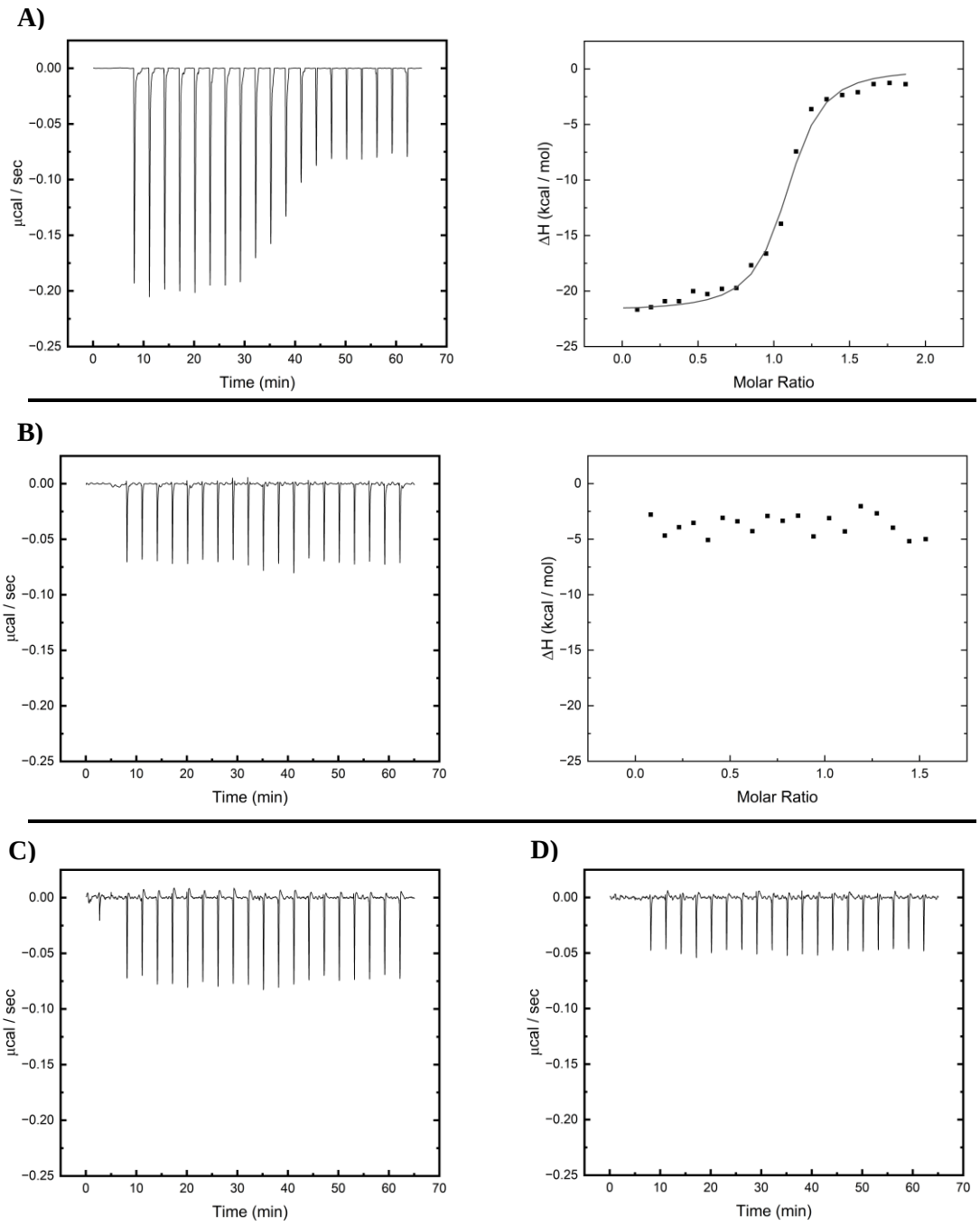


Figure 2.6: Binding isotherms and integrated heat plots of **A)** 0.3 M NaCl 15mer TBA functionalized gold nanoparticles titrated into thrombin – concentration of 15mer TBA is 50 µM, concentration of thrombin is 5.5 µM. **B)** CoV-1C-RBD aptamer functionalized gold nanoparticles titrated into thrombin – concentration of CoV-1C-RBD aptamer is 41 µM, concentration of thrombin is 5.5 µM. **C)** 0.3 M NaCl 15mer TBA functionalized gold nanoparticles titrated into blank buffer, **D)** CoV-1C-RBD aptamer functionalized gold nanoparticles titrated into blank buffer.

The binding isotherm and integrated heat plots of immobilized 15mer TBA on 10 nm gold nanoparticles demonstrate a novel application to ITC studies – thermodynamic characterization of binding interactions between immobilized 15mer TBA and target proteins in solution. The thermodynamic profile is compared to homogeneous 15mer TBA in Table 3. While there are a few notable differences, a thorough discussion of how the loading density affects target binding between immobilized 15mer TBA and target thrombin is presented in Chapter 3.

Table 2.3: Thermodynamic profiles of replicate trials of ITC experiments containing 15mer TBA functionalized gold nanoparticles, homogeneous 15mer TBA, and CoV-1C-RBD aptamer functionalized gold nanoparticles.

| | Strands / particle | Loading Density (strands / $cm^2$) | [Aptamer] (μM) | [Thrombin] (μM) | ΔH (kcal / mol) | -T ΔS (kcal / mol) | ΔG (kcal / mol) | Kd (nM) |
|---|---|---|---|---|---|---|---|---|
| **0.3M NaCl Aged** | 27 | $8.60 \times 10^{12}$ | 50 | 5.5 | -19.5 | 9.45 | -10 | 45.6 |
| | | | 50 | 5.5 | -20.2 | 9.52 | -9.86 | 48 |
| | | | 50 | 5.5 | -18.4 | 8.14 | -10.3 | 30.9 |
| **Free 15mer TBA** | N/A | N/A | 50 | 5.5 | -20.5 | 11 | -9.52 | 106 |
| | | | 50 | 5.5 | -22.3 | 12.8 | -9.47 | 115 |
| | | | 50 | 5.5 | -20.4 | 10.8 | -9.59 | 93 |
| **CoV-RBD-1C Aptamer fxn AuNP aged to 0.5M NaCl** | 31 | $8.80 \times 10^{12}$ | 41 | 5.5 | - | - | - | - |
| | | | 41 | 5.5 | - | - | - | - |
| | | | 41 | 5.5 | - | - | - | - |

## 2.4 Conclusion

ITC is a powerful tool in characterizing binding interactions between aptamers and target proteins. With precise knowledge of titrant and titrate concentrations, ITC can produce a complete thermodynamic profile between binding partners and elucidation of reaction mechanisms. However, ITC has traditionally been limited to interactions that take place in a solution. Understanding how immobilized aptamers on nanoparticle surfaces affect interactions with target proteins would help researchers optimize and determine how to achieve target binding.

Here we have highlighted several hurdles to nanoparticle incorporation into ITC experimental designs and illustrate how these barriers can be overcome. In doing so, we have opened the door to ITC characterization of nanomaterials featuring immobilized aptamers. We used 15mer TBA and thrombin to illustrate strategies for appropriate reaction stoichiometry, the importance of matching titrant and titrate buffers, and backfill with a passivating agent to prevent non-specific adsorption. Overcoming these barriers resulted in a successful characterization of binding between target thrombin and immobilized 15mer TBA on 10 nm gold nanoparticles. These ITC experimental designs can be adapted to various aptamer / target systems to thermodynamically characterize the binding process, demonstrating the versatility of ITC.

While ITC has many advantages, a few noteworthy limitations were also noted. ITC is reactant intensive because many biomolecular interactions do not produce large heat signatures. The concentration of immobilized aptamers is directly related to the concentration of nanoparticles, thus nanoparticles with low stock concentrations could require an impractical amount of starting materials. Additionally, because ~~different~~ unique aptamer sequences interact with the nanoparticles differently, the loading density is difficult to predict ~~a priori~~without investigation. While a range of loading densities can be generalized based on the surface functionalization approach, ITC requires precise knowledge of the number of binding ~~Therefore~~sites. Therefore, the loading density must be characterized to ensure proper stoichiometry.

## 2.5 References


(1) Freire, E.; Mayorga, O. L.; Straume, M. Isothermal Titration Calorimetry. *Analytical Chemistry* **1990**, *62* (18), A950-A959. DOI: DOI 10.1021/ac00217a002.

(2) Ladbury, J. E.; Chowdhry, B. Z. Sensing the heat: The application of isothermal titration calorimetry to thermodynamic studies of biomolecular interactions. *Chemical Biology* **1996**, *3* (10), 791-801. DOI: Doi 10.1016/S1074-5521(96)90063-0.

(3) Li, Y. J.; Wang, X. D.; Zhang, Y. L.; Nie, G. J. Recent Advances in Nanomaterials with Inherent Optical and Magnetic Properties for Bioimaging and Imaging-Guided Nucleic Acid Therapy. *Bioconjugate Chemistry* **2020**, *31* (5), 1234-1246. DOI: 10.1021/acs.bioconjchem.0c00126.

(4) Pica, A.; Krauss, I. R.; Parente, V.; Tateishi-Karimata, H.; Nagatoishi, S.; Tsumoto, K.; Sugimoto, N.; Sica, F. Through-bond effects in the ternary complexes of thrombin sandwiched by two DNA aptamers. *Nucleic Acids Research* **2017**, *45* (1), 461-469. DOI: 10.1093/nar/gkw1113.

(5) Sun, X.; Song, L.; Liu, N. A.; Shi, J. P.; Zhang, Y. Chromium-Doped Zinc Gallate Near-Infrared Persistent Luminescence Nanoparticles in Autofluorescence-Free Biosensing and Bioimaging: A Review. *ACSes Applied Nano Materials* **2021**, *4* (7), 6497-6514. DOI: 10.1021/acsanm.1c01115.

(6) Troisi, R.; Balasco, N.; Autiero, I.; Vitagliano, L.; Sica, F. Exosite Binding in Thrombin: A Global Structural/Dynamic Overview of Complexes with Aptamers and Other Ligands. *International Journal of Molecular Sciences* **2021**, *22* (19). DOI: ARTN 10803

10.3390/ijms221910803.

(7) Gu, Q. F.; Cao, H. H.; Zhang, Y. H.; Wang, H. Y.; Petrek, Z. J.; Shi, F. K.; Josephs, E. A.; Ye, T. Toward a Quantitative Relationship between Nanoscale Spatial Organization and Hybridization Kinetics of Surface Immobilized Hairpin DNA Probes. *ACSes Sensors* **2021**, *6* (2), 371-379. DOI: 10.1021/acssensors.0c01278.

(8) Southern, E. M.; Casegreen, S. C.; Elder, J. K.; Johnson, M.; Mir, K. U.; Wang, L.; Williams, J. C. Arrays of Complementary Oligonucleotides for Analyzing the Hybridization Behavior of Nucleic-Acids. *Nucleic Acids Research* **1994**, *22* (8), 1368-1373. DOI: DOI 10.1093/nar/22.8.1368.

(9) Minton, A. P. Excluded Volume as a Determinant of Protein-Structure and Stability. *Biophysical Journal* **1980**, *32* (1), 77-79. DOI: Doi 10.1016/S0006-3495(80)84917-4.

(10) Minton, A. P. Effect of a concentrated "inert" macromolecular cosolute on the stability of a globular protein with respect to denaturation by heat and by chaotropes: A statistical-thermodynamical model. *Biophysical Journal* **2000**, *78* (1), 101-109. DOI: Doi 10.1016/S0006-3495(00)76576-3.

(11) Lin, P. H.; Chen, R. H.; Lee, C. H.; Chang, Y.; Chen, C. S.; Chen, W. Y. Studies of the binding mechanism between aptamers and thrombin by circular dichroism, surface plasmon resonance and isothermal titration calorimetry. *Colloids and Surfaces B-Biointerfaces* **2011**, *88* (2), 552-558. DOI: 10.1016/j.colsurfb.2011.07.032.

(12) Nallagatla, S. R.; Heuberger, B.; Haque, A.; Switzer, C. Combinatorial Synthesis of Thrombin-Binding Aptamers Containing iso-Guanine. *J Comb Chem* **2009**, *11* (3), 364-369. DOI: 10.1021/cc800178m.

(13) Prozeller, D.; Morsbach, S.; Landfester, K. Isothermal titration calorimetry as a complementary method for investigating nanoparticle-protein interactions. *Nanoscale* **2019**, *11* (41), 19265-19273. DOI: 10.1039/c9nr05790k.

(14) Mirkin, C. A.; Letsinger, R. L.; Mucic, R. C.; Storhoff, J. J. A DNA-based method for rationally assembling nanoparticles into macroscopic materials. *Nature* **1996**, *382* (6592), 607-609. DOI: DOI 10.1038/382607a0.

(15) Liu, B.; Liu, J. Freezing Directed Construction of Bio/Nano Interfaces: Reagentless Conjugation, Denser Spherical Nucleic Acids, and Better Nanoflares. *Journal of the American Chemical Society* **2017**, *139* (28), 9471-9474, Article. DOI: 10.1021/jacs.7b04885..

(16) Hao, Y.; Li, Y. J.; Song, L.; Deng, Z. X. Flash Synthesis of Spherical Nucleic Acids with Record DNA Density. *Journal of the American Chemical Society* **2021**, *143* (8), 3065-3069. DOI: 10.1021/jacs.1c00568.

(17) Zhao, W. A.; Chiuman, W.; Lam, J. C. F.; McManus, S. A.; Chen, W.; Cui, Y. G.; Pelton, R.; Brook, M. A.; Li, Y. F. DNA aptamer folding on gold nanoparticles: From colloid chemistry to biosensors. *Journal of the American Chemical Society* **2008**, *130* (11), 3610-3618. DOI: 10.1021/ja710241b.

(18) Liang, P. P.; Canoura, J.; Yu, H. X.; Alkhamis, O.; Xiao, Y. Dithiothreitol-Regulated Coverage of Oligonucleotide-Modified Gold Nanoparticles To Achieve Optimized Biosensor Performance. *Acs Applied Materials & Interfaces* **2018**, *10* (4), 4233-4242. DOI: 10.1021/acsami.7b16914.

(19) Tsai, D. H.; Cho, T. J.; DelRio, F. W.; Gorham, J. M.; Zheng, J. W.; Tan, J. J.; Zachariah, M. R.; Hackley, V. A. Controlled Formation and Characterization of

Dithiothreitol-Conjugated Gold Nanoparticle Clusters. *Langmuir* **2014**, *30* (12), 3397-3405. DOI: 10.1021/la500044y.

(20) Hurst, S.; Lytton-Jean, A.; Mirkin, C. Maximizing DNA loading on a range of gold nanoparticle sizes. *Analytical Chemistry* **2006**, *78* (24), 8313-8318, Article. DOI: 10.1021/ac0613582..

(21) Archer, W. R.; Schulz, M. D. Isothermal titration calorimetry: practical approaches and current applications in soft matter. *Soft Matter* **2020**, *16* (38), 8760-8774. DOI: 10.1039/d0sm01345e.

(22) Macaya, R. F.; Schultze, P.; Smith, F. W.; Roe, J. A.; Feigon, J. Thrombin-Binding DNA Aptamer Forms a Unimolecular Quadruplex Structure in Solution. *Proceedings of the National Academy of Sciences of the United States of America* **1993**, *90* (8), 3745-3749. DOI: DOI 10.1073/pnas.90.8.3745.

(23) Padmanabhan, K.; Padmanabhan, K. P.; Ferrara, J. D.; Sadler, J. E.; Tulinsky, A. The Structure of Alpha-Thrombin Inhibited by a 15-Mer Single-Stranded-DNA Aptamer. *Journal of Biological Chemistry* **1993**, *268* (24), 17651-17654.

(24) Tasset, D. M.; Kubik, M. F.; Steiner, W. Oligonucleotide inhibitors of human thrombin that bind distinct epitopes. *Journal of Molecular Biology* **1997**, *272* (5), 688-698. DOI: DOI 10.1006/jmbi.1997.1275.

(25) Bock, L. C.; Griffin, L. C.; Latham, J. A.; Vermaas, E. H.; Toole, J. J. Selection of Single-Stranded-DNA Molecules That Bind and Inhibit Human Thrombin. *Nature* **1992**, *355* (6360), 564-566. DOI: DOI 10.1038/355564a0.

(26) Russo Krauss, I.; Merlino, A.; Randazzo, A.; Novellino, E.; Mazzarella, L.; Sica, F. High-resolution structures of two complexes between thrombin and thrombin-binding aptamer shed light on the role of cations in the aptamer inhibitory activity. *Nucleic Acids Research* **2012**, *40* (16), 8119-8128. DOI: 10.1093/nar/gks512.

(27) Desai, T.; Hansford, D.; Leoni, L.; Essenpreis, M.; Ferrari, M. Nanoporous anti-fouling silicon membranes for biosensor applications. *Biosensors & Bioelectronics* **2000**, *15* (9-10), 453-462, Article. DOI: 10.1016/S0956-5663(00)00088-9..

(28) Zhang, F.; Skoda, M. W. A.; Jacobs, R. M. J.; Zorn, S.; Martin, R. A.; Martin, C. M.; Clark, G. F.; Goerigk, G.; Schreiber, F. Gold nanoparticles decorated with oligo(ethylene glycol) thiols: Protein resistance and colloidal stability. *Journal of Physical Chemistry A* **2007**, *111* (49), 12229-12237. DOI: 10.1021/jp074293v.

(29) Zhao, W. T.; Hsing, I. M. Facile and rapid manipulation of DNA surface density on gold nanoparticles using mononucleotide-mediated conjugation. *Chemical Communications* **2010**, *46* (8), 1314-1316. ~~DOI: 10.1039/b920696e.~~

(30) Song, Y.; Song, J.; Wei, X.; Huang, M.; Sun, M.; Zhu, L.; Lin, B.; Shen, H.; Zhu, Z.; Yang, C. Discovery of Aptamers Targeting the Receptor-Binding Domain of the SARS-CoV-2 Spike Glycoprotein. *Analytical Chemistry* **2020**, *92* (14), 9895-9900~~, Article. DOI: 10.1021/acs.analchem.0c01394.~~.

# Chapter 3: Impact of Immobilized Aptamer Loading Density on Target Binding

## 3.1 Introduction

Aptamers are short DNA or RNA oligonucleotides that selectively bind to target molecules with high affinity and specificity.[1] A handful of unique attributes, such as durability in extreme environments, small size, and ease of chemical modification underscore aptamers as versatile and modular recognition elements for sensing platforms when compared to traditionally used antibodies.[2, 3] While some applications use aptamers in solution, many others immobilize aptamers on a nanomaterial.[4-6] Nanomaterials are choice components for sensor signal transduction due to rapid response times and high signal to noise ratios.[7-10] Conjugating aptamers to nanomaterials has the potential to greatly improve the reproducibility and sensitivity of many sensing platforms for point of care diagnostics, environmental monitoring, and food safety screening.[11-14]

Many sensing studies that incorporate aptamers as molecular recognition elements tend to focus on evaluating figures of merit such as limit of detection, reproducibility, and specificity.[15-20] While these metrics are valuable for evaluating sensor performance, a better understanding of target binding by these immobilized aptamers, one of the key processes that determine sensor performance, could help rationally improve sensor design and fabrication.

An important open question is how the local environment experienced by immobilized aptamers impacts their ability to recognize targets. Once immobilized, the effective concentration and local environment of aptamers are much different from those in a dilute solution. In this crowded environment, aptamers experience increased electrostatic repulsion and steric hindrance from neighboring aptamers as well as bound target analytes.[21, 22] As follows, the ability of the aptamer to recognize a target analyte cannot be extrapolated from behaviors in the dilute solution, where these interactions are negligible.

Indeed, numerous studies that investigated the hybridization of complementary DNA (cDNA) with immobilized DNA strands on flat surfaces showed that the binding affinity decreases upon increasing the DNA probe density, showcasing the significance of crowding effects on immobilized DNA probes.[23-25] However, non-covalent interactions between aptamers and target analytes are distinct from base-pairing interactions and thus, the impacts of surface density on target binding are likely to differ. Xiao *et al.* investigated the effect of surface crowding on target binding by aptamers immobilized on a flat surface.[6] A novel immobilization strategy that suppresses the local clustering of probe molecules was found to improve the signal gain and the limit of detection for a variety of aptamer-based biosensors, suggesting that steric hindrance and electrostatic repulsion between aptamers in close proximity may hinder target binding, similar to how surface crowding impacts DNA hybridization. To investigate the effects of aptamer crowding on gold nanoparticles, Gooding *et al.* measured the binding affinity and kinetics of the interferon gamma target on DNA aptamer conjugated gold nanoparticles using a fluorescent tag that reports the binding induced conformational changes of the aptamer probes.[4] They found that both the binding affinity and binding rate constant increased when the aptamer loading density was increased from 1.27 ×

$10^{11}$ strands / $cm^2$ to $3.42 \times 10^{12}$ strands/$cm^2$. This trend appears to contrast with the prevailing assumption that the target binding is hindered at higher DNA probe densities.[26-28] It is unclear whether this trend holds for other loading densities and other aptamers. Furthermore, while coupling signal generation to aptamer conformational changes upon target binding enables signal transduction, unambiguous interpretation of the fluorescence signal can be challenging: the increase in fluorescent signal may be caused by target binding, which can induce conformational changes, or the crowding effects, which can destabilize the nucleic acids secondary structures and cause signal increase even without enhancement in target binding.[29] Hence a label-free approach that can directly quantify binding affinity could eliminate such ambiguity. Moreover, the origin of this counter-intuitive crowding effect remains elusive due to a lack of comprehensive thermodynamic studies that could illuminate the mechanisms behind this effect.

Here we use isothermal titration calorimetry (ITC) to systematically investigate the impacts of surface crowding on target binding to aptamer functionalized nanoparticles. ITC is used to quantify the binding affinity and understand the thermodynamic driving forces behind the counterintuitive relationship between aptamers in crowded environments and their enhanced interactions with target analytes. The surface loading density of thrombin-binding aptamer-functionalized 10 nm gold nanoparticles is precisely controlled and then introduced to thrombin, revealing the thermodynamic profile of aptamer/target binding, including changes in enthalpy, free energy, and entropy. The thermodynamic profiles are compared across varying aptamer loaded surface densities, exposing the crowding effects on target binding. ITC, a label free approach, does not rely on an aptamer conformational change for signal generation. The decoupling of the signal generation from the target capture process serves to reduce the ambiguity of the signal generation. Gold nanoparticles, which are featured in many sensing platforms, serve as a model system as they are easily modifiable, but their size and curvatures are relevant to other nanomaterials that can be used for target capture purposes.

While our study confirms Gooding's finding[4] that increasing loading density on the gold nanoparticle can improve binding affinity, thermodynamic characterization using ITC reveals new mechanistic insights into binding under increasingly crowded conditions. The enthalpic cost increases with a higher density, confirming the roles of steric/electrostatic repulsion. However, crowding reduces the entropic costs of target binding. This entropic compensation is more than sufficient for offsetting the enthalpic penalty, leading to higher affinities at higher densities. Additionally, we found that the binding affinity declines precipitously when the loading density is above a certain threshold. While aptamer target interactions tend to be specific, this study highlights the utility of ITC as a method of understanding binding mechanisms in crowded environments for better optimization and engineering of high affinity aptamer-based sensors.

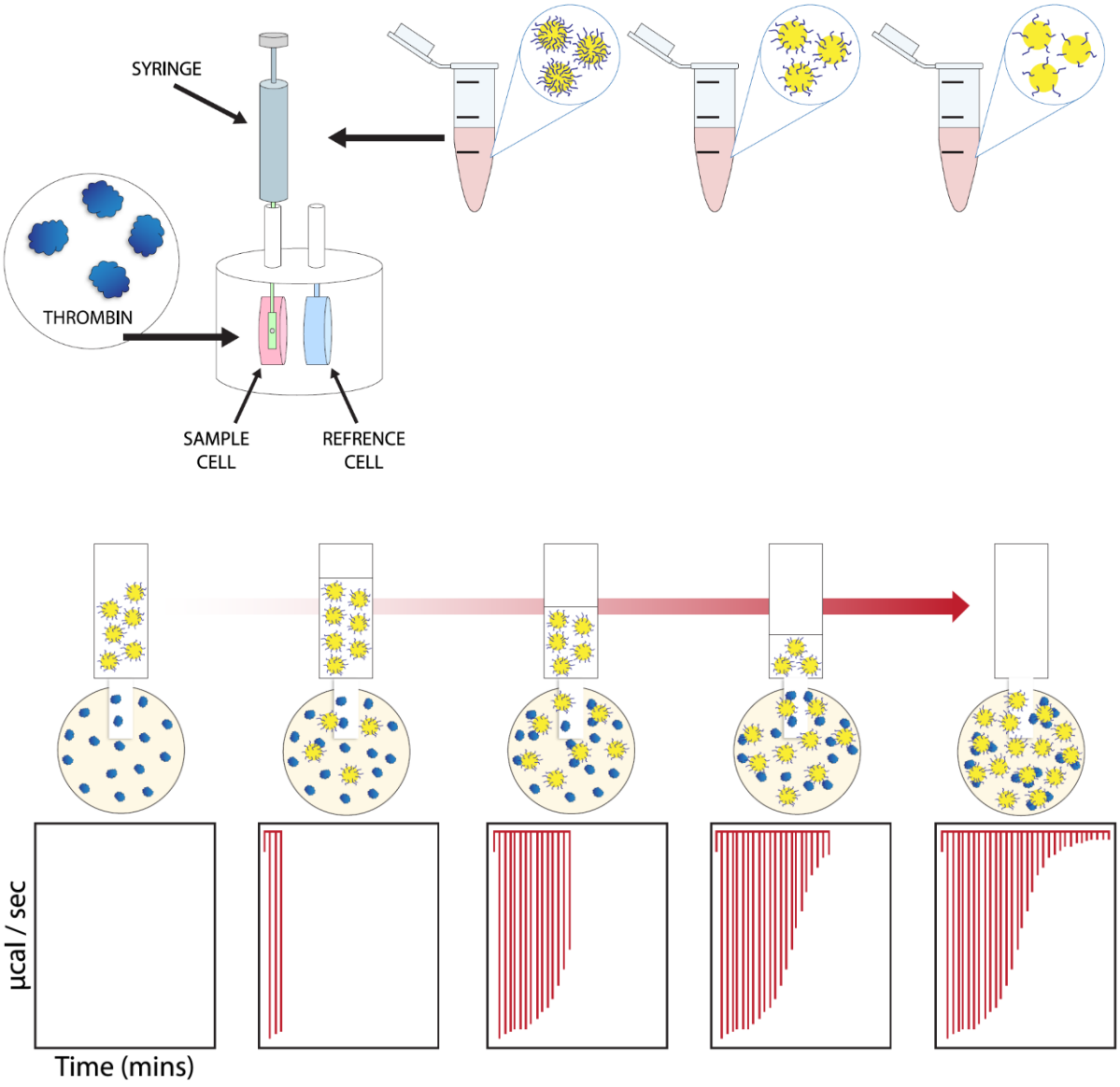


Figure 3.1: Schematic of reaction set up. 15mer thrombin binding aptamer (TBA) is immobilized on 10 nm gold nanoparticle surface. Gold nanoparticles with varying loading densities are loaded into the sample well and incrementally introduced to thrombin residing in the sample well. Evolved heat from aptamer target association is monitored using ITC.

## 3.2 Methods and Materials

### Chemicals and Supplies

Potassium chloride (KCl), magnesium chloride ($MgCl_2$), sodium citrate dihydrate, tris borate EDTA (TBE), polyethylene glycol (PEG) 8000, sodium chloride (NaCl), tris acetate, and tris

(2-carboxyethyl)phosphine hydrochloride (TCEP) were purchased from Fisher Scientific. Sodium dodecyl sulfate (SDS) and dithiothreitol (DTT) were purchased from Sigma-Aldrich. Butanol was purchased from Spectrum Chemical Manufacturing Group. Calcium chloride hexahydrate ($CaCl_2$) was purchased from Acros Organics. Thiol-OEG-3 was purchased from Prochimia. All chemicals listed above were used without further purification or modifications. α-Thrombin (thrombin) was purchased from BSP Biosciences. Thiolated DNA aptamers were purchased from Integrated DNA Technologies (IDT). 10 nm diameter gold nanoparticles were purchased from Ted Pella in Redding, CA. 3 kDa Amicon columns were purchased from Millipore Sigma.

**Preparation of Thrombin**

α-Thrombin arrived from the manufacturer in a buffer containing 50 mM sodium citrate pH 6.5, 200 mM NaCl, and 0.1% PEG 8000. For brevity, this buffer will be referred to as BSP buffer in subsequent sections. 92 µL of 3.55 mg/mL α-thrombin was frozen in a -80º C freezer and subsequently freeze-dried using a Labconco freeze dryer at -90º C and 0.2 mbar for several hours. Once the freeze-drying process was completed, freeze dried α-thrombin and buffer components were resuspended in 1,606 µL of thrombin binding buffer (TBB), which consists of 20 mM tris acetate pH 7.4, 140 mM NaCl, 5 mM KCl, 1 mM $MgCl_2$, and 1 mM $CaCl_2$. The final concentration of α-thrombin was 5.5 µM. Samples were aliquoted and frozen until use. The buffer used as the solvent for purified gold nanoparticle reactants was made by combining BSP and TBB in a ratio of 0.0573 : 1, respectively.

**Preparation of Conjugation Buffer**

The conjugation buffer (CB) is a mixture of BSP and TBB. The purpose of CB is to match the α-thrombin solution with the gold nanoparticle solution to remove buffer mismatches that can cause abnormal heat artifacts during ITC measurements.

CB was made by freeze-drying 20 mL of BSP buffer and resuspending in 349 mL of TBB. The resultant ratio of BSP buffer and TBB is 0.0573. CB was used during gold nanoparticle purification.

**Gold Nanoparticle Preparation**

- ❖ DNA preparation

Prior to gold nanoparticle functionalization, TCEP was used to reduce DNA containing a disulfide functional group into a monothiolated functional group. This monothiolated DNA linker is used to anchor DNA to the gold nanoparticle surface. TCEP was mixed with a DNA solution at a ratio of 400:1. The reaction mixture was allowed to react overnight before purification with a 3 kDa Amicon column. The reducing mixture containing thiolated DNA

and TCEP was loaded into an Amicon column and spun at 5,500 RCF for 90 minutes. A one-minute collection spin into a clean centrifuge tube eluted reduced DNA oligonucleotides for surface functionalization. The recovery yield ranged between 85 – 94%.

- ❖ Surface functionalization

DNA oligonucleotide surface functionalization took place using the procedure outlined in chapter 2. Briefly, DNA oligonucleotides were mixed with 10 nm gold nanoparticles in a 300:1 ratio. 10% SDS was added to reach a final SDS percentage of 0.1%. Following conjugation of DNA oligonucleotides, thiol-OEG was added to all samples to counter non-specific adsorption from proteins during the ITC experiments.[30]

**Salt Aging**

Salt aging was performed by techniques established in literature.[31, 32] Briefly, 5 M NaCl was added in increments of 0.1 M NaCl until the target concentration was reached. Thirty minutes elapsed between NaCl additions. Upon reaching the final salt concentration, the reaction mixture was allowed to react for 4 hours. Thiol-OEG-3 was added in a 300:1 ratio (with respect to gold nanoparticles) and allowed to react for 18 hours before purification.

**Freezing Method**

The freezing method of gold nanoparticle functionalization was performed by previously established methods.[33] DNA oligonucleotides and 10nm gold nanoparticles were mixed in a 300:1 ratio. The reaction mixture was then frozen in a -80º C freezer overnight. The following day, the reaction mixture was thawed and allowed to react with Thiol-OEG-3 in a 300:1 ratio (with respect to gold nanoparticles) for 18 hours before purification.

**Butanol Method**

Butanol dehydration to functionalize gold nanoparticles with single stranded DNA oligonucleotides was performed by previously established methodology.[34] DNA oligonucleotides and 10nm gold nanoparticles were mixed at a ratio of 300:1. Sufficient TCEP was added to produce a 1 mM concentration before adding n-butanol in 9:1 ratio (butanol: particle solution). Subsequently, the emulsion was vortexed for a few seconds. 200 µL of 0.5x TBE was added followed by another few seconds of vortex partitioning. The butanol excluding solution volume samples were concentrated by a 1-minute centrifugation at 2000 RCF. The ventral red particulate layer was carefully pipetted and transferred into a 2 mL Eppendorf DNA LoBind tube. Thiol-OEG-3 was added in a 300:1 ratio (with respect to gold nanoparticles) and allowed to react for 18 hours before purification.

**Purification of Gold Nanoparticles**

Gold nanoparticles were purified by centrifugation after the 18-hour incubation with Thiol-OEG-3. Gold nanoparticles were spun for 55 minutes at 4º C at 95,879 RCF using a Thermo Scientific Fiberlite F50L – 8 × 39 rotor in a Thermo Scientific Sorvall wX+ Ultra Series Centrifuge. About 90% of the supernatant was removed using a transfer pipette and replaced

with CB. A total of 6 centrifuge spins were performed. During the final centrifugation round, gold nanoparticles were left concentrated (around 0.800 – 1.9 µM).

ITC experiments are heavily dependent on reactant concentration. The concentration of DNA aptamer strands was determined by first measuring the concentration of gold nanoparticles. An aliquot of concentrated functionalized gold nanoparticles was diluted by a factor of 2000. This served to obtain a measurable signal while not diluting large volumes of concentrated gold nanoparticles. An absorbance reading at 520 nm using a Cary-60 UV-vis by Agilent Technologies was obtained. The concentration was calculated by dividing the measured absorbance by the extinction coefficient provided by the manufacturer ($9.55 \times 10^7$ $M^{-1}$ $cm^{-1}$). This concentration was multiplied by the number of DNA aptamers on the surface.

**Quantifying Immobilized Aptamers**

Following 10 nm gold nanoparticle functionalization and purification, a solution of 0.5 M DTT and 1.5 M NaCl was introduced to functionalized gold nanoparticles and allowed to incubate overnight. DTT removed immobilized aptamers from the solution while NaCl served to aggregate newly bare gold nanoparticles. The supernatant, containing previously immobilized aptamers, was collected after a 5-minute centrifuge spin at 5 k RCF. Aptamers were purified by NAP-5 size exclusion columns using ultrapure water as the mobile phase and quantified using absorbance at 260 nm from a Cary-60 UV-Vis by Agilent Technologies. Each sample of functionalized gold nanoparticles was performed and analyzed in triplicate to obtain a standard deviation of immobilized aptamers.

**ITC Experimental Conditions**

ITC experiments were performed on a Malvern PEAQ-ITC. All experiments featured thrombin in the sample well and aptamer functionalized gold nanoparticles in the syringe. All reactions took place at 25º C. 10 µcal / s was used as a reference power with feedback set to “high”. The stir speed was set to 750 RPM. The sample cell was loaded with 300 µL of thrombin in CB.

Twenty injections were used for each experimental trial. The first injection was 0.2 µL and served to remove any residual air from the loading process. Nineteen injections, each 2.0 µL over a 4.0 second interval, delivered functionalized gold nanoparticles to the sample well containing thrombin. The interval between injections was 180 seconds to ensure equilibration with the baseline reference power before the next sample injection. Each ITC experiment lasted about 60 minutes.

All reactions, apart from 0.9 M NaCl aged gold nanoparticles, were run in triplicate. 0.9 M NaCl aged gold nanoparticles were run in duplicate.

**Data Analysis**

Data analysis and interpretation was performed by the Malvern PEAQ-ITC analysis software using the single binding site method. Point to point subtraction between aptamer functionalized gold nanoparticles titrated into CB (blank) was used to control for heat of dilution.

Baseline smoothing for binding isotherms was carried out in Origin data analysis software. The heat spikes following titrant injection were masked and the resultant baseline was smoothed by adjacent averaging.

Integrated heat plots were plotted as exported from the Malvern PEAQ-ITC analysis software.

## 3.3 Results and Discussion

Before systematically investigating the crowding effect of target capture on gold nanoparticle surfaces, a baseline study of 15mer TBA's interaction with thrombin was used to validate the approach and better understand the role of the surface with respect to binding affinity. This positive control experiment featured free 15mer TBA in solution, without being tethered to the gold nanoparticle surface.

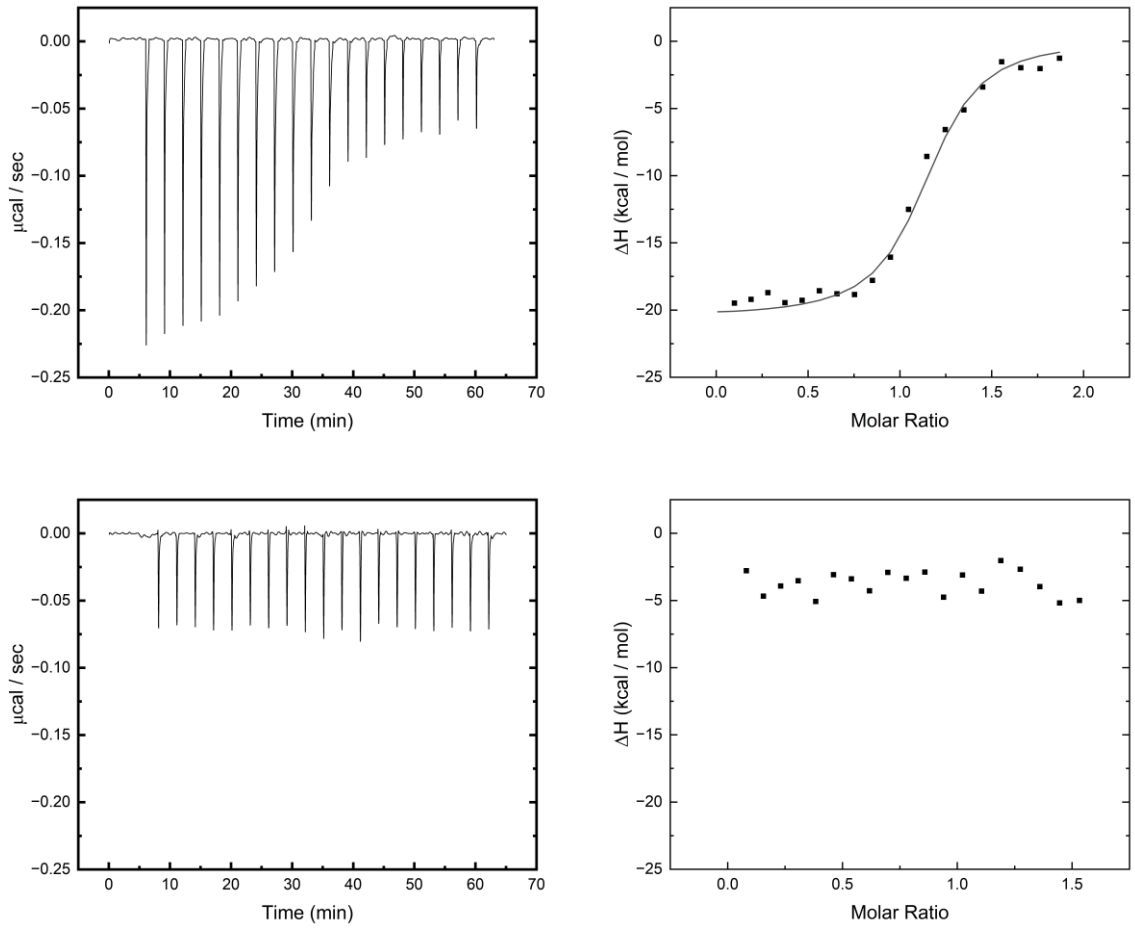


Figure 3.2: Binding isotherms and integrated heat plots for (top) free 15mer TBA and (bottom) CoV-1C-RBD aptamer functionalized gold nanoparticles. Concentration of free 15mer TBA is 50 µM. Concentration of CoV-1C-RBD is 41 µM. Thrombin concentration is 5.5 µM.

Figure 3.2 shows the generic ITC setup for reactants under investigation in this study. Thrombin was loaded into the sample well and the aptamer was titrated into the sample well from the syringe. The thermodynamic profile (table 3.1) obtained was in good agreement with previous ITC literature studies.[35]

A negative control experiment was performed to ensure the origin of evolved heat resulted from the association between thrombin and 15mer TBA rather than thrombin's association with a gold nanoparticle or non-specific interactions with the immobilized aptamer strand. 10 nm gold nanoparticles functionalized with CoV-1C-RBD, a DNA aptamer that recognizes Covid S1 spike protein, with a loading density of $8.8 \times 10^{12}$ strands / $cm^2$, were introduced to thrombin in an identical ITC setup.[36] While there is some heat generated from CoV-1C-RBD aptamer functionalized gold nanoparticles titrated into the sample cell containing thrombin, a blank titration of CoV-1C-RBD functionalized gold nanoparticles titrated into buffer (Figure 2.6D) reveals a similar heat signature. Thus, evolved heat from CoV-1C-RBD aptamer functionalized gold nanoparticles can be attributed to dilution upon injection into the sample cell rather than specific interactions between immobilized CoV-1C-RBD aptamers and thrombin. The heat signature of CoV-1C-RBD functionalized gold nanoparticles titrated into thrombin stands in contrast to 15mer-TBA functionalized gold nanoparticles where a clear binding trend is observed. A discussion of this trend can also be found in Chapter 2.

The effects of aptamer crowding on target binding was investigated by introducing 15mer TBA functionalized 10 nm gold nanoparticles to thrombin and measuring the heat evolved upon target binding. Central to crowding effects is the quantification of aptamer strands immobilized on the gold nanoparticle surface. To cover the entire range of loading densities, three different surface functionalization approaches were employed to fabricate gold nanoparticles. The final concentration of NaCl controls the DNA loading density of the salt aging method while the freezing and butanol dehydration methods feature higher loading densities. A discussion of these functionalization techniques is presented in Chapter 2.

The salt aging method was stopped at a final NaCl concentration of 0.3 M to fabricate aptamer functionalized gold nanoparticles with a loading density of $8.60 \times 10^{12}$ strands / $cm^2$, equating to 27 strands per 10 nm gold nanoparticle. This relatively bare loading density produced a heat signature that is characteristic of binding with thrombin. Immobilizing the aptamer strands on the gold nanoparticle surface resulted in a 41.5 nM binding affinity. Compared to the 105 nM binding affinity of the free aptamer, this represents a 60.5% improvement to binding affinity. The enthalpic change of the binding reaction between thrombin and 0.3 M NaCl functionalized gold nanoparticles decreased when compared to thrombin and the free 15mer TBA. This trend is unsurprising as crowding interactions are known to create steric hindrance and electrostatic repulsions which are unfavorable to target binding. Aptamer immobilized on gold nanoparticles show less unfavorable change in entropic contribution ($T\Delta S$) upon target binding when compared to free 15mer TBA. Conformational restriction upon binding in the free 15mer TBA system results in an entropic contribution change of -11.5 kcal /mol. The -9.04 kcal / mol entropic contribution change upon binding of the immobilized aptamer system is rationalized

by the inherently increased starting entropy of the functionalized gold nanoparticles – whose immobilized aptamers experience less degrees of freedom when immobilized.

Table 3.1: Relationship between surface functionalization method and aptamer strands per 10 nm gold nanoparticle. UV-Vis at 260 nm was used to quantify aptamer strands.

| Surface Functionalization Method | Average Number of DNA Aptamers per Gold Nanoparticle | Standard Deviation |
|---|---|---|
| **0.3 M NaCl** | 27 | 0.34 |
| **0.5 M NaCl** | 34 | 2.86 |
| **0.7 M NaCl** | 41 | 1.74 |
| **0.8 M NaCl** | 49 | 1.49 |
| **0.9 M NaCl** | 56 | 2.56 |
| **Freeze Method** | 69 | 2.65 |
| **Butanol Dehydration** | 124 | 7.41 |

Gold nanoparticle loading density was increased to $1.08 \times 10^{13}$ strands / $cm^2$ (34 strands per particle) by suspending the salt aging procedure upon arriving at 0.5 M NaCl. These gold nanoparticles experience enhanced target binding compared to the more sparely loaded gold nanoparticles discussed above. The 31.8 nM binding affinity of 34 strands per gold nanoparticle represents an improvement of 23.3% when compared to the 27 strands per particle binding affinity and a 69.7% improvement when compared to the free 15mer TBA. As crowding effects increase in the 34 strands per particle samples compared to the 27 strands per particle samples, enthalpic changes decrease because crowding creates a higher energy system

with increasing electrostatic repulsion. Increased crowding produced by the additional immobilized aptamer strands result in less unfavorable changes in entropic contribution when compared to less crowded aptamer functionalized gold nanoparticles because of the conformational restriction imposed by additional immobilized neighboring aptamer strands. Further increasing the aptamer loading density to $1.31 \times 10^{13}$ (41 strands per nanoparticle) yields better enhancement of target binding affinity to 14.5 nM – an 86.2% increase compared to free 15mer TBA. The trends of decreasing changes in enthalpy (-16.57 kcal / mol) and entropic contribution (-5.91 kcal / mol) are also observed. A summary of binding thermodynamic profiles between free / immobilized aptamers and thrombin is shown in table 3.3.

Table 3.2: Relationship to target binding affinity at varying aptamer loading densities. Binding affinity improvement observed as loading density increases.

| Loading Density (Strands / Gold Nanoparticle) | Affinity (nM) |
|---|---|
| **Free 15mer TBA** | 105 |
| **27** | 41.5 |
| **34** | 31.8 |
| **41** | 14.5 |

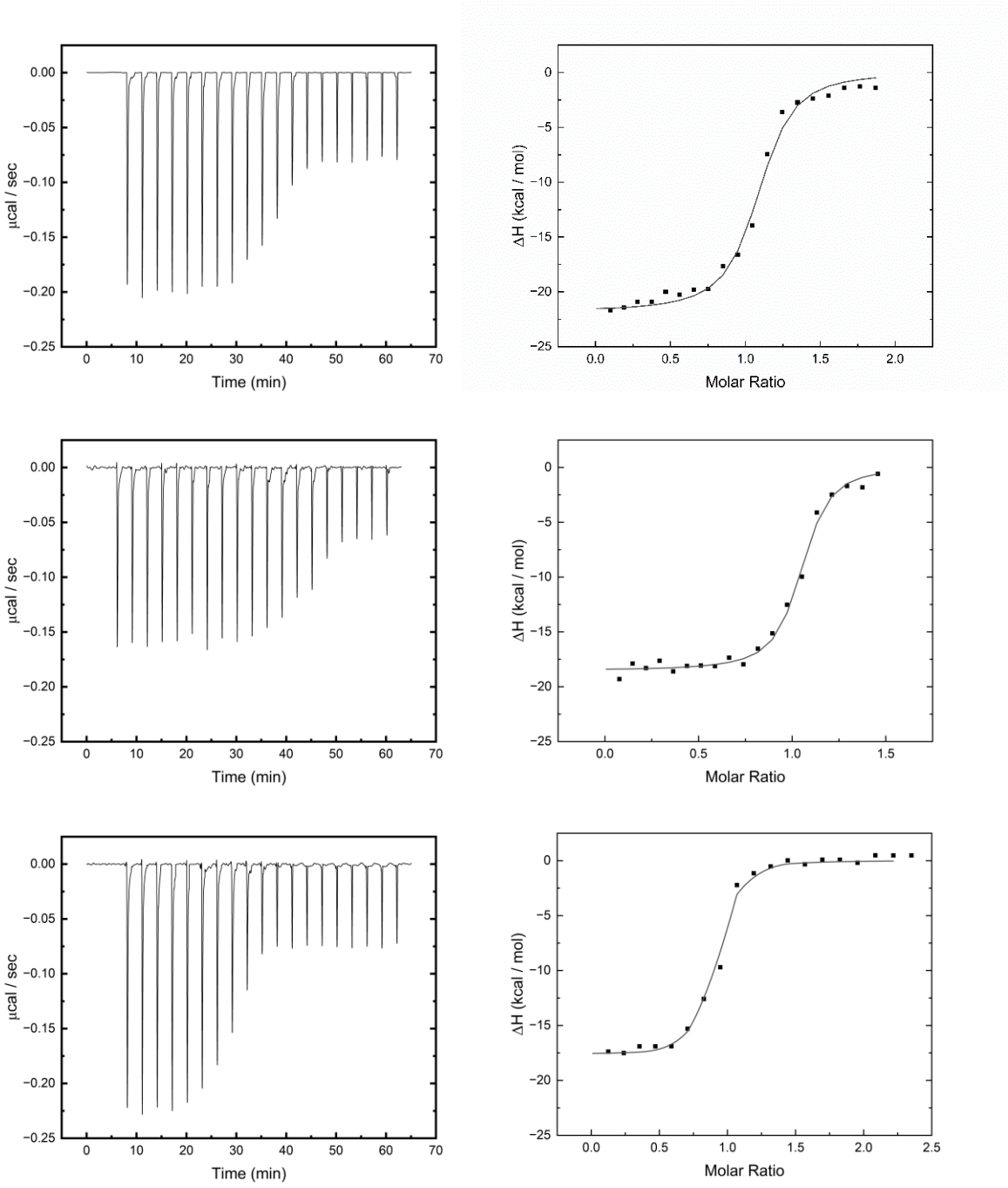


Figure 3.3: Binding isotherms (left) and integrated heat plots (right) of (top) 27 strands per gold nanoparticle [15mer TBA] = 50 µM, (middle) 34 strands per gold nanoparticle [15mer TBA] = 38 µM, (bottom) 41 strands per gold nanoparticle [15mer TBA] = 63 µM. Thrombin concentration is 5.5 µM.

Immobilized aptamers on gold nanoparticles exhibit less enthalpic change than homogeneous aptamers when binding to thrombin. The enthalpic penalty for thrombin binding increases as aptamer crowding increases. In other words, the enthalpic change upon target binding

decreases with increasing aptamer loading density. The volume change upon target binding is negligible, thus the enthalpy is approximately equal to the internal energy. In the free aptamer system, 15mer TBA forms non-covalent interactions with thrombin's exosite 1, lowering the energy of the system and releasing heat. The heat release is characteristic of an exothermic process and a negative enthalpic change upon binding. The dilute homogeneous solution does not contain a large magnitude of electrostatic repulsion between aptamer strands. However, the immobilized aptamer system contains aptamers that are in closer proximity to each other than the homogeneous aptamer system. Before target binding, electrostatic repulsions form a DNA brush extending away from the gold nanoparticle surface. After target binding takes place, aptamer conformation becomes further restricted, and aptamer secondary structure increases electrostatic repulsions between conformationally locked aptamers and neighboring strands. This final state is higher in internal energy from neighboring electrostatic repulsions. As follows, because the bound, immobilized aptamer energy is higher than the bound, homogeneous aptamer, the enthalpic change of the immobilized aptamer system decreases with respect to the homogeneous aptamer system. This trend of decreasing enthalpic change upon target binding is observed as loading density increases due to higher internal energies of crowded systems.

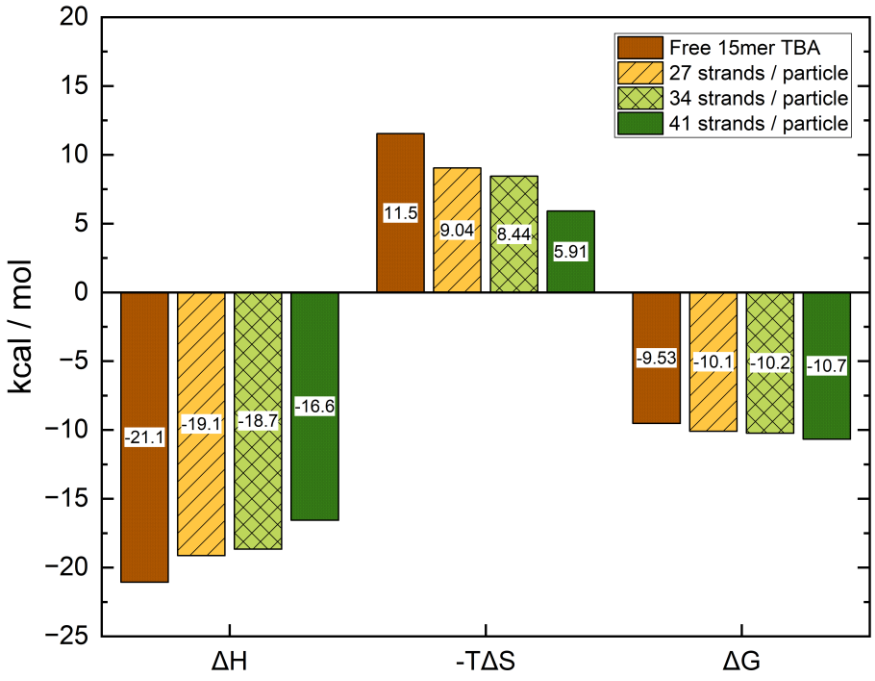


Figure 3.4: Thermodynamic profile of 15mer TBA interactions with thrombin at varying loading densities on 10 nm gold nanoparticles. ΔH and ΔS both decrease as loading density increases.

Immobilized aptamers on gold nanoparticles suffer less from unfavorable changes in entropic contribution than homogeneous aptamers when binding to thrombin. First, consider the free aptamer system. In the homogeneous aptamer solution, the aptamer exhibits considerable conformational freedom before target binding. However, upon binding to the target, non-covalent interactions with exosite 1 on the thrombin target result in the aptamer becoming conformationally locked. The sharp decrease in conformational degrees of freedom results in a large, unfavorable change in entropic contribution. On the other hand, for aptamers immobilized on a nanoparticle, before target binding, electrostatic repulsions between neighboring strands already limit aptamer conformational freedom. Therefore, compared to free aptamers, the degrees of conformational freedom for the immobilized aptamers do not decrease as much for target binding, i.e., aptamer immobilization prepays the entropic contribution penalty involved in target binding. The entropic compensation is enough to offset the entropic penalty from crowded aptamer systems. Furthermore, as crowding on the gold nanoparticle surface increases, unfavorable change in entropic contribution upon target binding decreases. This trend is rationalized by further restriction of aptamer conformational degrees of freedom by electrostatic repulsions and excluded volume effects from neighboring aptamer strands before target binding. In increasingly crowded systems, as neighboring aptamer strands restrict conformational freedom before target binding, the unfavorable entropic contribution changes after target binding are less pronounced.

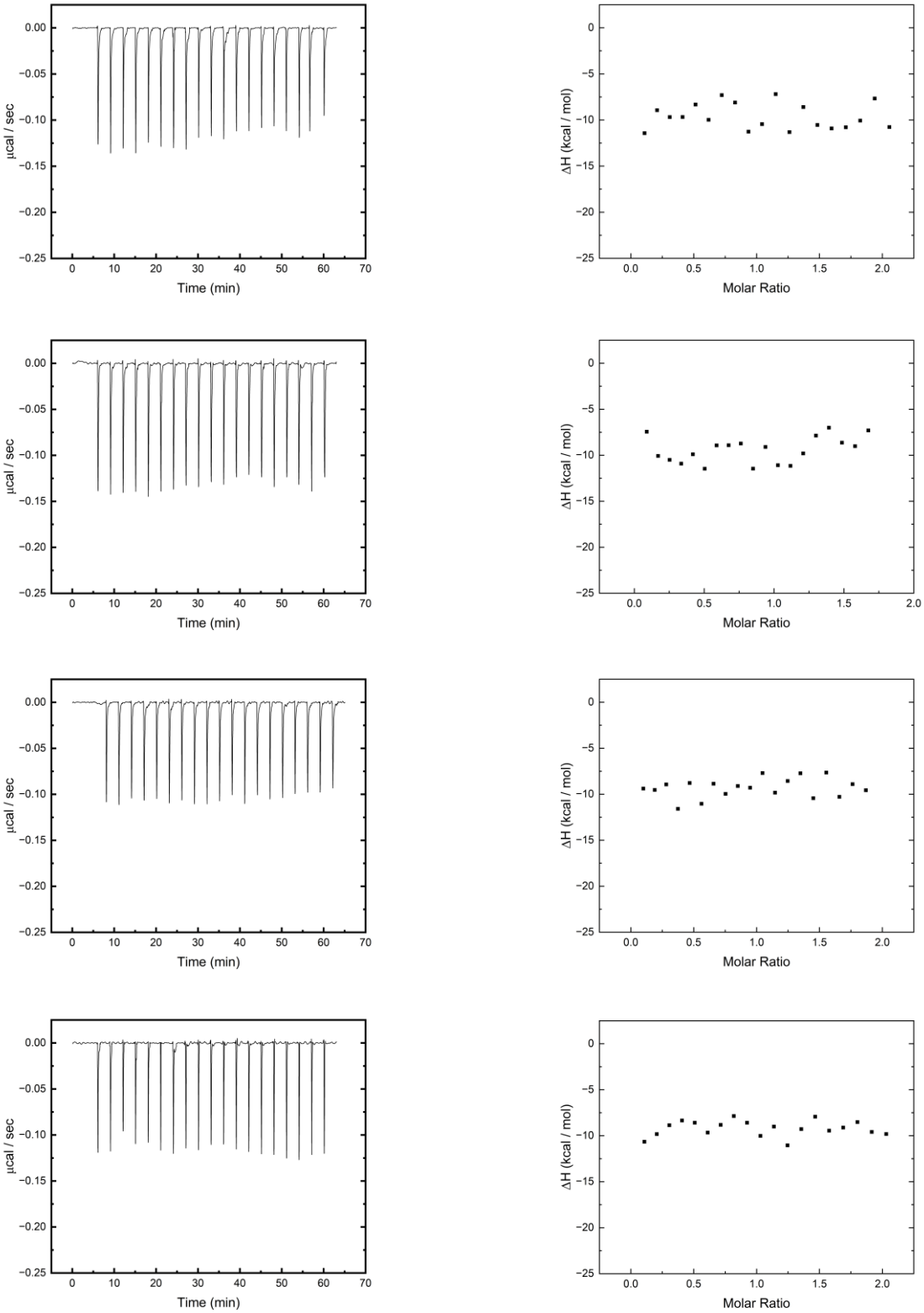


Figure 3.5: Binding isotherm and integrated heat plot of non-binding samples. A) 49 strands / particle. B) 55 strands / particle. C) 66 strands / particle. D) 114 strands / particle. 15mer TBA concentration is 50 µM for all plots. Thrombin concentration is 5.5 µM for all plots.

The loading density was further increased to investigate higher crowding regimes using higher salt aging concentrations along with the freeze and butanol dehydration methods. To the best of our knowledge, crowding regimes (< $1.5 \times 10^{13}$ strands / $cm^2$) have not been the subject of colloidal binding studies. Based on ITC measurements, the transition from binding to non-binding loading is quite abrupt. The loading density difference between the threshold of binding and non-binding is roughly 20%. Steric effects are likely to account for the non-binding behavior exhibited at higher loading densities. Despite the non-binding behavior observed at higher loading densities, figure 3.5 shows heat signatures upon titrant injection. Failure to achieve saturation at higher loading densities could be a result of slowed reaction kinetics under crowded conditions. Target binding kinetics is known to slow upon increasing loading density, however, Gooding *et al.* showed that increasing loading densities increased target binding kinetics on gold nanoparticle surfaces.[4, 28] More investigation into this nebulous region could determine the cutoff threshold for binding more accurately and elucidate more complex behaviors or potential transient target binding. Nevertheless, these results show that the loading density needs to be carefully controlled: a relatively high density is needed to maximize binding affinity; on the other hand, overcrowding the surface can lead to a precipitous decline of binding.

Our study suggests that the choice of the gold nanoparticle functionalization method is critical for aptamer / target binding. While there are parameters that can be changed in the various methods used to functionalize gold nanoparticles with DNA, methods that boast higher DNA surface densities, such as the freezing method and butanol dehydration, produce loading densities that are too high for target detection. The salt aging method of gold nanoparticle functionalization allows for suspending salt additions to closely tailor the final loading density – unlike the freezing or butanol dehydration methods that require the procedure be carried out to completion.

Table 3.3: Thermodynamic profiles of all ITC experiments and replicates.

| **Preparation Method** | **Strands / particle** | **Loading Density (strands / $cm^2$)** | **[Aptamer] (µM)** | **[Thrombin] (µM)** | **ΔH (kcal / mol)** | **-T ΔS (kcal / mol)** | **ΔG (kcal / mol)** | **Kd (nM)** |
|---|---|---|---|---|---|---|---|---|
| **Free TBA** | N/A | N/A | 50 | 5.5 | -20.5 | 11 | -9.52 | 106 |
| | | | 50 | 5.5 | -22.3 | 12.8 | -9.47 | 115 |
| | | | 50 | 5.5 | -20.4 | 10.8 | -9.59 | 93 |
| **CoV-RBD-1C Aptamer fxn AuNP aged to 0.5M NaCl** | 31 | $8.80 \times 10^{12}$ | 41 | 5.5 | - | - | - | - |
| | | | 41 | 5.5 | - | - | - | - |
| | | | 41 | 5.5 | - | - | - | - |
| **0.3M NaCl Aged** | 27 | $8.60 \times 10^{12}$ | 50 | 5.5 | -19.5 | 9.45 | -10 | 45.6 |
| | | | 50 | 5.5 | -20.2 | 9.52 | -9.86 | 48 |
| | | | 50 | 5.5 | -18.4 | 8.14 | -10.3 | 30.9 |
| | 34 | $1.08 \times 10^{13}$ | 38 | 5.5 | -18.5 | 8.22 | -10.3 | 29.4 |

| | | | | | | | | |
|---|---|---|---|---|---|---|---|---|
| **0.5M NaCl Aged** | | | 38 | 5.5 | -19.3 | 9.11 | -10.2 | 34.5 |
| | | | 38 | 5.5 | -18.2 | 7.9 | -10.3 | 31.5 |
| **0.7M NaCl Aged** | 41 | $1.31 \times 10^{13}$ | 63 | 5.5 | -15.8 | 5.1 | -10.7 | 13.7 |
| | | | 63 | 5.5 | -17.1 | 6.43 | -10.7 | 15.1 |
| | | | 63 | 5.5 | -16.8 | 6.2 | -10.6 | 14.6 |
| **0.8M NaCl Aged** | 49 | $1.56 \times 10^{13}$ | 57 | 5.5 | - | - | - | - |
| | | | 57 | 5.5 | - | - | - | - |
| | | | 57 | 5.5 | - | - | - | - |
| **0.9M NaCl Aged** | 55 | $1.75 \times 10^{13}$ | 47 | 5.5 | - | - | - | - |
| | | | 47 | 5.5 | - | - | - | - |
| **Freeze Method** | 66 | $2.10 \times 10^{13}$ | 50 | 5.5 | - | - | - | - |
| | | | 50 | 5.5 | - | - | - | - |
| | | | 50 | 5.5 | - | - | - | - |
| **Butanol Dehydration** | 114 | $3.63 \times 10^{13}$ | 50 | 5.5 | - | - | - | - |
| | | | 50 | 5.5 | - | - | - | - |
| | | | 50 | 5.5 | - | - | - | - |

## 3.4 Conclusion and Outlook

Here, we use aptamer functionalized 10 nm gold nanoparticles to characterize the thermodynamic profiles of immobilized aptamer binding to a protein target. ITC was used to gain mechanistic insight into enhanced aptamer target interactions under crowding conditions by varying the loading density of immobilized aptamers. Increasing aptamer loading density on gold nanoparticle surfaces resulted in an improvement to binding affinity between aptamers and target thrombin, but only up to a certain loading density. The mechanism for increased binding affinity was determined to be entropically based, as increasingly crowded surfaces reduce the entropic contribution penalty upon target binding when compared to less crowded surfaces and free aptamers. The entropic compensation is enough to offset the enthalpic penalty observed as loading density increases. The ability to utilize ITC for this study explains the mechanism for enhanced immobilized aptamer affinity for target proteins.

Our trends in binding affinity align with Gooding *et al.*'s conclusions;[4] however, it should be noted that the higher loading densities were used in this study. The highest crowding density used by Gooding *et al.* was $3.3 \times 10^{12}$ strands / $cm^2$ whereas the lowest crowding density used in this study was $8.8 \times 10^{12}$ strands / $cm^2$. Over the range of loading densities used by Gooding *et al.*, target binding affinity increased. However, Gooding did not use a loading density high enough to observe a precipitous decline in target binding. As such, in contrast to Gooding's conclusion, target binding affinity does not always increase as loading density increases.

The specific nature of aptamer interactions and conformational changes warrant caution when generalizing, but ITC can be utilized to investigate the intricacies of immobilized aptamers and their interactions with targets. While the optimal crowding density may be challenging to generalize, determining the loading density at which target binding ceases is crucial. For biosensing applications, optimizing the number of aptamer strands on an individual basis is

essential to achieve maximum sensitivity. This study provides insights into elucidating the optimal loading density by outlining an ITC experimental design and a method for quantifying aptamers on gold nanoparticle surfaces.

A previous investigation uncovered decreased binding affinity between 15mer-TBA and target thrombin when 15mer-TBA is immobilized on the 5' end of the aptamer.[37] These differences are likely attributed to conformational changes relative to the surface after target capture. In the study presented within, 15mer-TBA was immobilized using the 3' end, meaning steric hindrance is likely to decrease upon target binding as 15mer-TBA complex is removed from the surface. However, certain aptamers, such as the dopamine and glucose binding aptamer, are known to be displaced from the surface upon target binding.[38] This phenomenon represents an intriguing avenue for study on crowded systems as movement toward or away from surfaces may affect the ability of an aptamer to capture a target depending on the local environment. Aptamers that move further from the immobilized surface are likely to experience fewer crowding effects from neighboring aptamer strands, which would allow them to capture targets despite high loading densities. Because steric hindrance is alleviated during target binding, the effects of target crowding are hypothesized to be decreased when compared to conformational changes that result in migration toward the surface. As such, higher loading densities would not hinder target binding. ~~The specific nature of aptamer interactions and conformational changes warrant caution when generalizing, but ITC can be utilized to investigate the intricacies of immobilized aptamers and their interactions with targets.~~

This investigation was intentionally designed to study a relatively large protein target. However, much investigation remains in small molecule targets. In these systems, steric hindrance originating from the target is negligible, meaning that steric hindrance will only come from neighboring aptamers. Small molecules can more easily pass through the dense aptamer brush, but conformational changes required for target capture are likely to hinder target capture at sufficiently high aptamer loading densities. Furthermore, cutoff loading densities for target capture are likely higher for small molecule aptamers compared to aptamers designed for macromolecular target capture.

While this study underscores the mechanism for enhanced target binding under crowded conditions on colloidal gold nanoparticles, it leaves room for additional investigations to further probe the detailed interactions of immobilized aptamers and their targets. The role of nanoparticle curvature on the effect of gold nanoparticle crowding could be used to further optimize target capture. This study might fix aptamer loading density across nanoparticles ranging from 5 nm to 20 nm to better understand the role of the surface curvature. By nature of the curved surface, immobilized aptamers feel fewer crowding effects as they protrude from the surface and have fewer interactions with neighboring immobilized aptamers. However, as the size of the gold nanoparticle increases, the surface begins to resemble a planar surface.[39] Across similar loading densities, compared to larger nanoparticles, binding to smaller nanoparticles has more favorable enthalpy, i.e., $\Delta H$ is more negative. Fewer interactions with neighboring aptamers result in larger enthalpic changes after target binding on smaller gold

nanoparticles. Meanwhile, pronounced crowding interactions on larger gold nanoparticles result in an entropically driven target binding mechanism. Studies involving larger nanoparticles (>30 nm) will likely encounter practical limitations with stoichiometry suitable for ITC (Figure 2.4). Longer spacer regions would protrude aptamer recognition sequences further from the nanoparticle surface. The increased distance from the surface also results in increased distance from neighboring aptamer strands, which lowers the internal energy of the system. This decrease is likely to result in a larger enthalpic contribution to target binding when compared to shorter spacer regions at similar loading densities. Further investigation into spacer region length may discover the loading density cutoff for target capture. Because steric hindrance is alleviated with increasing spacer length, it is hypothesized that target binding will be observed at higher loading densities.

Target binding is a fundamental aspect of biosensing that plays a pivotal role in the effectiveness of biosensor technology. Despite its importance, the detailed mechanisms and intricacies of target binding are often not fully explored in many biosensing developments. This oversight can hinder the optimization and performance of biosensors. The design and fabrication of biosensors depend heavily on fabricating materials that maximize target binding to generate reproducible, reliable, and highly sensitive signal outputs. By delving into the specifics of how targets are captured – particularly the interactions between immobilized aptamers and target proteins in solution – rationally designed biosensing materials can be developed. The effectiveness of a biosensor is significantly influenced by how these aptamers are immobilized on its surface and how they interact with their target proteins. Optimizing factors such as loading density, surface chemistry, the orientation of aptamers, environmental and buffer conditions, and kinetic parameters of binding interactions is crucial. By understanding and manipulating these factors, it is possible to create biosensors with enhanced performance characteristics and rationalize biosensor figures of merit, such as limit of detection and response time. This in-depth understanding, along with the proper tools to characterize target binding interactions, leads to the rational design and fabrication of biosensors, which can offer superior sensitivity, specificity, and reproducibility.

## 3.5 References


(1) Bock, L. C.; Griffin, L. C.; Latham, J. A.; Vermaas, E. H.; Toole, J. J. Selection of Single-Stranded-DNA Molecules That Bind and Inhibit Human Thrombin. *Nature* **1992**, *355* (6360), 564-566. DOI: DOI 10.1038/355564a0.

(2) Jayasena, S. Aptamers: An emerging class of molecules that rival antibodies in diagnostics. *Clinical Chemistry* **1999**, *45* (9), 1628-1650, Article|Proceedings Paper..

(3) Mairal, T.; Özalp, V. C.; Sánchez, P. L.; Mir, M.; Katakis, I.; O'Sullivan, C. K. Aptamers:: molecular tools for analytical applications. *Analytical and Bioanalytical Chemistry* **2008**, *390* (4), 989-1007. DOI: 10.1007/s00216-007-1346-4.

(4) Chen, X. Q.; Lisi, F.; Bakthavathsalam, P.; Longatte, G.; Hoque, S.; Tilley, R. D.; Gooding, J. J. Impact of the Coverage of Aptamers on a Nanoparticle on the Binding Equilibrium and Kinetics between Aptamer and Protein. *ACSes Sensors* **2021**, *6* (2), 538-545. DOI: 10.1021/acssensors.0c02212.

(5) Kang, D.; Zuo, X.; Yang, R.; Xia, F.; Plaxco, K.; White, R. Comparing the Properties of Electrochemical-Based DNA Sensors Employing Different Redox Tags. *Analytical Chemistry* **2009**, *81* (21), 9109-9113, Article. DOI: 10.1021/ac901811n..

(6) Liu, Y. Z.; Canoura, J.; Alkhamis, O.; Xiao, Y. Immobilization Strategies for Enhancing Sensitivity of Electrochemical Aptamer-Based Sensors. *ACSes Applied Materials & Interfaces* **2021**, *13* (8), 9491-9499. DOI: 10.1021/acsami.0c20707.

(7) Kus-Liskiewicz, M.; Fickers, P.; Ben Tahar, I. Biocompatibility and Cytotoxicity of Gold Nanoparticles: Recent Advances in Methodologies and Regulations. *International Journal of Molecular Sciences* **2021**, *22* (20). DOI: ARTN 10952

10.3390/ijms222010952.

(8) Zhao, J.; Buldum, A.; Han, J.; Lu, J. Gas molecule adsorption in carbon nanotubes and nanotube bundles. *Nanotechnology* **2002**, *13* (2), 195-200, Article. DOI: 10.1088/0957-4484/13/2/312..

(9) Star, A.; Gabriel, J.; Bradley, K.; Gruner, G. Electronic detection of specific protein binding using nanotube FET devices. *Nano Letters* **2003**, *3* (4), 459-463, Article. DOI: 10.1021/nl0340172..

(10) Zhao, J.; Park, H.; Han, J.; Lu, J. Electronic properties of carbon nanotubes with covalent sidewall functionalization. *Journal of Physical Chemistry B* **2004**, *108* (14), 4227-4230, Letter. DOI: 10.1021/jp036814u..

(11) Mallikaratchy, P. Evolution of Complex Target SELEX to Identify Aptamers against Mammalian Cell-Surface Antigens. *Molecules* **2017**, *22* (2), Review. DOI: 10.3390/molecules22020215.

(12) Ni, S. J.; Zhuo, Z. J.; Pan, Y. F.; Yu, Y. Y.; Li, F. F.; Liu, J.; Wang, L. Y.; Wu, X. Q.; Li, D. J.; Wan, Y. Y.; et al. Recent Progress in Aptamer Discoveries and Modifications for Therapeutic Applications. *ACSes Applied Materials & Interfaces* **2021**, *13* (8), 9500-9519. DOI: 10.1021/acsami.0c05750.

(13) Sun, H. G.; Zu, Y. L. A Highlight of Recent Advances in Aptamer Technology and Its Application. *Molecules* **2015**, *20* (7), 11959-11980. DOI: 10.3390/molecules200711959.

(14) Zhou, W.; Hu, K. Q.; Kwee, S.; Tang, L.; Wang, Z. H.; Xia, J. F.; Li, X. J. Gold Nanoparticle Aggregation-Induced Quantitative Photothermal Biosensing Using a Thermometer: A Simple and Universal Biosensing Platform. *Analytical Chemistry* **2020**, *92* (3), 2739-2747. DOI: 10.1021/acs.analchem.9b04996.

(15) Aithal, S.; Mishriki, S.; Gupta, R.; Sahu, R. P.; Botos, G.; Tanvir, S.; Hanson, R. W.; Puri, I. K. SARS-CoV-2 detection with aptamer-functionalized gold nanoparticles. *Talanta* **2022**, *236*. DOI: ARTN 122841

10.1016/j.talanta.2021.122841.

(16) Cho, H.; Baker, B. R.; Wachsmann-Hogiu, S.; Pagba, C. V.; Laurence, T. A.; Lane, S. M.; Lee, L. P.; Tok, J. B. H. Aptamer-Based SERRS Sensor for Thrombin Detection. *Nano Letters* **2008**, *8* (12), 4386-4390. DOI: 10.1021/nl802245w.

(17) Liu, Y.; Tuleouva, N.; Ramanculov, E.; Revzin, A. Aptamer-Based Electrochemical Biosensor for Interferon Gamma Detection. *Analytical Chemistry* **2010**, *82* (19), 8131-8136. DOI: 10.1021/ac101409t.

(18) Moitra, P.; Alafeef, M.; Dighe, K.; Frieman, M. B.; Pan, D. Selective Naked-Eye Detection of SARS-CoV-2 Mediated by N Gene Targeted Antisense Oligonucleotide Capped Plasmonic Nanoparticles. *Acs Nano* **2020**, *14* (6), 7617-7627. DOI: 10.1021/acsnano.0c03822.

(19) Yang, L. Y.; Fu, C. C.; Wang, H. L.; Xu, S. P.; Xu, W. Q. Aptamer-based surface-enhanced Raman scattering (SERS) sensor for thrombin based on supramolecular recognition, oriented assembly, and local field coupling. *Analytical and Bioanalytical Chemistry* **2017**, *409* (1), 235-242. DOI: 10.1007/s00216-016-9992-z.

(20) Zhang, L. Y.; Fang, X. N.; Liu, X. B.; Ou, H. C.; Zhang, H. Y.; Wang, J. J.; Li, Q.; Cheng, H. Y.; Zhang, W. Y.; Luo, Z. F. Discovery of sandwich type COVID-19 nucleocapsid protein DNA aptamers. *Chemical Communications* **2020**, *56* (70), 10235-10238. DOI: 10.1039/d0cc03993d.

(21) Miyoshi, D.; Sugimoto, N. Molecular crowding effects on structure and stability of DNA. *Biochimie* **2008**, *90* (7), 1040-1051. DOI: 10.1016/j.biochi.2008.02.009.

(22) Ricci, F.; Lai, R. Y.; Heeger, A. J.; Plaxco, K. W.; Sumner, J. J. Effect of molecular crowding on the response of an electrochemical DNA sensor. *Langmuir* **2007**, *23* (12), 6827-6834. DOI: 10.1021/la700328r.

(23) Millan, K. M.; Mikkelsen, S. R. Sequence-Selective Biosensor for DNA-Based on Electroactive Hybridization Indicators. *Analytical Chemistry* **1993**, *65* (17), 2317-2323. DOI: DOI 10.1021/ac00065a025.

(24) Levicky, R.; Herne, T. M.; Tarlov, M. J.; Satija, S. K. Using self-assembly to control the structure of DNA monolayers on gold: A neutron reflectivity study. *Journal of the American Chemical Society* **1998**, *120* (38), 9787-9792. DOI: DOI 10.1021/ja981897r.

(25) Steel, A. B.; Herne, T. M.; Tarlov, M. J. Electrochemical quantitation of DNA immobilized on gold. *Analytical Chemistry* **1998**, *70* (22), 4670-4677. DOI: DOI 10.1021/ac980037q.

(26) White, R. J.; Phares, N.; Lubin, A. A.; Xiao, Y.; Plaxco, K. W. Optimization of electrochemical aptamer-based sensors via optimization of probe packing density and surface chemistry. *Langmuir* **2008**, *24* (18), 10513-10518. DOI: 10.1021/la800801v.

(27) Gong, P.; Levicky, R. DNA surface hybridization regimes. *Proceedings of the National Academy of Sciences of the United States of America* **2008**, *105* (14), 5301-5306. DOI: 10.1073/pnas.0709416105.

(28) Peterson, A. W.; Heaton, R. J.; Georgiadis, R. M. The effect of surface probe density on DNA hybridization. *Nucleic Acids Research* **2001**, *29* (24), 5163-5168. DOI: DOI 10.1093/nar/29.24.5163.

(29) Watkins, H. M.; Simon, A. J.; Ricci, F.; Plaxco, K. W. Effects of Crowding on the Stability of a Surface-Tethered Biopolymer: An Experimental Study of Folding in a Highly Crowded Regime. *Journal of the American Chemical Society* **2014**, *136* (25), 8923-8927. DOI: 10.1021/ja411486g.

(30) Zhang, F.; Skoda, M. W. A.; Jacobs, R. M. J.; Zorn, S.; Martin, R. A.; Martin, C. M.; Clark, G. F.; Goerigk, G.; Schreiber, F. Gold nanoparticles decorated with oligo(ethylene

glycol) thiols: Protein resistance and colloidal stability. *Journal of Physical Chemistry A* **2007**, *111* (49), 12229-12237. DOI: 10.1021/jp074293v.

(31) Mirkin, C. A.; Letsinger, R. L.; Mucic, R. C.; Storhoff, J. J. A DNA-based method for rationally assembling nanoparticles into macroscopic materials. *Nature* **1996**, *382* (6592), 607-609. DOI: DOI 10.1038/382607a0.

(32) Hurst, S.; Lytton-Jean, A.; Mirkin, C. Maximizing DNA loading on a range of gold nanoparticle sizes. *Analytical Chemistry* **2006**, *78* (24), 8313-8318, Article. DOI: 10.1021/ac0613582..

(33) Liu, B.; Liu, J. Freezing Directed Construction of Bio/Nano Interfaces: Reagentless Conjugation, Denser Spherical Nucleic Acids, and Better Nanoflares. *Journal of the American Chemical Society* **2017**, *139* (28), 9471-9474, Article. DOI: 10.1021/jacs.7b04885..

(34) Hao, Y.; Li, Y. J.; Song, L.; Deng, Z. X. Flash Synthesis of Spherical Nucleic Acids with Record DNA Density. *Journal of the American Chemical Society* **2021**, *143* (8), 3065-3069. DOI: 10.1021/jacs.1c00568.

(35) Nallagatla, S. R.; Heuberger, B.; Haque, A.; Switzer, C. Combinatorial Synthesis of Thrombin-Binding Aptamers Containing iso-Guanine. *Journal of Combinatorial Chemistry* **2009**, *11* (3), 364-369. DOI: 10.1021/cc800178m.

(36) Song, Y.; Song, J.; Wei, X.; Huang, M.; Sun, M.; Zhu, L.; Lin, B.; Shen, H.; Zhu, Z.; Yang, C. Discovery of Aptamers Targeting the Receptor-Binding Domain of the SARS-CoV-2 Spike Glycoprotein. *Analytical Chemistry* **2020**, *92* (14), 9895-9900, Article. DOI: 10.1021/acs.analchem.0c01394..

(37) Baldrich, E.; Restrepo, A.; O'Sullivan, C. K. Aptasensor development: Elucidation of critical parameters for optimal aptamer performance. *Analytical Chemistry* **2004**, *76* (23), 7053-7063. DOI: 10.1021/ac049258o.

(38) Nakatsuka, N.; Yang, K.; Abendroth, J.; Cheung, K.; Xu, X.; Yang, H.; Zhao, C.; Zhu, B.; Rim, Y.; Yang, Y.; et al. Aptamer-field-effect transistors overcome Debye length limitations for small-molecule sensing. *Science* **2018**, *362* (6412), 319+, Article. DOI: 10.1126/science.aao6750..

(39) Hill, H. D.; Millstone, J. E.; Banholzer, M. J.; Mirkin, C. A. The Role Radius of Curvature Plays in Thiolated Oligonucleotide Loading on Gold Nanoparticles. *ACScs Nano* **2009**, *3* (2), 418-424. DOI: 10.1021/nn800726e.

# 4.1 Appendix

**Free 15mer TBA**

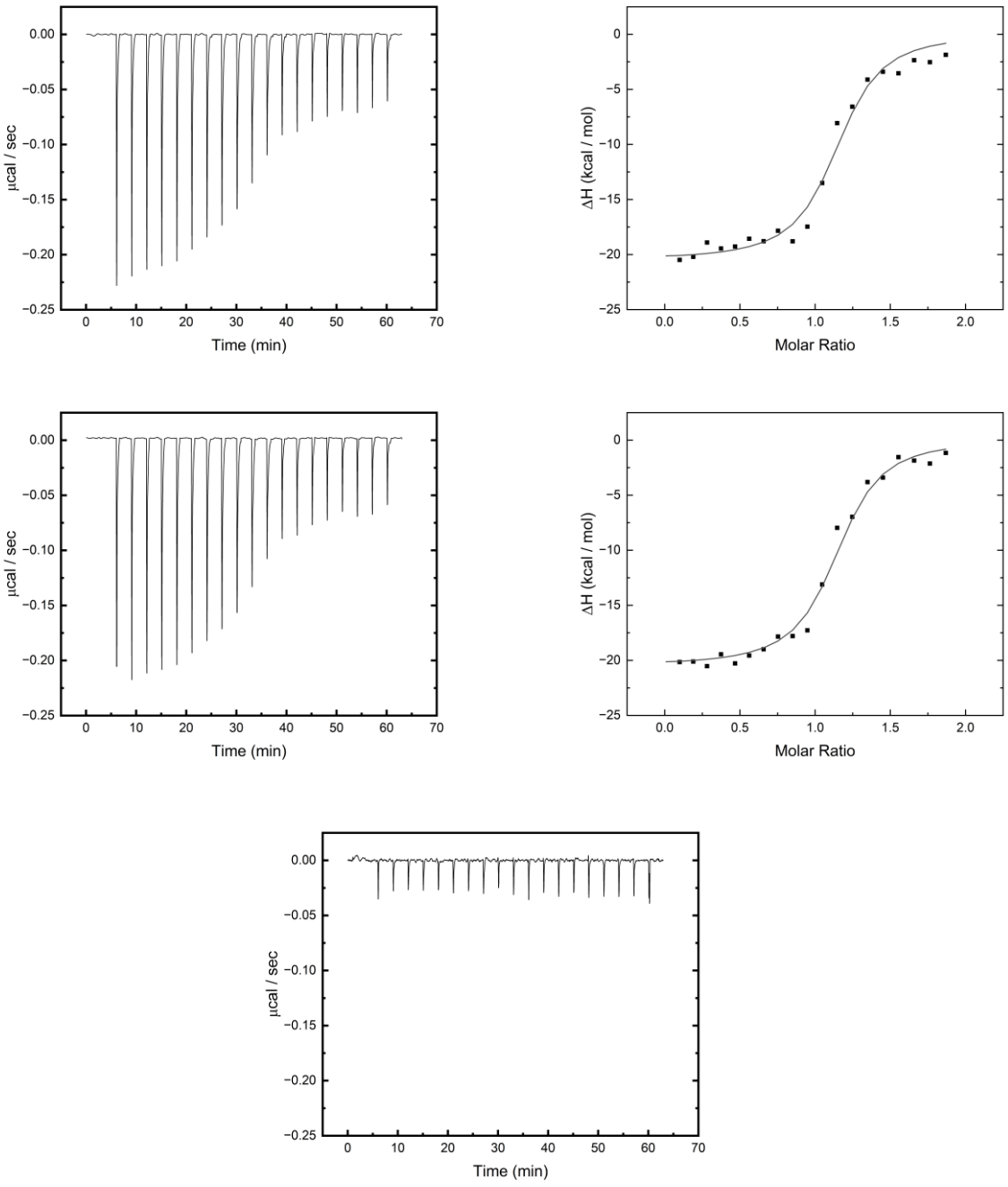


Figure A1: Replicate trials of homogeneous 15mer TBA with thrombin. For both replicates, concentration of 15mer TBA is 50 µM, concentration of thrombin is 5.5 µM. Bottom plot is 15mer TBA titrated into buffer (no thrombin in sample cell).

**Negative control**

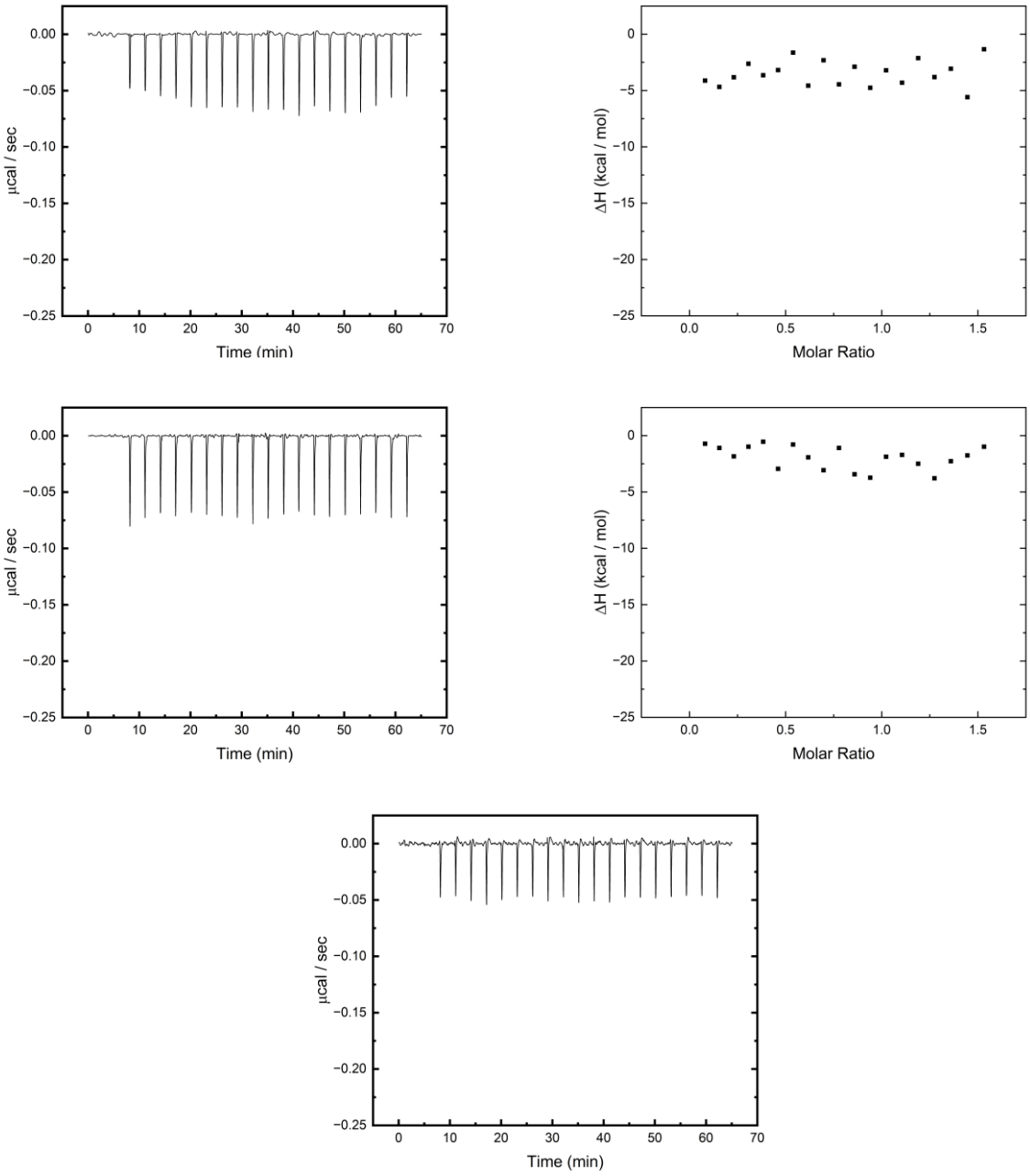


Figure A2: Replicate trials of CoV-1C-RBD aptamer functionalized 10 nm gold nanoparticles with thrombin. In both replicates, concentration of CoV-1C-RBD aptamer is 41 µM, concentration of thrombin is 5.5 µM. Bottom plot is CoV-1C-RBD titrated into buffer (no thrombin in sample cell).

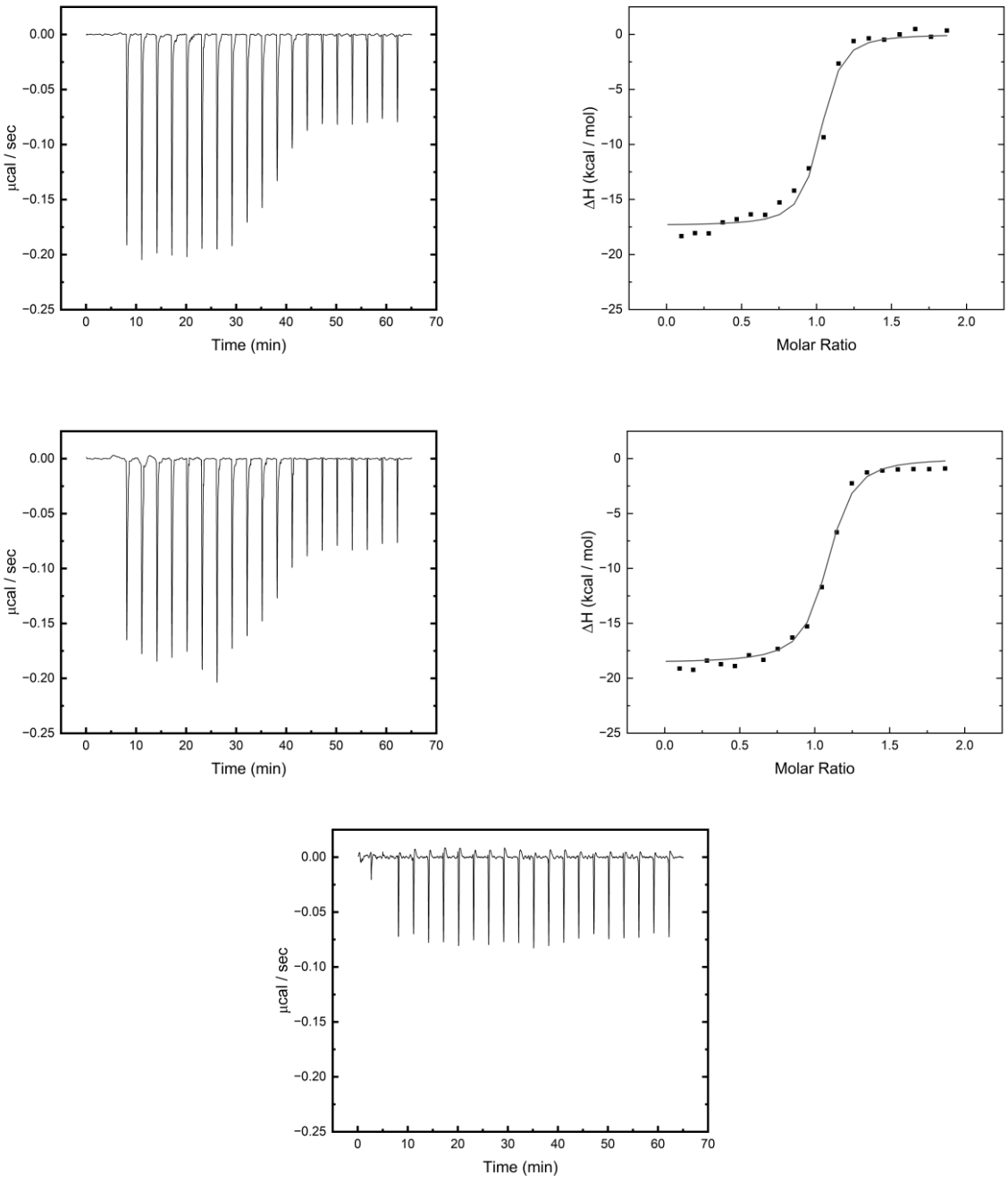


Figure A3: Replicate trials of homogeneous 0.3 M NaCl aged gold nanoparticles functionalized with 15mer TBA titrated into thrombin. In both replicates, concentration of 15mer TBA is 50 µM, concentration of thrombin is 5.5 µM. Bottom plot is 0.3 M NaCl aged gold nanoparticles functionalized with 15mer TBA titrated into buffer (no thrombin in sample cell).

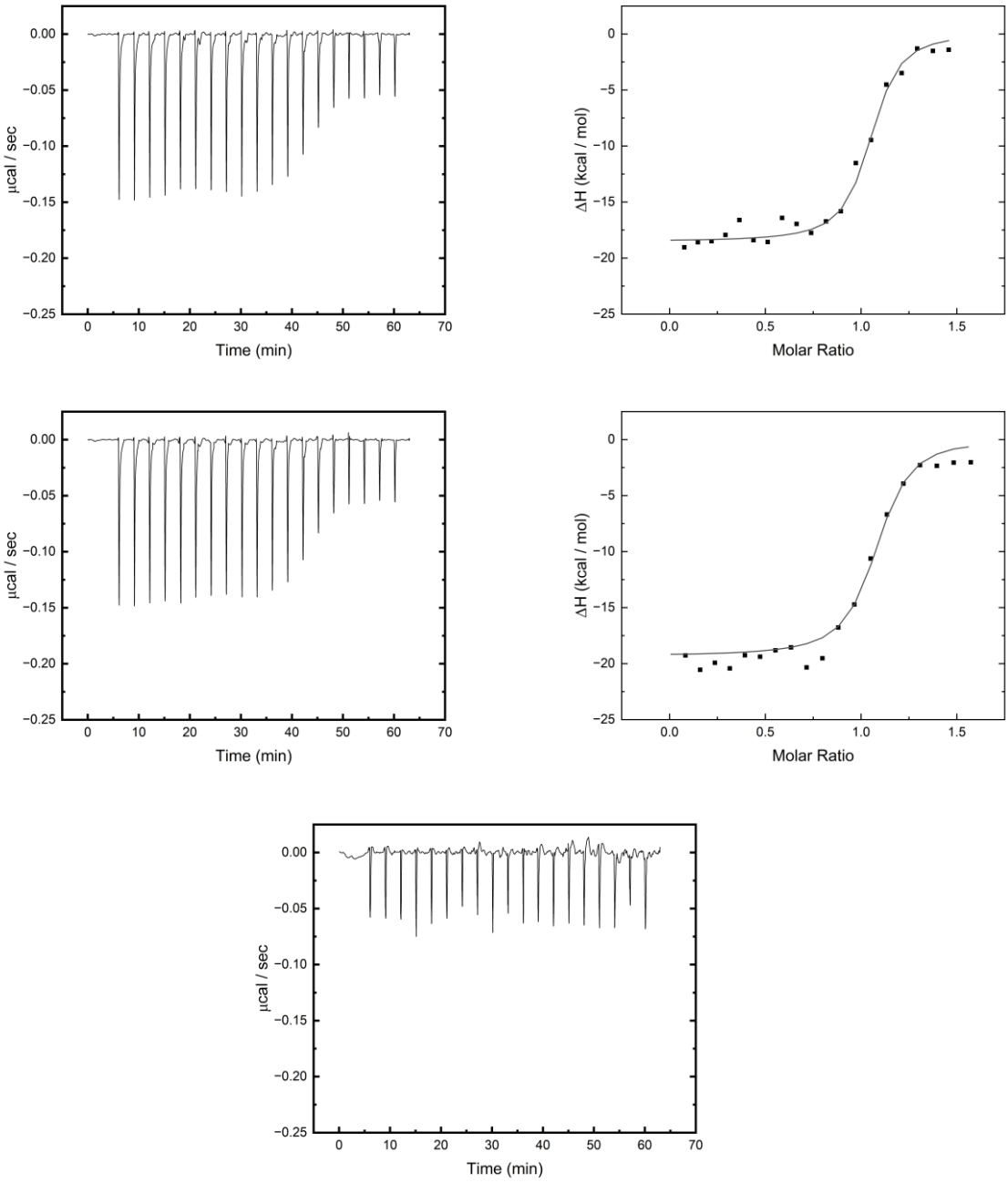


Figure A4: Replicate trials of homogeneous 0.5 M NaCl aged gold nanoparticles functionalized with 15mer TBA titrated into thrombin. In both replicates, concentration of 15mer TBA is 37 µM, concentration of thrombin is 5.5 µM. Bottom plot is 0.5 M NaCl aged gold nanoparticles functionalized with 15mer TBA titrated into buffer (no thrombin in sample cell).

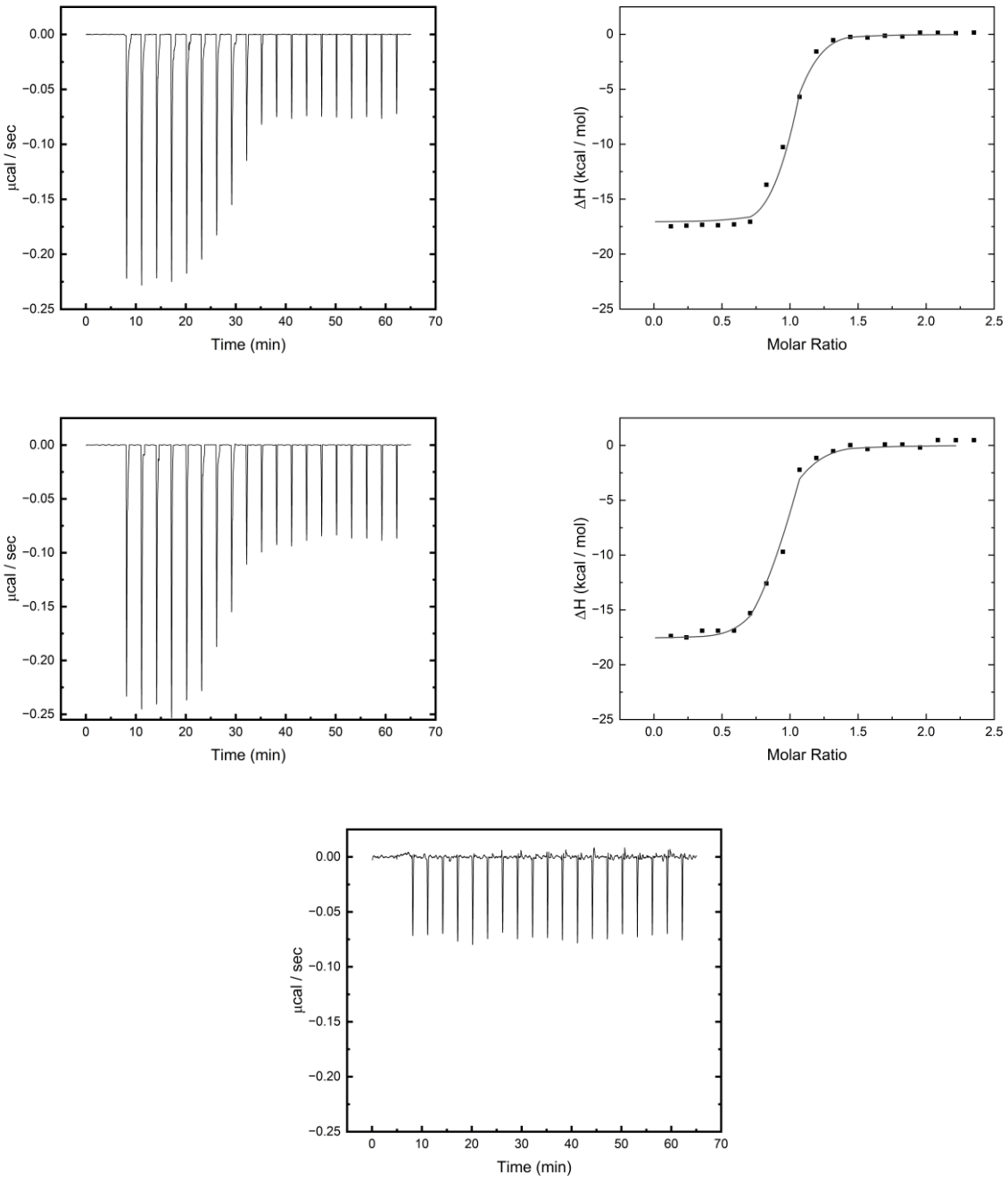


Figure A5: Replicate trials of homogeneous 0.7 M NaCl aged gold nanoparticles functionalized with 15mer TBA titrated into thrombin. In both replicates, concentration of 15mer TBA is 61 µM, concentration of thrombin is 5.5 µM. Bottom plot is 0.7 M NaCl aged gold nanoparticles functionalized with 15mer TBA titrated into buffer (no thrombin in sample cell).

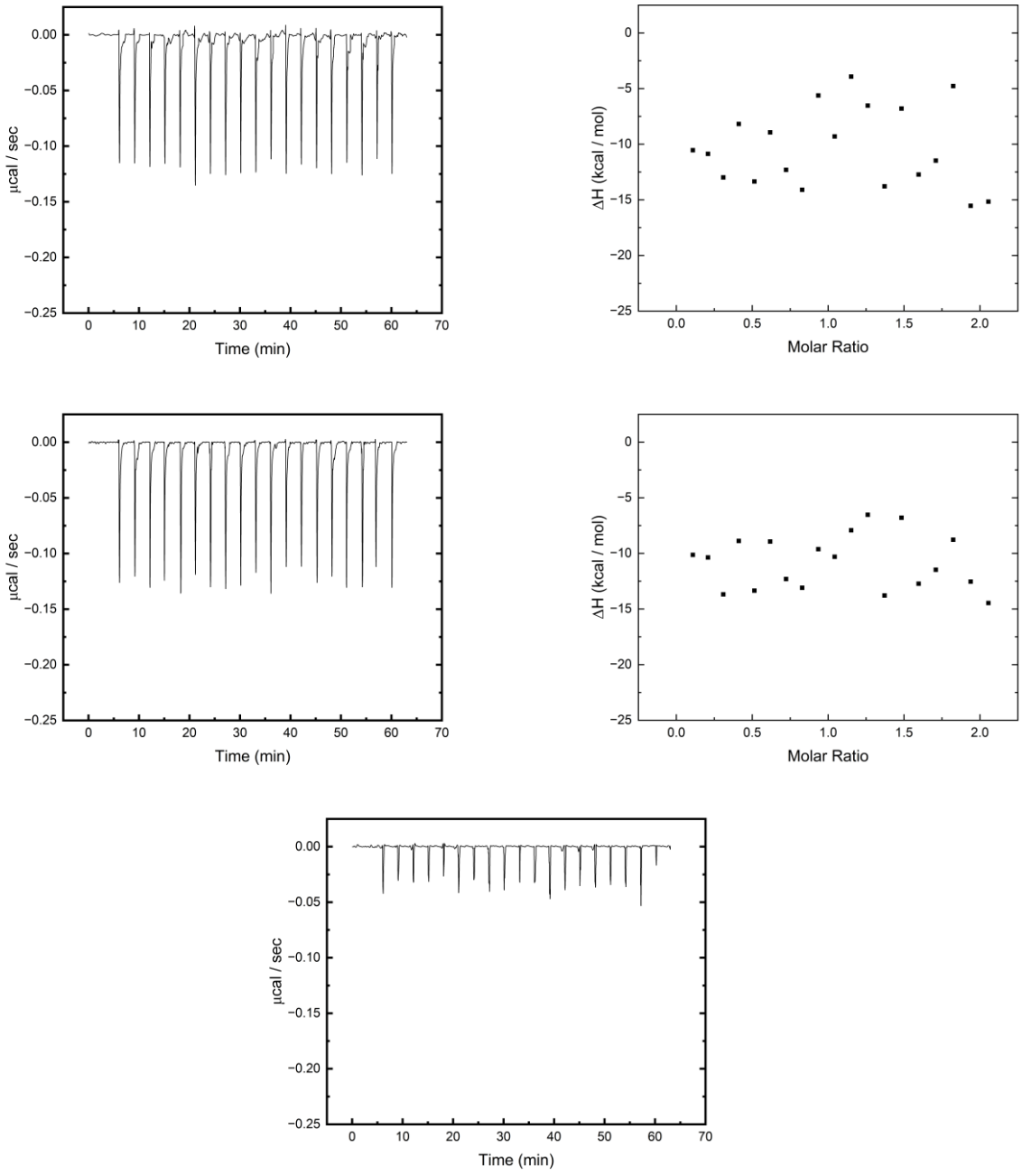


Figure A6: Replicate trials of homogeneous 0.8 M NaCl aged gold nanoparticles functionalized with 15mer TBA titrated into thrombin. In both replicates, concentration of 15mer TBA is 50 µM, concentration of thrombin is 5.5 µM. Bottom plot is 0.8 M NaCl aged gold nanoparticles functionalized with 15mer TBA titrated into buffer (no thrombin in sample cell).

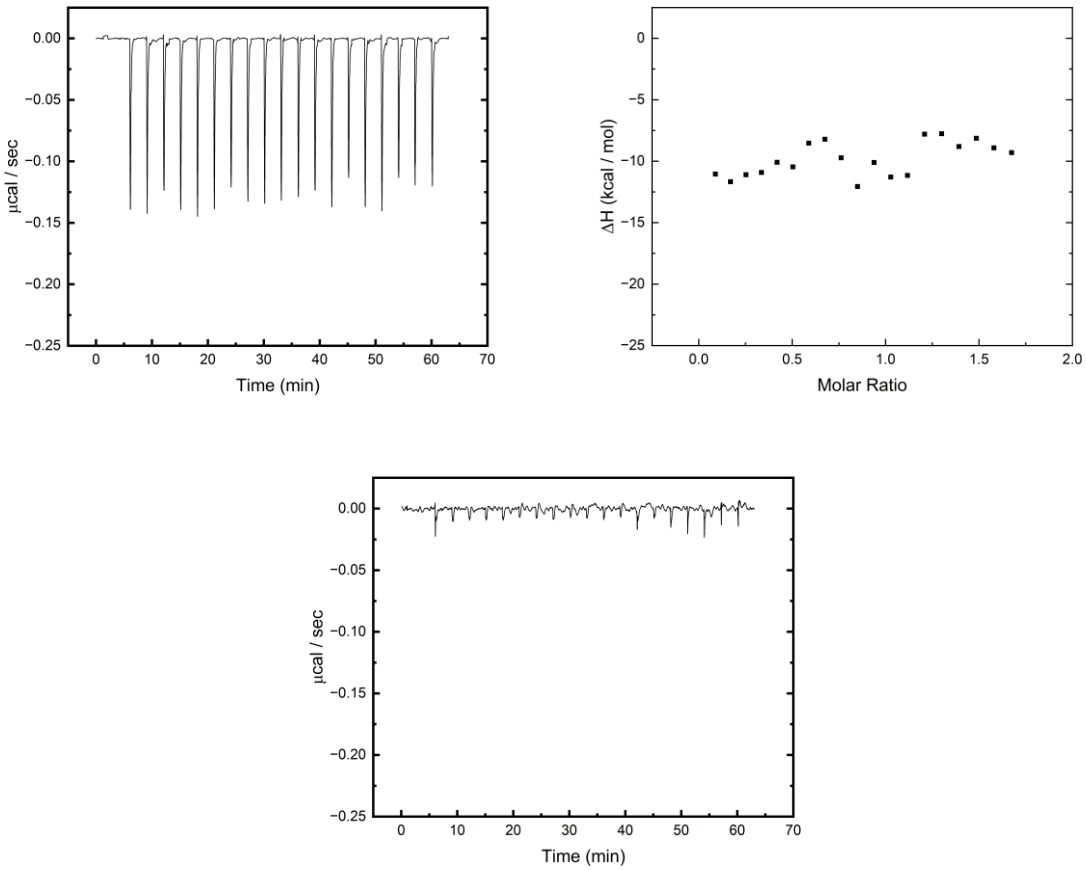


Figure A7: Replicate trial of 0.9 M NaCl aged gold nanoparticles functionalized with 15mer TBA titrated into thrombin. In both replicates, concentration of 15mer TBA is 50 µM, concentration of thrombin is 5.5 µM. Bottom plot is 0.9 M NaCl aged gold nanoparticles functionalized with 15mer TBA titrated into buffer (no thrombin in sample cell).

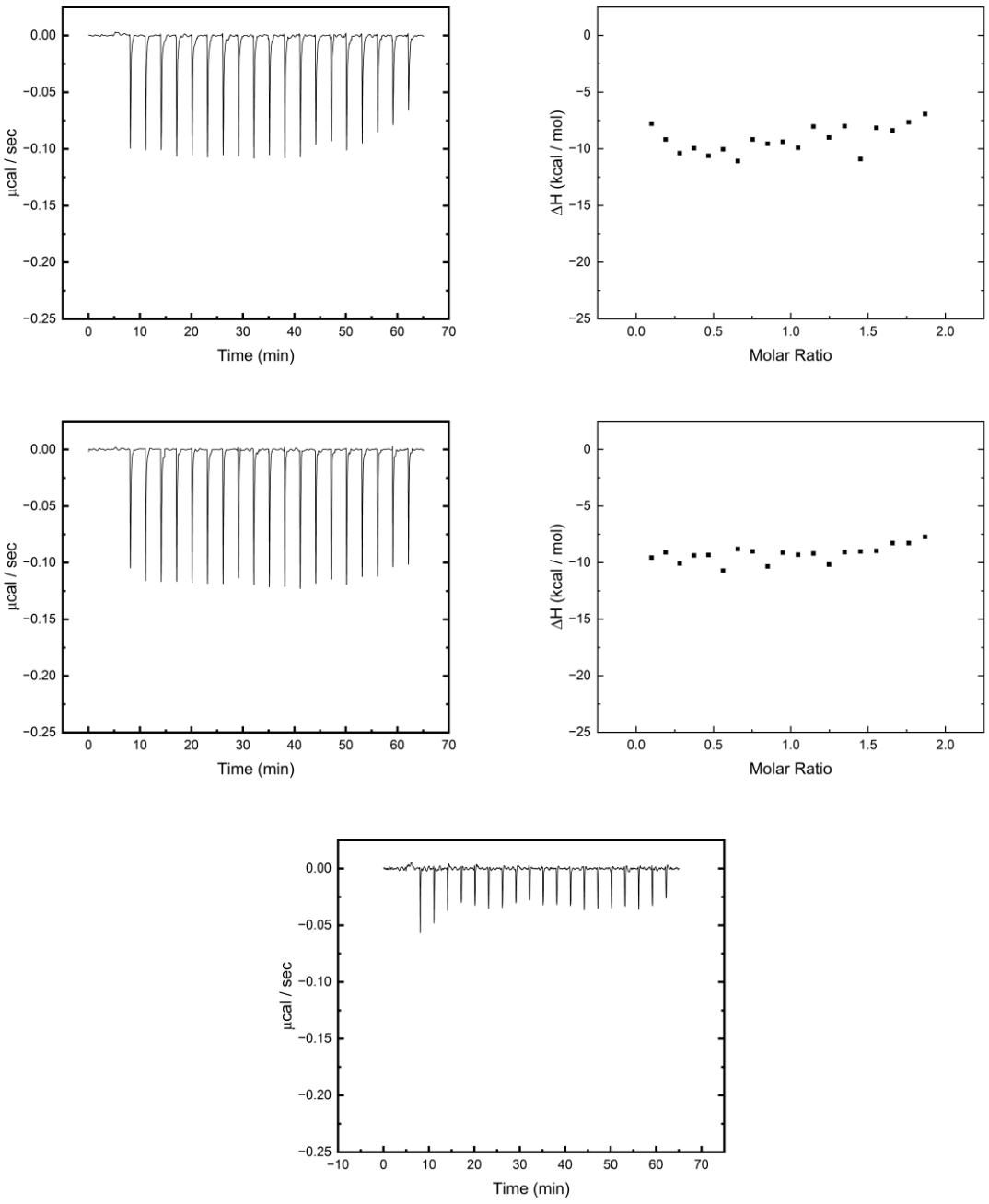


Figure A8: Replicate trials of 15mer TBA functionalized gold nanoparticles prepared by the freezing method titrated into thrombin. In both replicates, concentration of 15mer TBA is 50 µM, concentration of thrombin is 5.5 µM. Bottom plot is 15mer TBA functionalized gold nanoparticles prepared by the freezing method titrated into buffer (no thrombin in sample cell).

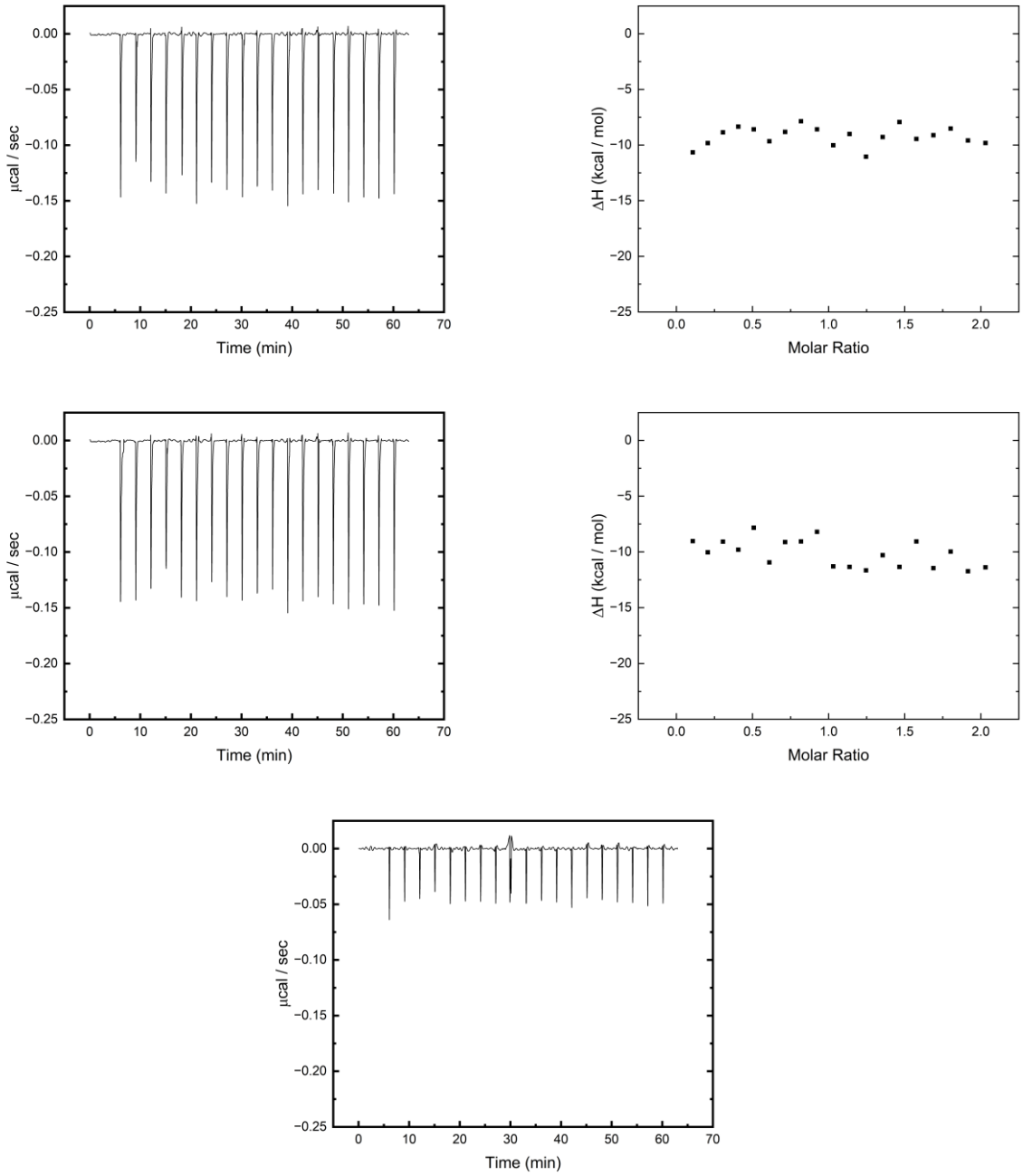


Figure A9: Replicate trials of 15mer TBA functionalized gold nanoparticles prepared by the butanol dehydration method titrated into thrombin. In both replicates, concentration of 15mer TBA is 50 µM, concentration of thrombin is 5.5 µM. Bottom plot is 15mer TBA functionalized gold nanoparticles prepared by the butanol dehydration method titrated into buffer (no thrombin in sample cell).

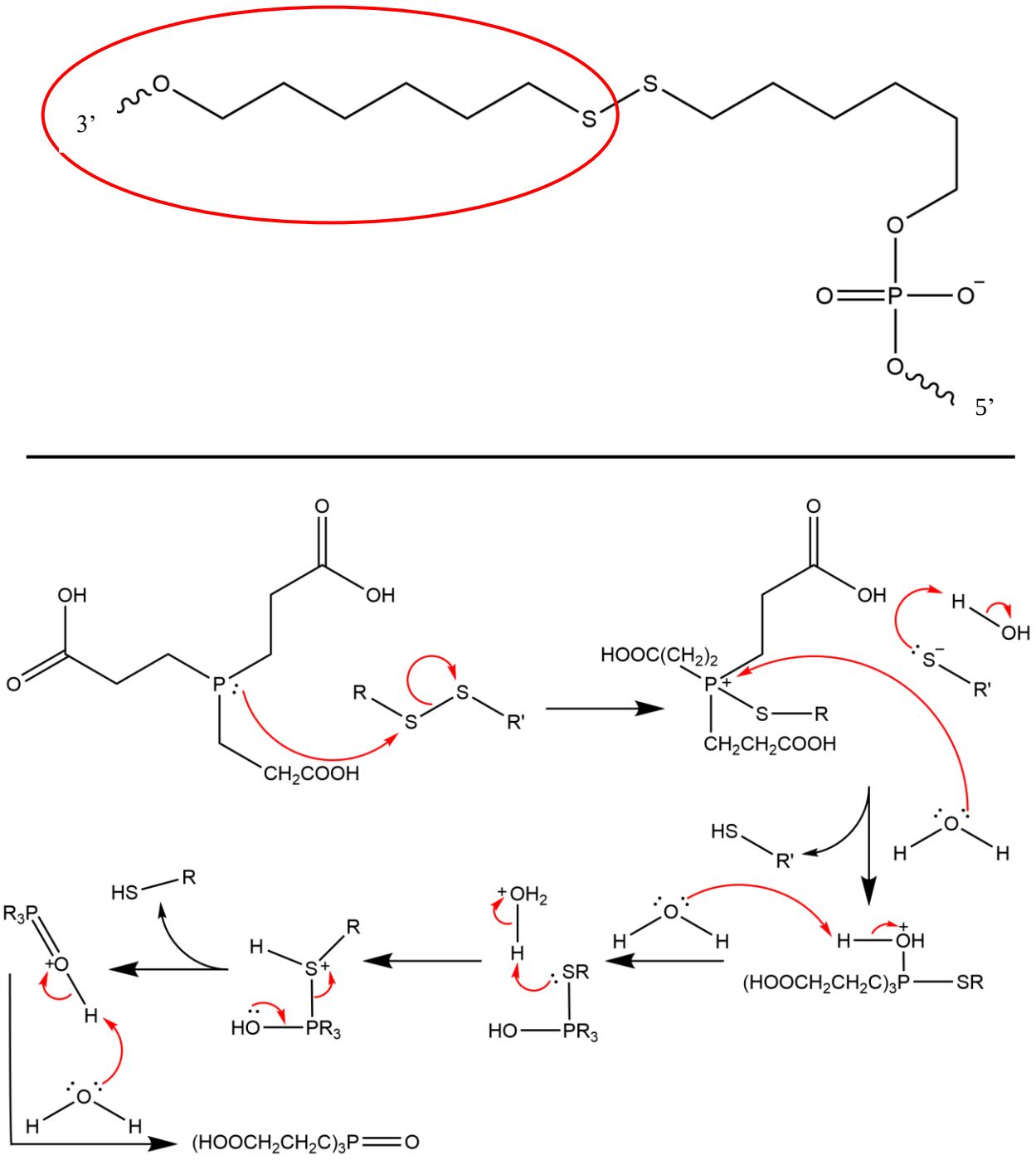


Figure A10: (Top) Thiolated linker of 15mer TBA. Protecting group (circled in red) is removed upon DNA reduction. (Bottom) Mechanism for TCEP reduction of di-sulfide functionalized aptamers. Result is a mono-thiolated DNA aptamer after reduction.

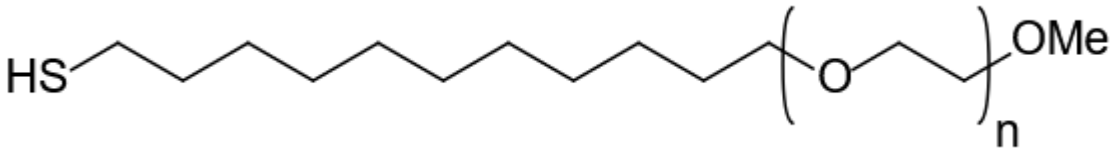


Figure A11: Structure of thiolated oligoethylene glycol (thiol-OEG). For experiments within this dissertation, n is equal to 3.

Table A1: Data table for aptamer quantification experiments.

| Sample Identification | Salt Age Target | Volume Collected (L) | Absorbance | Dilution Factor | Concentration DNA (M) | Total Strands | Strands per AuNP | Average Number of Strands | Standard Deviation |
|---|---|---|---|---|---|---|---|---|---|
| 15mer-TBA_PolyA_0.7M-NaCl_1 | 0.7M NaCl | 6.52E-04 | 0.165 | 1 | 6.22E-07 | 2.44E+14 | 3.92E+01 | 41 | 1.74 |
| 15mer-TBA_PolyA_0.7M-NaCl_2 | 0.7M NaCl | 6.54E-04 | 0.179 | 1 | 6.75E-07 | 2.66E+14 | 4.26E+01 | | |
| 15mer-TBA_PolyA_0.7M-NaCl_3 | 0.7M NaCl | 6.51E-04 | 0.1707 | 1 | 6.44E-07 | 2.53E+14 | 4.05E+01 | | |
| 15mer-TBA_PolyA_0.3M-NaCl_1 | 0.3M NaCl | 6.61E-04 | 0.1004 | 1 | 3.78E-07 | 1.51E+14 | 2.72E+01 | 27 | 0.341 |
| 15mer-TBA_PolyA_0.3M-NaCl_2 | 0.3M NaCl | 6.70E-04 | 0.0997 | 1 | 3.76E-07 | 1.52E+14 | 2.74E+01 | | |
| 15mer-TBA_PolyA_0.3M-NaCl_3 | 0.3M NaCl | 6.73E-04 | 0.101 | 1 | 3.81E-07 | 1.54E+14 | 2.79E+01 | | |
| 15mer-TBA_PolyA_0.9M-NaCl_1 | 0.9M NaCl | 6.45E-04 | 0.1779 | 1 | 6.71E-07 | 2.61E+14 | 5.75E+01 | 56 | 2.56 |
| 15mer-TBA_PolyA_0.9M-NaCl_2 | 0.9M NaCl | 6.61E-04 | 0.1724 | 1 | 6.50E-07 | 2.59E+14 | 5.71E+01 | | |
| 15mer-TBA_PolyA_0.9M-NaCl_3 | 0.9M NaCl | 6.91E-04 | 0.1527 | 1 | 5.76E-07 | 2.40E+14 | 5.29E+01 | | |
| 15mer-TBA_PolyA_0.8M-NaCl_1 | 0.8M NaCl | 6.68E-04 | 0.1526 | 1 | 5.75E-07 | 2.32E+14 | 5.11E+01 | 49 | 1.49 |
| 15mer-TBA_PolyA_0.8M-NaCl_2 | 0.8M NaCl | 6.80E-04 | 0.1426 | 1 | 5.38E-07 | 2.20E+14 | 4.86E+01 | | |
| 15mer-TBA_PolyA_0.8M-NaCl_3 | 0.8M NaCl | 6.60E-04 | 0.1464 | 1 | 5.52E-07 | 2.20E+14 | 4.85E+01 | | |
| 15mer-TBA_PolyA_Freeze_1 | FREEZE | 6.71E-04 | 0.2041 | 1 | 7.70E-07 | 3.11E+14 | 6.72E+01 | 69 | 2.65 |
| 15mer-TBA_PolyA_Freeze_2 | FREEZE | 6.91E-04 | 0.213 | 1 | 8.03E-07 | 3.34E+14 | 7.22E+01 | | |
| 15mer-TBA_PolyA_Freeze_3 | FREEZE | 6.96E-04 | 0.1998 | 1 | 7.53E-07 | 3.16E+14 | 6.83E+01 | | |
| 15mer-TBA_PolyA_Butanol_1 | Butanol | 6.71E-04 | 0.0807 | 1 | 3.04E-07 | 1.23E+14 | 1.16E+02 | 124 | 7.41 |
| 15mer-TBA_PolyA_Butanol_2 | Butanol | 6.83E-04 | 0.0885 | 1 | 3.33E-07 | 1.37E+14 | 1.29E+02 | | |
| 15mer-TBA_PolyA_Butanol_3 | Butanol | 6.60E-04 | 0.0906 | 1 | 3.41E-07 | 1.36E+14 | 1.28E+02 | | |
| 15mer-TBA_PolyA_0.5M-NaCl_1 | 0.5M NaCl | 6.91E-04 | 0.0968 | 1 | 3.65E-07 | 1.52E+14 | 3.18E+01 | 34 | 2.86 |
| 15mer-TBA_PolyA_0.5M-NaCl_2 | 0.5M NaCl | 6.71E-04 | 0.1169 | 1 | 4.41E-07 | 1.78E+14 | 3.73E+01 | | |
| 15mer-TBA_PolyA_0.5M-NaCl_3 | 0.5M NaCl | 6.82E-04 | 0.1022 | 1 | 3.8E-07 | 1.58E+14 | 3.32E+01 | | |
| | | | | | | Total AuNP | | | |

| | | | | | | | | | |
|---|---|---|---|---|---|---|---|---|---|
| 10nm-AuNP_0.9M-NaCl | 0.9M NaCl | 2.00E-04 | 1.078 | 3.33 | 3.76E-08 | 4.53E+12 | | | |
| 10nm-AuNP_0.7M-NaCl | 0.7M NaCl | 2.00E-04 | 0.743 | 6.66 | 5.18E-08 | 6.24E+12 | | | |
| 10nm-AuNP_0.3M-NaCl | 0.3M NaCl | 2.00E-04 | 0.66 | 6.66 | 4.60E-08 | 5.54E+12 | | | |
| 10nm-AuNP_FREEZE | FREEZE | 2.00E-04 | 0.979 | 3.75 | 3.84E-08 | 4.63E+12 | | | |
| 10nmAuNP-Butanol | Butanol | 2.00E-04 | 0.1599 | 5.26 | 8.81E-09 | 1.06E+12 | | | |
| 10nm-AuNP_0.8M-NaCl | 0.8M NaCl | 2.00E-04 | 0.4849 | 4.57 | 2.32E-08 | 2.80E+12 | | | |
| 10nm-AuNP_0.5M-NaCl | 0.5M NaCl | 2.00E-04 | 0.2083 | 18.18 | 3.97E-08 | 4.78E+12 | | | |
| | | | | | | | | | |
| AuNP Extinction Coefficient ($M^{-1}$ $cm^{-1}$) | | | | | | | | | |
| 9.55E+07 | | | | | | | | | |
| DNA Extinction Coefficient ($M^{-1}$ $cm^{-1}$) | | | | | | | | | |
| 265000 | | | | | | | | | |

Table A2: DNA Aptamer sequence and extinction coefficient information.

| Aptamer Name | Sequence | Extinction Coefficient ($M^{-1}$ $cm^{-1}$) |
|---|---|---|
| 15mer Thrombin Binding Aptamer (TBA) | 5' – GGTTGGTGTGGTTGGAAAAAAA AAA –Thiol Linker 3' | 265,000 |
| CoV-1C-RBD Aptamer | 5′- CAGCACCGACCTTGTGCTTTGG GAGTGCTGGTCCAAGGGCGTTA ATGGACATTTT – Thiol Linker 3' | 514,600 |